ELYSIUM

34th Annual AHS International Student Design Competition

24 Hour Hovering Machine
Conceptual Design

Sponsored by Sikorsky A Lockheed Martin Company

UNIVERSITY OF MARYLAND

Alfred Gessow Rotorcraft Center
Department of Aerospace Engineering
University of Maryland
College Park, MD 20742

Alfred Gessow Rotorcraft Center
Department of Aerospace Engineering
University of Maryland
College Park, MD 20740 U.S.A.

To the American Helicopter Society:

The members of the University of Maryland Graduate Student Design Team hereby grant AHS full permission to distribute the enclosed Executive Summary and Final Proposal for the 34th Annual Design Competition as they see fit.

Thank you,

The UMD Graduate Design Team

Alfred Gessow Rotorcraft Center
Department of Aerospace Engineering
University of Maryland
College Park, MD 20740 U.S.A.

Daniel Escobar
Graduate Student (Team Leader)
descobar@umd.edu

Tyler Sinotte
Graduate Student
tsinotte@gmail.com

Peter Oas
Graduate Student
peter.oas@gmail.com

Bumseok Lee
Graduate Student
bslee@umd.edu

Brent Mills
Graduate Student (ARL)
brent.t.mills.civ@mail.mil

Dylan Jude
Graduate Student
djude@umd.edu

William Craig
Graduate Student
wscraig@umd.edu

Dr. Bharath Govindarajan
Faculty Advisor
bharath@umd.edu

Dr. Vengalattore Nagaraj
Faculty Advisor
vnagaraj@umd.edu

Dr. Inderjit Chopra
Faculty Advisor
chopra@umd.edu

ACKNOWLEDGEMENTS

Contents

List of Figures

List of Tables

Elysium Requirements and Compliance

Mission Profile Compliance	Design Solution	Section
Carry a Non-Productive Payload with ground weight no less than 176.4 lb (80 kg)	Elysium can carry 210 lb (95 kg) of payload	Table 14.1
The aircraft shall be unoccupied, i.e., fly autonomously or receive commands from a Ground Controller	Elysium carries a simulated human test dummy, and the onboard autopilot is capable of fully autonomous control	Sec. 12.1
Hover for 24 Hours at three Hover Stations	Elysium has a hover endurance of xx hours	Sec. 3.2
Travel 0.54 nm (1 km) between hover Stations	Elysium has a range of 1460 nm (2703 km)	Sec. 3.2 Sec. 19.2
Shall not trap gases that have density lower than ambient air. All closed cavities of the aircraft must be vented to the atmosphere	Elysium's fuel tanks are properly vented to the atmosphere	Sec: 11.11
Energy, shall not be collected by the aircraft from man-made sources	Elysium only uses energy from the on-board fuel	Sec. 5.2.2 Ch. 11
No part of the machine may be jettisoned during flight	Elysium does not jettison any parts during the flight as shown through the weight analysis	Table 14.1
The vehicle must use technologies so that it can be designed, built, and tested within the next 3-5 years	Every component aboard and all designed systems of Elysium meet this requirement	Ch. 21
Hover shall be defined as when the aircraft is supported exclusively by aerodynamic forces	Elysium is supported in hover purely by the aerodynamic lift of its two rotors	Ch. 7
Hover shall be defined as when the aircraft has zero relative velocity with respect to a ground observer station, both longitudinally and laterally, and has no change in altitude	Elysium's closed loop control system is capable of quickly returning to a hover condition after gust from	Ch. 15.5
Hover shall be defined as out-of-ground-effect (HOGE) at an altitude at least twice the vehicle dimension	By RFP definition, HOGE for Elysium is greater than 102 ft (31 m), and Elysium's mission defines a hover altitude of 1,500 ft (457.2 m)	Sec. 3.2
Hover shall be defined as flight time during which wind speeds do not exceed 9.71 kt (5m/s)	Elysium's sizing mission accounts for 45 min of time every 24 hours to account for wind gusts	Sec. 19.5
Maintain vehicle centroid within Hover Sphere	Elysium control system can return the vehicle to its original location only travelling 25 ft (7.6m)	Sec. 15.5

Documentation Requirement Compliance	Section
Conceptual Design Trade Studies	Ch. 5
Vehicle Description	Ch. 6
Propulsion System Data	Ch. 11
Hover Performance Data	Ch. 19
Forward Flight Performance Data	Ch. 19
Mission Performance Data	Ch.19
Air Vehicle Design & Subsystem Drawings	Ch. 11
Aerodynamic Data	Ch. 19
Loads & Criteria Data	Ch. 18
Mass Properties Data	Ch. 14
Manufacturing & Cost Data	Ch. 21
Additional Graduate Student Tasks:	--
a) Simulation & Flight Control Laws Development	Ch. 15
b) Stress Analysis & Fatigue Substantiation	Ch. 9 & Ch.10
c) Aerodynamic Design Substantiation	Ch. 19
d) Propulsion System Details	Ch. 11

Three View

51.0 ft (15.55 m)
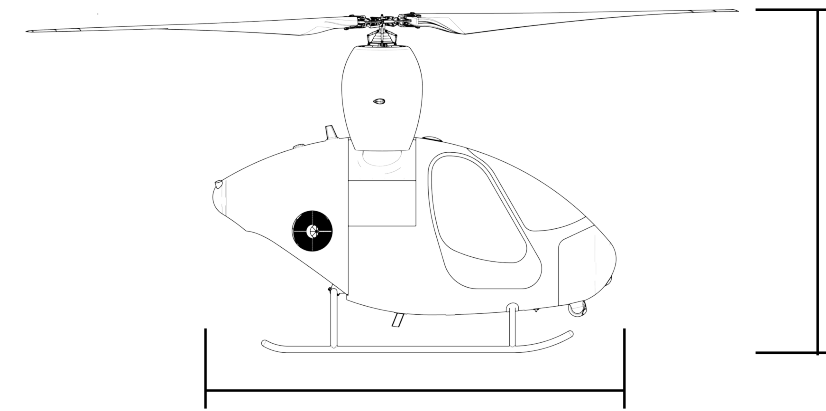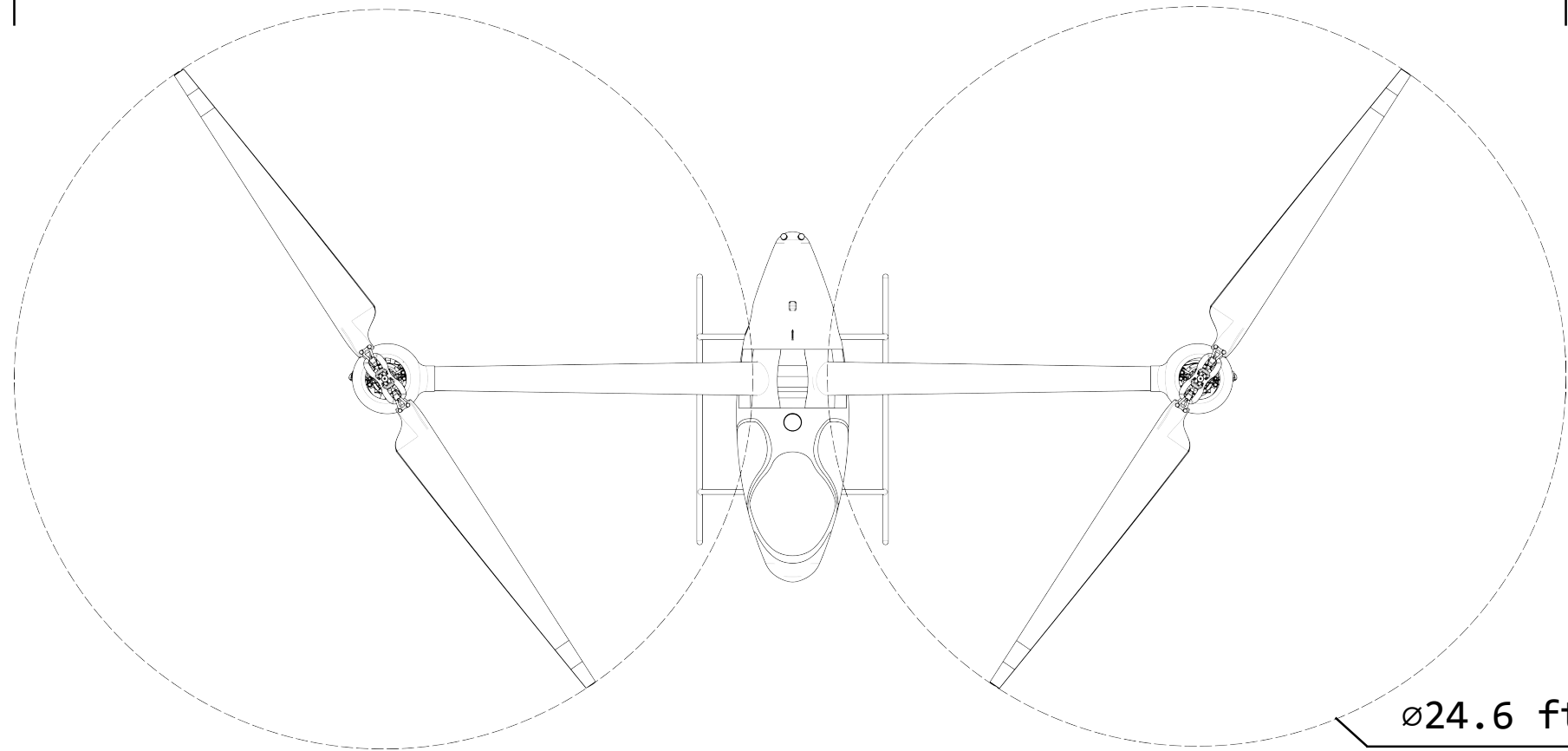
⌀24.6 ft
(7.49 m)

6.3 ft
(1.92 m)

11.7 ft
(3.56 m)
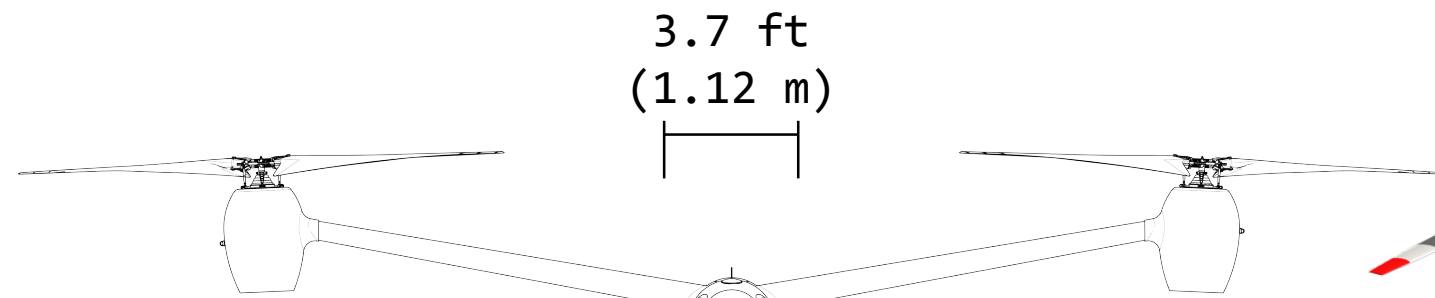
3.7 ft
(1.12 m)

1.1 ft
(0.33 m)

6.4 ft
(1.95 m)

29.6 ft (9.02)

1 Introduction

The role of rotorcraft has changed dramatically since their inception. Initially conceived as vehicles with superior hover capabilities, helicopters have morphed into vehicles with a vast range of capabilities such as high-speed forward flight and long endurance loitering. Consequently, designing a vehicle to satisfy these requirements typically results in a compromise in performance for individual flight regimes because of competing and contradicting requirements. The goal of efficient high speed forward flight has caused helicopter design to diverge from optimal hover performance.

The *Igor I. Sikorksy 24 Hour Hover Challenge*, and the *AHS International 34th Annual Student Design Competition* Request for Proposal (RFP) aim to bridge the gap between current rotorcraft and the necessary technology to achieve highly efficient hover. These challenges hope to spark innovations and step changes in helicopter technology towards the goal of sustained efficient hover. The RFP calls for inventions in structures, propulsion system, and rotor aerodynamic efficiency. A top to bottom re-evaluation of every choice that goes into helicopter design is required to achieve this goal of superior performance, more efficient hover than any current helicopter design, and to be cost effective and reliable.

Through the application of innovative design methodology and design driven technical substantiation, the 2017 University of Maryland Graduate Design Team proudly presents *Elysium* Technology Demonstrator; a 1812 lb (822 kg) autonomous twin rotor hybrid electric helicopter that demonstrates 24 hours of hover flight with unprecedented performance, efficiency and reliability. By implementing a minimalist approach to structural, propulsion system, and rotor aerodynamic design, *Elysium* meets and surpasses all RFP requirements through a lightweight, safe, and mission flexible package.

Elysium is designed as a technology demonstrator (TD), i.e., an experimental vehicle designed to complete a full-flight test regime and showcase its superior technology and capability. Historically, these vehicles (designated 'XV' and/or 'TD') have been built with the intention of showcasing a particular technology, such as high-speed forward flight (Hughes XV-9, Sikorsky X2-TD), noise reduction or convertible concepts (Bell's XV-3 and XV-15). Once successful, these TDs can be translated to military and commercial vehicles. In the same vein, *Elysium* identifies and demonstrates the technology required to achieve sustainable and efficient hover for 24 hours.

FIGURE 1.1: *Elysium* Technology Demonstrator (TD) vehicle concept performing the 24-hour hover challenge.

The design methodology for *Elysium* is focused on the key design metrics of: (1) Minimizing gross take off weight and fuel weight, (2) Ensuring superior reliability through reducing mechanical complexity, and (3) Innovative application of state-of-the-art technology to create a superior vehicle platform. This report will outline the methodology utilized in arriving at the final *Elysium* system design and explain the features of the aircraft that make it a superior technology for accomplishing the proposed mission.

TABLE 1.1: Overview of *Elysium*

Sub-system	Innovation
Hover Efficiency	A hover optimized design results in the ability to hover for 24 hours at 1,500 ft, ISA+10°C while still demonstrating other typical helicopter attributes, such as 20 knot (37 km/hr) cruise speed at 1500 ft (457.2m).
Twin Rotor	A dual non-overlapping rotor design isolates aerodynamic interference and combines with a highly efficient propulsion system to allow on-board generated power to be used primarily for thrust generation
Optimized Aerodynamics	Two-bladed rotor utilizes high-lift airfoils to ensure an unprecedented FM through the mission of 0.84, while using inboard reflex airfoils to reduce pitch link loads
Variable Tip Speed	Rotor RPM scheduling results in a constant blade loading along the entire mission duration to maintain maximum rotor efficiency
Lightweight Structure	Innovative lightweight composite structure and a reliable semi-articulated hub maintains a weight empty fraction of 0.60
Control	Swashplate control for quick reliable control and gust response allowing *Elysium* to operate up to a 65 ft/sec horizontal gusts
Creative Hybrid Propulsion	Hybrid electric-piston propulsion system is designed to achieve low specific fuel consumption over the duration of the entire mission, while allowing for upgrades in the future
Mechanical Simplicity	Mechanical simplicity across all subsystems drastically increases overall vehicle reliability and time between scheduled maintenance while minimizing maintenance costs
Health Monitoring	Onboard self-monitoring for faster maintenance and in-flight status
Avionics	Avionics allow for fully autonomous flight as well as low-workload optionally piloted in day and night conditions

2 Analysis of 24 Hour Mission

Before detailed design into a solution for the RFP, an investigation into the current state-of-the-art and impact of vehicle and rotor parameters, such as disk loading, empty weight fraction, figure of merit, and specific fuel consumption, was carried out. While recognizing that helicopters are designed for different mission requirements, a simplified momentum theory based analysis of typical single main rotor helicopters was carried out with the goal of determining which vehicle characteristics had to be improved to achieve the 24 hour hover goal.

2.1 Current Helicopter Estimates

In addition to the momentum theory analysis, a literature review into aircraft endurance records was important to understand the achievements and limitations of current technology. From

1989, the longest refueled manned helicopter flight lasted 50 hours in a Bell 47B, and from 1966 the longest non-refueled manned helicopter flight lasted 15 hours and 8 minutes in a modified Hughes YOH-6A. The only modifications to the YOH-6A were the removal of non flight critical structural components to reduce the empty weight and increase endurance. More recently, in 2008, the Boeing and DARPA A160 Hummingbird set the record for the longest unmanned helicopter flight of 18 hours and 41 minutes. These record breaking flights prove that while current helicopter technology is capable of meeting a 24 hour non-hovering flight without any payload in terms of reliability requirements and flight endurance, the same is not clear for a pure *hovering* mission where the challenges are different, especially with a payload requirement.

A momentum theory study was conducted using characteristics of five existing single main rotor helicopters: YOH-6A, UH-60, CH-53K, CH-54B, and the Robinson R22, to estimate their maximum hovering capabilities. These helicopters represent a broad range of current technologies, weight classes, rotor geometries, engine size and cost levels. In addition to using the helicopter parameters, the following engineering assumptions were made: (1) induced power factor of 1.15, (2) transmission efficiency of 0.95, (3) standard sea level atmospheric conditions, and (4) each aircraft's allowable fuel was the difference between maximum gross take-off weight and empty weight. While the last assumption might require additional fuel tanks to be installed to re-purpose the payload capacity for fuel storage, this simplistic exercise ignores this requirement.

TABLE 2.1: Current helicopter endurance estimates

	YOH-6A	**UH-60**	**CH-53K**	**CH-54B**	**R22**
Empty Weight (lb)	1,400	10,624	33,226	19,234	796
Maximum Weight (lb)	3,549	23,500	84,700	47,000	1,363
Radius (ft)	13.7	26.8	39.5	36.0	12.6
V_{Tip} (ft/s)	693.2	723.6	766.3	698.4	635.0
Blade Loading	0.099	0.101	0.075	0.0866	2.7
Disk Loading (lb/sqft)	6.0	10.4	17.3	11.5	2.7
Empty Weight Fraction	39.4%	45.2%	39.2%	40.9%	58.4%
SFC (lb/hp/hr)	0.77	0.43	0.39	0.45	0.35
Max. Hover Time (Hr)	**15.6**	**16.0**	**16.7**	**17.1**	**17.4**

Table 2.1 shows the results from these calculations. It is important to note that, for these calculations to be accurate, fuel consumption must be accounted for by updating the vehicle weight at each time-step of the numerical integration when estimating the endurance. These calculations show that current typical helicopter technology is incapable of achieving the required 24 hour hover mission and fall short by approximately 7–8 hours. These aircraft were not specifically designed for a hover mission and therefore are not optimized for hover. From the data presented in Table 2.1, the R22 stands out as a lightweight helicopter with the highest hovering endurance for the 24 hour hover challenge. The R22 has a combination of low empty weight fraction, low tip velocity, and low specific fuel consumption, which allows the vehicle to achieve this high level of endurance.

2.2 RFP Plots

The RFP provides preliminary insight into the design space by looking at the hover performance of a coaxial helicopter over 24 hours using a specific fuel consumption of 0.35 lb/hp/hr (0.21

(a) Constant C_T and FM   (b) Variable C_T at V_{tip} of 650 ft/s   (c) Variable C_T at V_{tip} of 400 ft/s
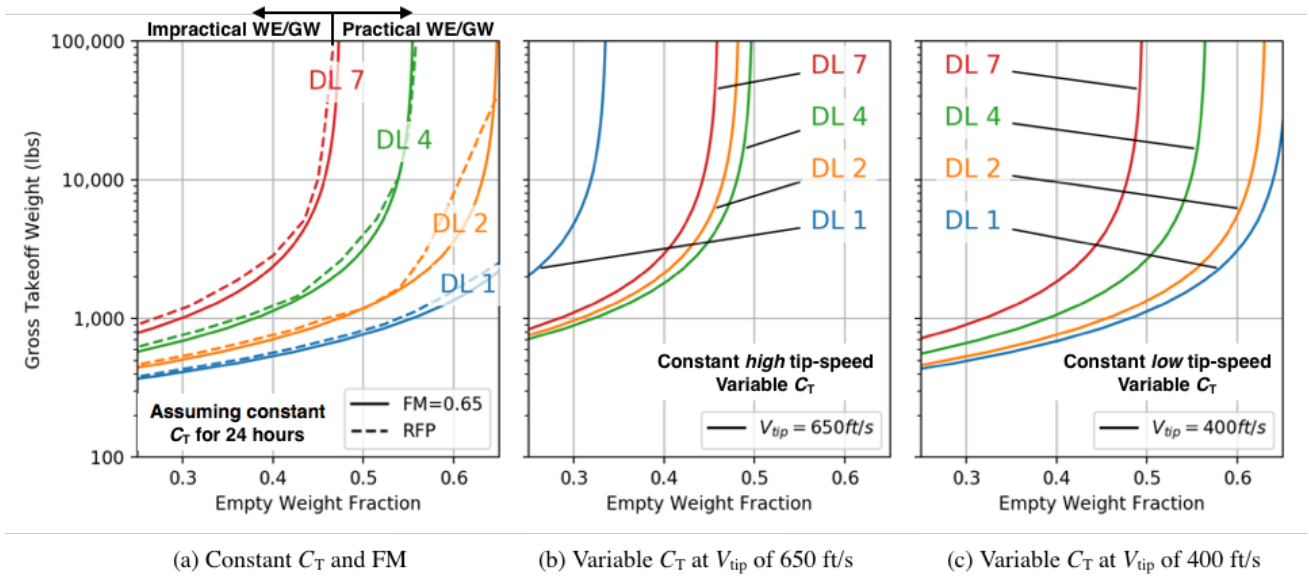
FIGURE 2.1: Comparison between the assumption of constant FM and constant tip speed.

kg/kw/hr). The first provided plot of gross take-off weight versus empty weight at various disk-loadings is recreated in Fig. 2.1(a) in an attempt to decipher the technical reasoning behind the RFP. It was observed that, through trial and error, a constant Figure of Merit (FM) of 0.65 could best approximate the data provided by the RFP. The trend from Fig. 2.1(a) suggests a step-change in technology is required to obtain the low disk-loading and empty-weight fraction of a feasible vehicle in the range of 2,000–5,000 lbs (907–2,267 kg), which is the premise upon which the current RFP is based.

Note that for these calculations, the thrust cannot be assumed constant throughout the entire mission as there is a constant fuel burn which reduces the overall weight of the vehicle. A study was conducted subdividing the 24 hour interval into 10 minute segments, which implies that the thrust coefficient ($C_T = T/(\rho A(\Omega R)^2)$) of the rotor will decrease if the rotor tip-speed remains unchanged. Consequently, the use of a constant FM can lead to misleading results, because a typical helicopter would not be able to maintain a constant FM as C_T changes, as indicated by

$$FM = \frac{P_{\text{ideal}}}{P_{\text{actual}}} = \frac{C_T^{3/2}/\sqrt{2}}{\kappa C_T^{3/2}/\sqrt{2} + C_{P_0}} \tag{2.1}$$

Alternatively, from a simple modified momentum theory analysis, the rotor power can be broken down into the induced and profile power components

$$P_{\text{actual}} = \frac{\kappa T^{3/2}}{2\rho A} + \rho A V_{\text{tip}}^3 \left(\frac{\sigma C_{d0}}{8} \right) \tag{2.2}$$

where κ is the induced power factor, and C_{d0} is the average rotor drag coefficient. Using recommended values from Leishman [1], $\kappa = 1.15*1.20$ (for induced and interference losses), $C_{d0} = 0.01$ and $\sigma = 0.04$ results in a very different trend. Figures 2.1(b) and 2.1(c) show the variation of gross take-off weight (GW) with empty weight fraction (WE) for representative constant rotor tip speeds of 650 ft/s (198 m/s) and 400 ft/s (122 m/s), respectively. The tip speed has a drastic effect on hover performance especially as thrust changes over time because the profile power term in Eq. 2.2 scales with $\sim V_{\text{tip}}^3$. For the higher tip-speed of 650 ft/s (198 m/s), while the rotor

may initially have been very efficient with a full-fuel tank, at the end of the 24-hour mission the induced power decreases while the profile power stays the same. The trend in gross take-off weight with varying disk loading is also different with and without the assumption of a constant FM (with varying C_T), i.e., Figs. 2.1(a) and 2.1(b), respectively. With a higher constant tip speed, the empty weight fraction of the design falls in the "impractical" WE/GW range, as defined in the RFP; however, a lower tip speed alleviates that requirement.

When analyzed, the provided plots from the RFP provide insight into the direction required for the design of the helicopter. A constant FM is advantageous and can be achieved *if C_T is held* constant throughout the 24 hour mission. This target can be achieved through a variation in rotor RPM or a variation in rotor radius. Furthermore, a FM of 0.65 matches the results provided in the RFP, which is quite low by the state-of-the-art standards. Therefore, *Elysium* uses a variable RPM to maintain a constant FM (see Section 5.1.3) and optimized blade aerodynamics (see Section 7) to achieve a nearly constant FM of 0.847 throughout the mission. Furthermore, a comprehensive analysis of hover performance and rotor tip speed is presented in Section 5.

3 Mission Requirements

The RFP states the mission is to hover for a total duration of 24 hours, in three separate hover stations spaced 0.54 nm (1 km) apart from each other. Therefore, *Elysium* is required to operate in hover for nearly the entire duration of the mission. Consequently, hover efficiency is a paramount requirement for completing this mission effectively. The design of a VTOL hovering machine is unique, and a large number of possible configurations were considered before choosing *Elysium's* twin rotor design, which demonstrated the capability to meet all the requirements presented by the RFP for the minimal gross take-off weight.

The hover stations are defined as 65.6 ft (20 m) radius spheres that are separated by a minimum distance of 0.54 nm (1 km) from one another, where the position is defined with respect to each sphere's centroid. The RFP specifies a zero ground speed hover condition, and stipulates that wind speeds must be less than 16.4 ft/s (5 m/s) for the flight regime to be considered hover, independent of the true ground speed. This rule is interpreted as a deterrence to any solution claiming a constant local wind velocity with the goal of power savings, and not as a rule that the vehicle will operate in a location that will never see wind gusts above the stated limit.

Furthermore, the RFP does not specify details about the mission profile, such as atmospheric conditions, altitude, forward flight speed, or location. Therefore, a sizing mission was chosen for *Elysium* while satisfying simultaneously the RFP requirements and those imposed upon in as a technology demonstrator. The sizing mission was chosen to be a particularly demanding mission, so that *Elysium* would be capable of broader variety of possible missions. Additionally, an ideal mission was determined, where maximum endurance could be attained with a specific set of optimistic flight conditions, outlined in Section 19.

3.1 Flight Conditions

As a technology demonstrator, *Elysium's* design was not diluted by the need to design for exceptional weather conditions. For an experimental technology demonstrator, flight test personnel have the option to select test days with favorable weather for flying. Although the permitted flight conditions limit flight testing, they are not the ultimate limits of *Elysium* and in practice *Elysium* could successfully complete its mission in far more adverse weather conditions. The

permitted weather conditions for flight testing of *Elysium* include:

- Wind speeds less than 20 knots (33.8 ft/s, 0.3 m/s)

- Turbulence no greater than intermittent light turbulence as defined by in the FAA Aeronautical Information Manual (Table 7-1-10 in Section 7-1-23)

- Temperature less than ISA+10°C at altitude

- Precipitation of light rain, defined as a maximum of 0.10 inches per hour (no hail or snow)

- No lightning or thunder

- No possibility of blade icing

These levels were chosen by inspecting the average weather for the year of 2016–2017 in five US cities: (1) College Park, MD, (2) Tuscon, AZ, (3) Chicago, IL, (4) West Palm Beach, FL, and (5) Fairbanks, AK, as shown in Fig. 3.1(a). Daily METAR (Meteorological Aerodrome Report) data of average and maximum, temperature, wind speed, and precipitation was analyzed for determining these weather conditions. From this data and the stated allowable conditions, *Elysium* would be permitted to flight test an average of 172 days, 47%, out of the year in

Location	Unfavorable weather conditions					Available Flight Testing Days (percentage of year)	
	Icing	Wind (> 20 knots)	Temperature (> ISA + 10⁰C)	Rain (> 10 inches)	Total days		
West Palm Beach, FL	0	93	168	182	265	100	27%
Chicago, IL	50	121	45	164	240	125	34%
College Park, MD	21	20	67	126	198	167	46%
Fairbanks, AK	164	9	2	168	282	83	23%
Tuscon, AZ	0	42	171	81	221	144	39%

(a) Weather conditions for a calender year at five representative cities
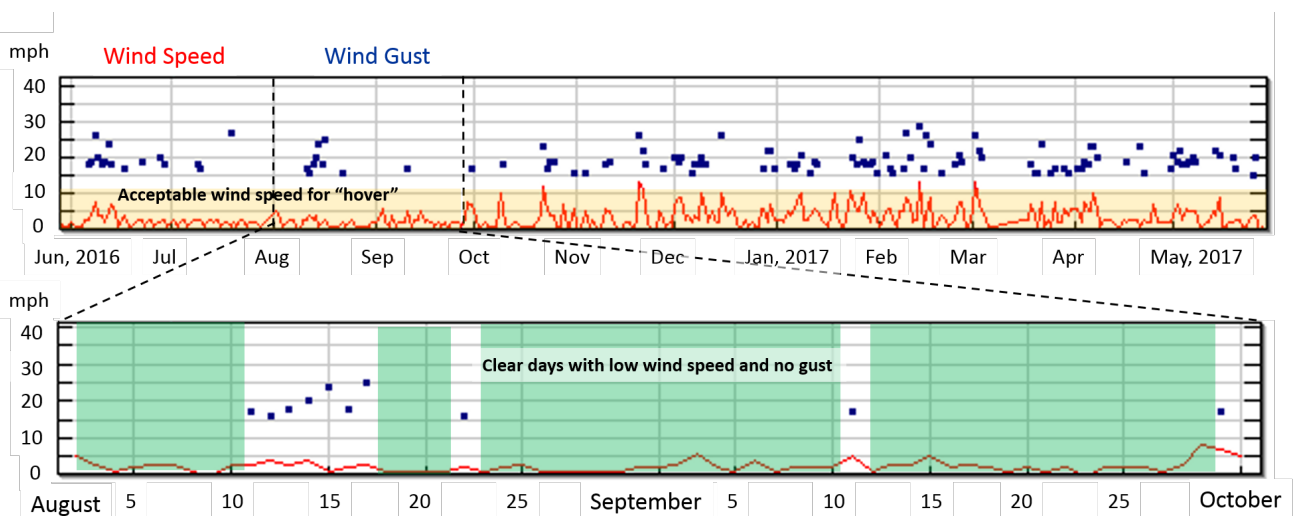
(b) Wind and gust weather data in College Park, MD

FIGURE 3.1: Weather data for a calender year at five cities in the United States with focus on the wind conditions at College Park, MD.

2016 for the five cities. As a technology demonstrator, *Elysium* was not designed for operation in extreme weather conditions. However, the chosen conditions do not limit *Elysium* from operating as a typical helicopter in a normal helicopter environment. Figure 3.1(b) shows the maximum wind and gust profile in College Park, MD, over the 2016–2017 year. For most of the year, the average wind speed is below the limits for "hover" as specified in the RFP. The frequency of high levels of gust is low and as shown in the expanded view in Fig. 3.1(b), there are many days that are highly favourable for flight testing of *Elysium*.

3.2 Sizing Mission

Figure 3.2 illustrates *Elysium's* sizing mission. The sizing mission consists of hovering for 24 hours at 1,500 ft (457m), ISA + 10°C. The mission begins with a 5 minute idle at mean sea level (ISA), then *Elysium* performs a vertical climb to the hover altitude at a rate of 150 ft/min (48 m/s), cruises a distance of 0.54 nm (1 km) at a forward velocity of 20 knots (37 km/h) to reach the first hover station, and hovers for a total of 8 hours at that station. The cruise and hover segments are then repeated for the final two hover stations. Finally, *Elysium* vertically descends at a rate of 150 ft/min (48 m/s) and ends with a reserve of 45 minutes in hover.

The details of each segment are detailed as follows

1. **Pre-flight:** After all pre-flight check have been completed, *Elysium* will start up, perform system checks, and idle on the ground for 5 minutes. The idle period allows for the engine to warm up, and all on-board sensors to calibrate. The necessary communication links between *Elysium* and the ground station will be secured at this time before take-off.

2. **Take-off and Climb:** *Elysium* will increase power for take-off, and begin vertical climb immediately after take-off. The vertical climb will take approximately 10 minutes at 150 ft/min (48 m/min) to reach the hover altitude of 1,500 ft (457 m) ISA+10°C. Since this phase sizes the propulsion system, a relatively low vertical climb rate minimizes the power required and thus the overall weight of the vehicle. The onboard GPS will indicate when *Elysium* reaches the hover altitude and desired hover coordinates.

3. **Hover:** *Elysium* will transition from climb to hover and the hover timer will start as soon as *Elysium* reaches the pre-determined centroid location of the first hover station, and achieves zero ground velocity. *Elysium* will maintain hover, as defined in the RFP, through the onboard auto pilot to mitigate the effects of any gusts. Excluding any time when wind velocity is greater than 16.4 ft/s (5 m/s) and when the vehicle does not have zero ground velocity due to transients in gust corrections, the hover timer will run continuously until a hover duration of eight hours has been achieved. At this point, *Elysium* will transition to forward flight.

4. **Cruise:** *Elysium* will transition from hover to a forward flight cruise velocity of 20 knots (37 km/h). The flight path will be a direct line, with no altitude change, to the second predetermined hover location, a distance of 0.54 nm (1 km) from the first hover station. The cruise between hover stations will last 2 minutes, until *Elysium* reaches the next way point. The autopilot will navigate to the next hover station using the onboard GPS and avionics suite to avoid obstacles or collisions with any other aircraft.
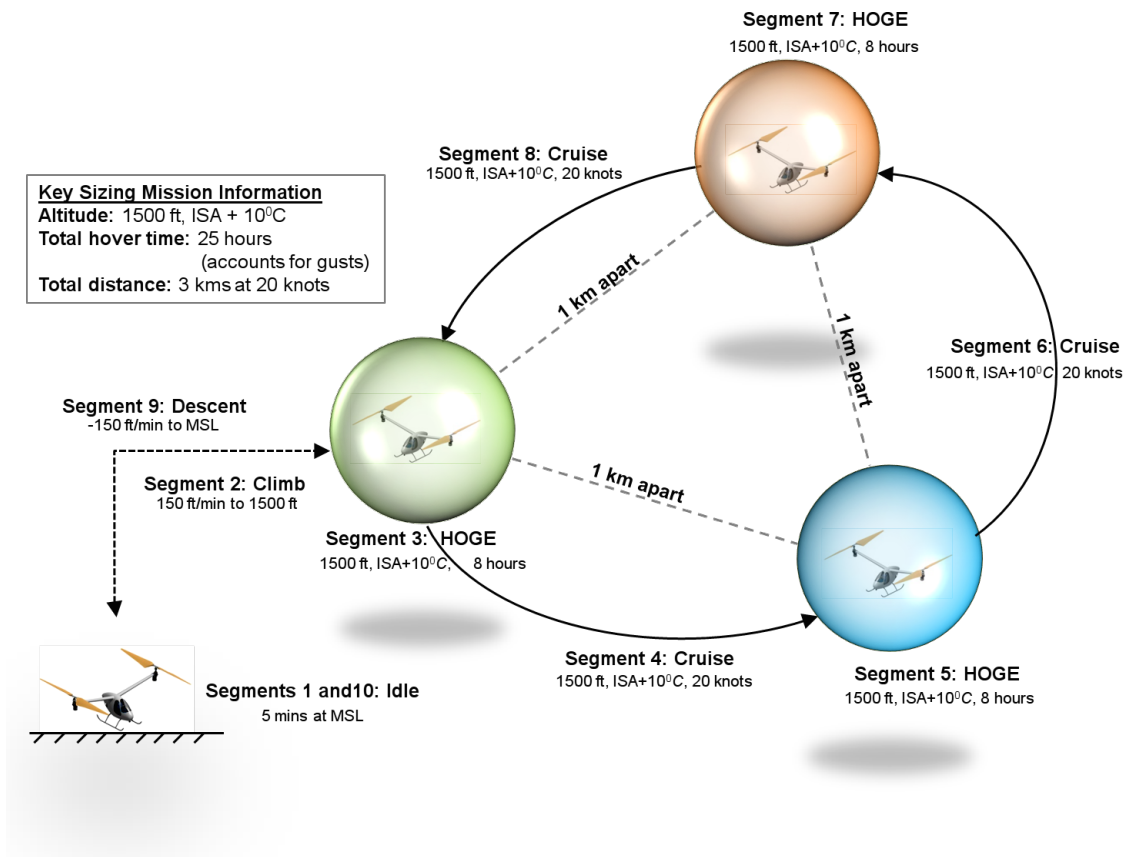
FIGURE 3.2: Schematic of the sizing mission for *Elysium*.

5. **Repeat Hover and Cruise:** At the GPS coordinates of the next hover station, *Elysium* will transition to hover and repeat steps (3) and (4) twice to achieve the RFP specified a total hover duration of 24 hours and range of 1.62 nm (3 km).

6. **Descent and Landing:** Upon completion of the final cruise segment, *Elysium* will decelerate, and enter a vertical descent of 150 ft/min (48 m/s). After 10 minutes, *Elysium* will reach the ground where the radar altimeter will provide precise distance date for an autonomous landing. The onboard cameras will guarantee a clear landing zone, for both the vehicle safety and any personnel or animals on the ground. Once *Elysium* has landed and before rotor slowing or engine shutdown, a full systems check will sweep all onboard systems to ensure correct operation and report any unusual behavior or need for maintenance checks.

3.3 Multi-Mission Capabilities

The RFP presents a 24 hour hover mission, but does not specify a specific application that fits this mission profile. There are many possible missions that would benefit from the long endurance, reliability, controllability, and size of *Elysium*.

- **Observation:** A common use of modern helicopters is to provide constant aerial surveillance of ground activity such as traffic, natural disasters, or other emergency situations. Current helicopters used for these mission types have very limited endurance capabilities

and need to be refueled or replaced with a new aircraft and crew every few hours. Blimps and lighter-than-air aircraft do not possess the controllability required for effectively conducting many of these missions, and higher altitude fixed-wing reconnaissance vehicles and satellites can be difficult to coordinate over a desired location and can have compromised imagery due to cloud cover or other atmospheric effects.

- **Communications:** A stationary and controllable aerial platform could be used as temporary communication arrays. In disaster areas, where local infrastructure has been destroyed or disabled, *Elysium* could hover over the effected area and quickly re-establish necessary communication links that would otherwise take significant manpower and effort to establish from the ground. For the military, *Elysium* could act as part of a forward staging area to establish communication and internet to support tactical operation in remote locations that would otherwise require much more complicated organization.

- **Survey Services:** Although not truly hover, *Elysium* would excel at long endurance missions requiring data collection and surveying while in low speed flight. Global imaging system mapping of terrain or atmospheric data collection would benefit from *Elysium's* 24 hour endurance capability and simultaneously increase productivity and reduce cost when compared to current helicopters.

- **Air Taxi:** The non-refueled multi-mission flexibility of *Elysium* could also potentially be employed for an urban air taxi service. In a downtown urban environment, *Elysium* could perform many individual missions in a single 16 hour work day, 6:00 am to 10:00 pm, to be serviced and refueled at night. Each vehicle would then be ready for a full day of passengers the next morning. Not needing to return to a refueling station during the operating day allows for a far greater number of passenger miles traveled per day, therefore increasing profits. Not needing to build a large network of refueling stations would also significantly cut infrastructure costs, one of the most significant market barriers of electric cars.

4 Configuration Selection

The AHS Design challenge requires that the vehicle be capable of hovering for 24 hours in three hover stations, each of which is a distance of 0.54 nm (1 km) apart, but does not specify details about the vehicle's operational use or any other mission requirements; therefore, many important design decisions are left to the designers' discretion. Consequently, there is an opportunity to make fundamental design decisions that can lead to effective and innovative solutions.

The Analytical Hierarchy Process (AHP) was used to determine the customer needs and provide a basis for comparison between configurations. From a broad range of needs, the eight most important criteria are ranked based on their order of importance to develop the voice of the customer. A House of Quality (HoQ) matrix was developed to identify customer requirements and determine the key engineering design factors to satisfy the customers' needs. With a technical basis to compare each configuration, a Pugh decision matrix ranked the top 9 aircraft configurations. The down-selection process began with the assessment of the Pugh matrix ranking, but additional analysis was necessary to reach a final vehicle configuration.

4.1 Voice of the Customer

4.1.1 Selection Criteria

As a technology demonstrator, *Elysium* needs to meet a set of criteria that is not necessarily required for a production aircraft. From analysis of the RFP and design requirements of a technology demonstrator, 30 customer criteria were identified and defined. This list was evaluated on a scale from 'Barely Applicable' to 'Absolutely Necessary'. The top eight criteria were then prioritized more vigorously in an Analytical Hierarchy Process (AHP) matrix to use in configuration comparisons. These top criteria are defined below, in no specific order.

- **Hover Efficiency:** The maximum possible Power Loading, thrust divided by power (T/P), integrated over the entire mission length.

- **Innovation:** Novel or original technical design at the configuration level.

- **Reliability:** Low probability of failure, classified as inability to complete the mission, under normal operating conditions.

- **Disturbance Rejection:** Ability to maintain or recover a given flight condition after experiencing a wind gust.

- **Technology Maturity:** Assessment of initial faults or inherent problems that necessitate further development. Technology maturity is quantified by the United States Department of Defense (DoD) Technology Readiness Levels (TRLs).

- **Cost:** Total cost, in terms of monetary, man hours, and environmental impact, to design develop, build, and maintain the configuration.

- **Durability:** Ability to withstand abnormally rough atmospheric or environmental conditions; a measure of robustness.

- **Safety:** The safety of personnel on the ground during the entire mission and in the case of any failures.

4.1.2 Analytical Hierarchy Process

Having identified customer criteria, the Analytical Hierarchy Process (AHP) was used to objectively compare the relative importance of each criteria to the specified mission. Knowing the most critical aspects of a 24 hour hover mission is necessary to properly select a configuration. The AHP technique uses pair-wise comparisons between criteria. In the AHP matrix, a given criteria in the left-most column is independently compared against each criteria across the top row. A value of greater than one (> 1.0) means the left-column criteria is more important than the top-row criteria. Similarly, a value of less than one (< 1.0) implies the opposite.

The AHP matrix, Fig. 4.1, shows the criteria ranking and thereby the importance of each criteria for the 24 hour mission. It should be noted that these eight criteria are all important for a successful final design, and the prioritization through the AHP matrix is viewed as a relative metric.

The AHP values within each column are normalized by the column sum, then averaged by row. This gives a Normalized Priority for each row, which can be ordered to provide the final ranking.
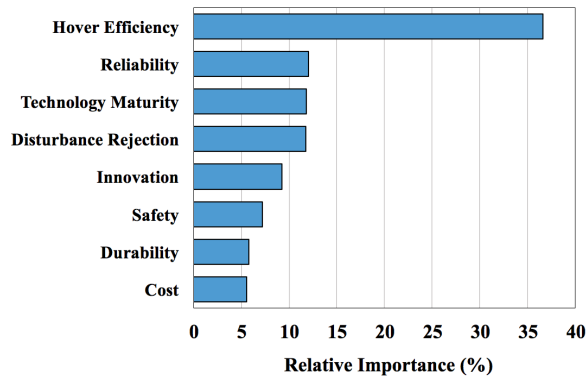
FIGURE 4.1: Relative ranking of customer criteria through the Analytical Hierarchy Process (AHP).

The ranking shows that hover efficiency is by far the most important customer criteria, followed by reliability, technology maturity, and disturbance rejection. It is without surprise that hover efficiency is so highly ranked, but the following three criteria are more illuminating. Innovation, safety, durability, and cost are key to program success, but are relatively less important compared to the top four criteria.

TABLE 4.1: Selection Criteria Weight from Analytical Hierarchy Process.

	Hover Efficiency	Innovation	Reliability	Disturbance Rejection	Technology Maturity	Cost	Durability	Safety	Normalized Priority	Rank
Hover Efficiency	**1.00**	5.00	3.00	5.00	5.00	5.00	5.00	5.00	**0.366**	**1**
Innovation	0.20	**1.00**	1.00	1.00	1.00	1.00	3.00	1.00	**0.093**	**5**
Reliability	0.33	1.00	**1.00**	1.00	3.00	3.00	1.00	1.00	**0.120**	**2**
Disturbance Rejection	0.20	1.00	1.00	**1.00**	0.33	3.00	3.00	3.00	**0.118**	**4**
Technology Maturity	0.20	1.00	0.33	1.00	**1.00**	3.00	3.00	1.00	**0.118**	**3**
Cost	0.20	1.00	0.33	0.33	0.33	**1.00**	1.00	1.00	**0.055**	**8**
Durability	0.20	0.33	0.33	0.33	0.33	1.00	**1.00**	1.00	**0.048**	**7**
Safety	0.20	1.00	1.00	0.33	1.00	1.00	1.00	**1.00**	**0.072**	**6**

4.2 Considered Configurations

Having established a basis to compare configurations, the next step is identifying and exploring possible configurations for the vehicle design. A large variety of vehicle configurations were considered for this mission, but many were quickly rejected because of fundamental drawbacks in terms of the customer criteria established by the AHP in Section 4.1.2, most importantly hover performance. Some of the possible choices are highlighted and defined below:

- **Single Main Rotor:** The single main rotor (SMR) is a proven configuration with very high technology readiness levels. SMRs possess low disk loadings, greater reliability, and relatively low mechanical complexity. With only a single main rotor, this configuration necessitates an anti-torque device for yaw stability and control. The incorporation of anti-torque with a tail rotor requires additional power, which does not contribute towards lift or thrust. Because the single main rotor configuration carries additional power requirements, it may not be the optimal choice. Additional analysis in configuration sizing to make a conclusive decision is detailed in Section 5.4.
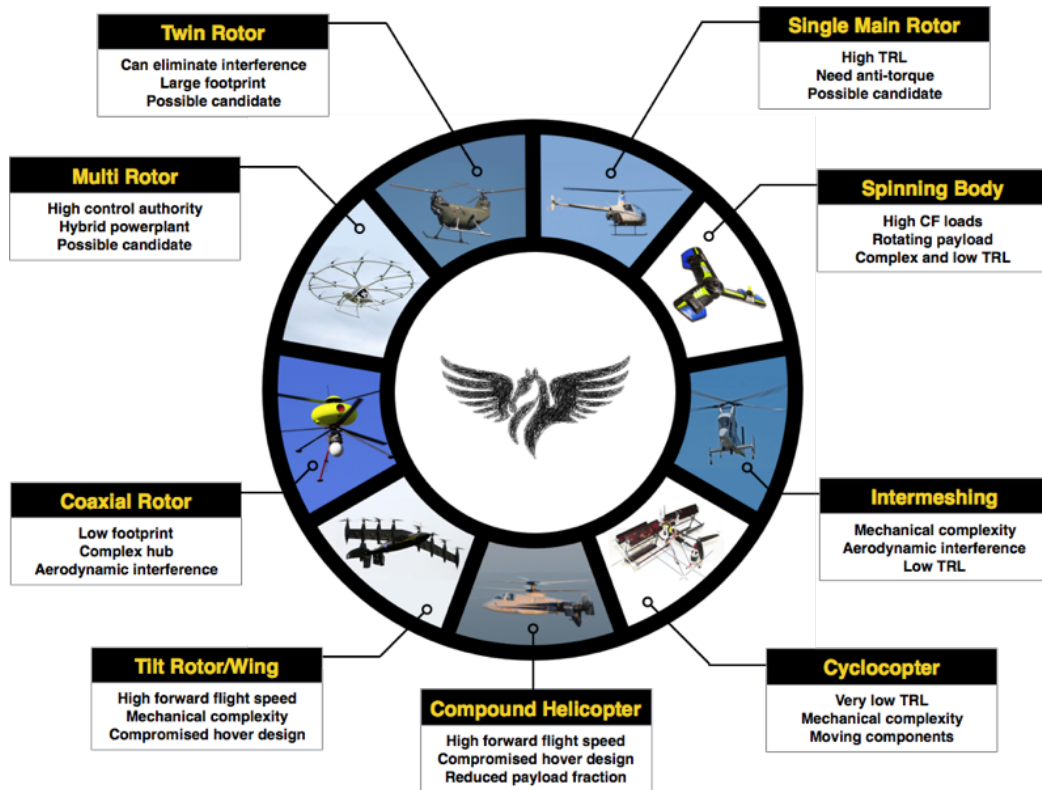
FIGURE 4.2: Notional representations of configurations considered in the selection process.

- **Coaxial Rotor:** (Two contra-rotating rotors) A coaxial rotor configuration allows for greater total thrust for a given vehicle footprint, which is of great advantage for vehicles that need to operate in confined spaces, such as onboard ships or urban canyons. The coaxial rotor suffers from interference effects because the lower rotor operates in the wake of the upper rotor; this interference is described in greater detail in Section 5.4. For this mission, hover performance is the driving design parameter. The coaxial rotor has the aerodynamic disadvantage of rotor interference, but the structural advantage of a smaller footprint and therefore minimal structural weight. Additionally, coaxial rotors require a complex hub, where the upper rotor controls must pass through the lower rotor. The mechanical complexity introduces unnecessary reliability and durability issues. A conclusive decision on the coaxial rotor cannot be made without additional analysis into the configuration sizing.

- **Twin Rotor:** (Tandem and side-by-side) The twin rotor design has two equal sized rotors used for lift, thrust, and control. An example of the twin rotor is the Boeing CH-47 Chinook. While the Chinook flies with a front and back orientation, here the twin rotor may also be defined as a side-by-side configuration. The advantage of a side-by-side configuration is that, in hover, all power is going towards lift, and not to yaw control, as in a single main rotor. The twin configuration can have overlapping or non-overlapping rotors. In the non-overlapping case, there is no interference loss between the rotors, which is an advantage over coaxial or inter-meshing rotor configurations. The twin configuration appears to exhibit high hover endurance characteristics, but additional analysis is necessary to make a conclusive decision; this is detailed in Section 5.4.

- **Multi-rotor:** (More than two rotors) Multi-rotor VTOL aircraft are defined as using a large number of rotors to produce thrust and lift, and achieve control. There are countless possible combinations of rotor number, size, and layout. A common multi-rotor configuration is the quad-rotor with four rotors that typically use an electric propulsion system and differential RPM for control. The multi-rotor configuration is not defined by this single vehicle and was considered independently from control scheme or power train. The multi-rotor configuration needs support structure to connect each rotor. Because there are no established weight models in AFDD/NDARC for multi-rotor configurations, a weight model was developed to size a multi-rotor aircraft for the RFP mission given a number of rotors and rotor radius, and a detailed explanation of this model is given in Section 5.3. Additional analysis in configuration sizing to make a conclusive decision is therefore necessary and detailed in Section 5.4.

- **Compound Helicopter:** Compound rotorcraft can be thrust augmented, lift augmented or thrust-and-lift augmented, and are designed to primarily expand the vehicle's forward flight envelope. The presence of lift and/or thrust augmentation helps offload the rotor, which alleviates the constraints of conventional helicopter designs allowing for increased efficiency in forward flight. Compound helicopters have greater capability than conventional helicopters in terms of forward flight maximum speed and efficiency, but provide no advantage in hover, which is the most important metric for a 24 hour hover mission. Compound helicopters suffer from a reduced payload fraction, which is a consequence of the increased complexity required for the augmentation systems. For these reasons, compound helicopters, of any type, were eliminated from configuration.

- **Inter-meshing:** Inter-meshing rotors allow for greater thrust than a single main rotor and a smaller footprint than a tandem configuration, but interference between the two main rotors degrades hover performance and increased mechanical complexity causes reliability issues. The mechanical complexity of the dual hub with a connecting shaft is an unnecessary feature for a hover mission. The inter-meshing rotor inherently has degraded hover performance over two isolated rotors and offers no advantages for a hover mission, so can therefore can be eliminated from consideration because of the importance of hover performance.

- **Spinning Body:** There are many possible designs of a spinning body rotorcraft, and many were considered to satisfy this mission. Some concepts included a spinning wing with either tip jets or tip propellers, coaxial rotors with the body spinning along with one of the rotors, and fastening two fixed wing aircraft to fly in a circular pattern to keep the centroid stationary. The myriad of concepts for this configuration were eliminated from consideration because of the inherent issues, such as the need for additional mechanical complexity to keep the payload non-rotating, the reduced reliability at high centrifugal loadings and low technology readiness levels.

- **Tilt-rotor/wing:** Tilt-rotor/wing is defined where the rotors operate in both edgewise and axial modes. The configuration is capable of VTOL in edgewise mode and transitions to axial mode for efficient high speed forward flight. Tilt-rotor/wing aircraft require additional hardware and machinery to accomplish this transition. The advantages in forward flight are achieved at a sacrifice to hover performance, because of the high disk loadings and additional weight due to the mechanically complex tilting mechanisms. The additional weight and mechanical complexity of the tilting mechanism offer no benefits in terms of

hover efficiency and negatively impact the configuration's reliability. Tilt-rotor/wing configurations can be eliminated because of their focus on forward flight efficiency at a cost to hover efficiency, while offering no unique advantages for the 24 hour hover mission.

- **Cyclocopter:** The cyclocopter configuration is defined as a rotorcraft that employs cycloidal rotors to achieve lift, thrust, and control. There are a couple of proven cyclocopter configurations: one has two cycloidal rotors and a conventional rotor for pitch control, and another has four cycloidal rotors for lift, thrust, and all controls. The cycloidal rotor has been shown to have higher power loading for a given disk loading than a conventional vertical rotation axis rotor. Unfortunately, the mechanical complexity and high number of moving components make the cyclocopter configuration susceptible to failure and introduce reliability issues. Micro aerial vehicle scale cyclocopters have been proven at the university research level, but cyclocopters at the size necessary for a 176.4 lb payload have not been successfully demonstrated thus far. Large cyclocopters have been shown to have issues with excessively large bending moment [2]. For these reasons, the cyclocopter configuration was eliminated.

4.3   Configuration Selection: Pugh Matrix

The customer criteria and their corresponding weightings from the AHP in Sec 4.1.2 were used to evaluate each of the identified possible configurations from Section 4.2 in a Pugh decision matrix. The Pugh matrix is shown in Table 4.2. The Pugh matrix identified two groups of configurations. The compound, intermeshing, spinning body, tilt-rotor/wing, and cyclocopter configurations were eliminated based on their low scoring in the Pugh matrix. The single main rotor, coaxial rotor, twin-rotor, and multi-rotor all received very similar scores in the Pugh matrix and could not be down-selected any further without additional analysis. As demonstrated by the rankings in the AHP matrix, hover efficiency is the most important factor in the down-selection process. Intuition or qualitative metrics are not sufficient to measure a configurations hover efficiency, as defined by mission integrated power loading, and thus a more qualitative comparison was deemed necessary. To this end, a sizing code was developed to "fly" each configuration through the mission profile and determine a preliminary hover efficiency in order to achieve a final selection. This sizing code assisted in determining the vehicle configuration in terms of the number of rotors and rotor positioning, providing quantitative results for the aerodynamic characteristics of each configuration.

TABLE 4.2: Pugh decision matrix shows the various configurations ranked against the weighted AHP customer criteria.

	Weights	SMR	Coax	Compound	Twin	Inter-meshing	Spinning Body	Multi-rotor	Tilt-rotor/ Tilt-wing	Cyclocopter
Hover Efficiency	0.366	0	0	-1	1	-1	-2	1	-1	1
Reliability	0.120	0	-1	-1	0	0	-1	1	-1	-3
Technology Maturity	0.118	0	0	-1	0	-1	-3	0	-1	-3
Disturbance Rejection	0.118	0	1	1	1	1	-1	-1	0	-1
Innovation	0.093	0	1	2	1	1	-3	1	1	2
Safety	0.072	0	1	-1	1	1	-2	-1	1	-2
Durability	0.058	0	1	-1	1	1	-1	2	-1	-3
Cost	0.055	0	1	-1	0	0	-1	0	-1	-2
Score		0.0000	0.2755	-0.4861	0.7063	-0.1437	-1.8597	0.5049	-0.5526	-0.7088

Key:
1 - No Relation
2 - Low Relation
3 - High Relation

FIGURE 4.3: The House of Quality to determine the Voice of the Customer.

Requirement	Weights (1-5)	Empty Weight Fraction	Power Loading	Disk Loading	Blade Loading (Ct/sigma)	Tip Speed	Autorotative Index	Hub Drag	Velocity Best Range	Blade Aerodynamics	Flat Plate Area	Blade Tip Design	Blade Structures	Hub Type	Engine SFC	Installed Power	Engine Power to Weight	Drivetrain Design	Fuel Storage	Primary Control Actuators	Avionics	Material Selection	Landing Gear Configuration	Vibration Suppression Devices	Payload Access	Fuselage Modularity	Fuselage Vertical Download	Cockpit Design	Redundancy	HUMS	Crashworthy Structure
Operational Requirements																															
Hover for 24 Hours	5	3	3	3	3	3	1	1	1	3	1	3	2	2	3	2	3	3	3	1	1	3	2	1	1	1	3	1	1	1	1
Carry payload of 176.4 lb (80kg)	5	3	3	3	3	2	1	1	1	3	3	3	2	2	3	2	3	3	2	1	1	3	3	3	3	3	1	1	3	1	1
Gust Mitigation	5	1	1	3	3	3	1	1	1	3	2	2	2	3	1	1	1	1	1	3	3	2	1	1	1	1	1	1	1	1	1
Range	4	3	3	3	3	3	1	3	3	3	3	3	2	3	3	1	3	2	2	1	3	2	1	1	1	1	1	1	1	1	1
Autonomy	5	1	1	2	1	2	2	1	1	1	1	1	1	1	1	1	1	1	1	2	3	1	2	2	1	1	1	1	2	3	3	1
Control Response	5	1	1	3	3	3	1	1	1	1	1	1	2	3	1	1	1	1	1	3	3	2	1	1	1	1	1	1	3	1	1
Max Flight Speed	5	1	1	2	3	1	1	3	3	3	3	3	3	3	1	3	3	1	1	2	1	3	2	3	1	1	1	1	1	1	1
Cruise Speed	4	1	3	2	3	1	1	3	3	3	3	3	3	3	1	2	3	1	1	1	1	2	2	3	1	1	1	2	1	1	1
Max Rate of Climb	4	1	3	2	3	2	1	3	1	3	2	2	1	1	1	3	3	1	1	1	1	2	1	1	1	1	1	2	1	1	1
G-limit/Accelerations	4	1	1	2	3	2	1	2	1	2	1	2	3	3	1	2	1	1	2	3	2	2	2	1	1	1	1	1	3	1	1
Multi-mission capable	5	2	2	2	2	1	2	1	2	2	1	1	2	2	1	2	1	1	2	2	3	1	2	2	2	3	1	2	3	1	1
Load/unload payload	4	1	1	1	1	1	1	1	1	1	1	1	1	1	1	1	1	1	1	1	1	1	1	1	3	3	1	3	1	1	1
Ability to upgrade technology	5	2	1	1	1	1	1	1	1	1	1	1	1	1	3	2	3	3	2	3	1	1	1	1	1	3	1	3	3	3	1
Design Requirements																															
Reliability	5	1	1	1	1	1	1	1	1	1	1	1	3	2	1	1	1	3	3	3	3	3	2	3	1	1	1	3	3	3	3
Noise	5	1	1	2	2	3	1	1	1	3	1	3	1	1	1	1	1	3	1	1	1	1	1	1	1	1	1	1	1	1	1
Vibration Levels	5	1	1	1	1	3	1	1	1	2	2	3	3	3	1	1	1	3	1	1	1	3	1	3	1	1	1	3	2	1	1
Platform/Modularity	5	1	1	1	1	1	1	1	1	1	1	1	1	1	1	1	1	3	2	2	3	2	2	1	3	1	1	3	3	2	2
Pilot Workload	5	1	1	1	1	1	3	1	1	1	1	1	1	2	1	1	1	1	3	3	1	1	1	2	1	2	1	3	3	2	1
Inter-changeability of Parts	4	1	1	1	1	1	1	1	1	1	1	1	1	3	1	1	1	3	3	3	3	2	3	1	1	1	1	3	1	1	1
Aesthetics	5	1	1	1	1	1	1	1	1	2	1	1	2	2	1	1	1	1	1	1	1	2	3	1	2	3	1	2	1	1	1
Landing Pad Independence	5	1	1	3	1	1	1	1	1	1	1	1	1	1	1	1	1	1	1	3	1	1	3	1	2	3	1	3	2	1	1
Cost & Development																															
Baseline Vehicle Selling Price	3	2	1	1	1	1	1	1	1	1	1	1	2	2	2	2	3	3	3	3	3	2	3	1	1	2	1	3	3	3	3
Manufacturing Costs	3	2	2	1	1	1	1	1	1	2	1	1	3	3	1	1	1	3	3	3	3	2	3	2	2	2	1	3	3	2	3
Hourly operating Cost	4	1	3	3	1	3	1	2	2	2	2	1	3	3	2	3	2	3	3	2	2	1	2	1	1	1	1	2	2	2	1
Maintenance Costs	4	2	1	1	1	1	1	1	1	1	1	1	3	3	1	1	3	3	3	3	3	3	3	3	1	1	1	2	2	2	2
Total Life-cycle Costs	3	1	1	1	1	1	1	1	1	1	1	1	3	3	3	3	3	3	3	3	3	3	3	1	1	2	1	3	3	2	2
Hover Fuel Efficiency	5	3	3	3	3	3	1	1	1	3	1	3	1	1	3	1	3	3	1	3	2	1	1	1	1	3	1	1	1	1	1
Pollution	5	1	3	3	3	3	1	1	2	3	2	2	2	3	3	2	3	2	1	1	1	1	1	1	1	1	1	1	1	1	1
End of Life Recyclability	4	2	1	1	1	1	1	1	1	1	1	1	3	3	1	1	1	3	3	3	3	3	1	1	1	1	1	2	2	2	2
Safety																															
Autorotation Capability	4	1	1	1	2	3	3	1	1	1	1	1	3	3	1	1	1	1	3	3	1	3	1	1	1	1	1	1	1	3	3
Crashworthiness	5	1	1	1	1	2	1	1	1	1	1	1	3	3	1	1	1	3	3	3	3	3	3	1	2	2	1	3	1	1	3
Ground Safety	4	1	1	3	1	1	1	1	1	1	1	1	2	2	1	3	1	3	3	2	2	1	2	1	3	3	1	3	1	2	3
Survivability	5	1	1	2	2	2	3	1	1	1	1	1	2	2	1	2	1	3	3	3	3	1	1	1	1	1	1	3	3	1	3
Mean time between repairs/failures	4	1	1	1	1	2	1	1	1	1	1	1	1	3	2	2	1	3	3	3	2	3	1	3	1	1	1	2	3	3	3
Detectability	2	1	1	2	2	3	1	1	1	3	1	3	1	1	1	1	1	1	1	3	1	3	2	2	1	1	1	2	1	1	1
Raw Score		216	234	287	277	310	192	196	194	268	223	258	301	335	223	78	103	141	111	140	104	95	78	119	66	88	83	155	98	87	83
Rank		11	8	4	5	2	14	12	13	6	9	7	3	1	9	28	21	16	19	17	20	23	28	18	30	24	26	15	22	25	26

5 Initial Vehicle Sizing

An in-house sizing code was developed using momentum theory to model aerodynamics in hover, forward flight, climb, and descent. The Aero Flight Dynamics Directorate (AFDD) weight model [3] was used for for preliminary estimates of component empty weights. However, these empty weight models are based on historic data from full-scale helicopters and tiltrotors; therefore, their applicability to *Elysium's* weight class and for multi-rotor systems is questionable. For a more detailed analysis of structure weight specific to the *Elysium*, a custom 3D finite-element code was developed to provide accurate estimates of the size of the beams and support members for aircraft with more that one rotor; see Section 5.3 for details. The aerodynamics and structural weight algorithms were developed by the authors and are computed iteratively until convergence.

As shown in the left-hand column of the sizing algorithm schematic in Fig. 5.1, the inputs to the algorithm include both mission-specific parameters such as weather, mission profile, as well as vehicle-specific information for performance and geometry. In the aerodynamic analysis, the inputs are converted to dimensional rotor properties and each mission segment is marched
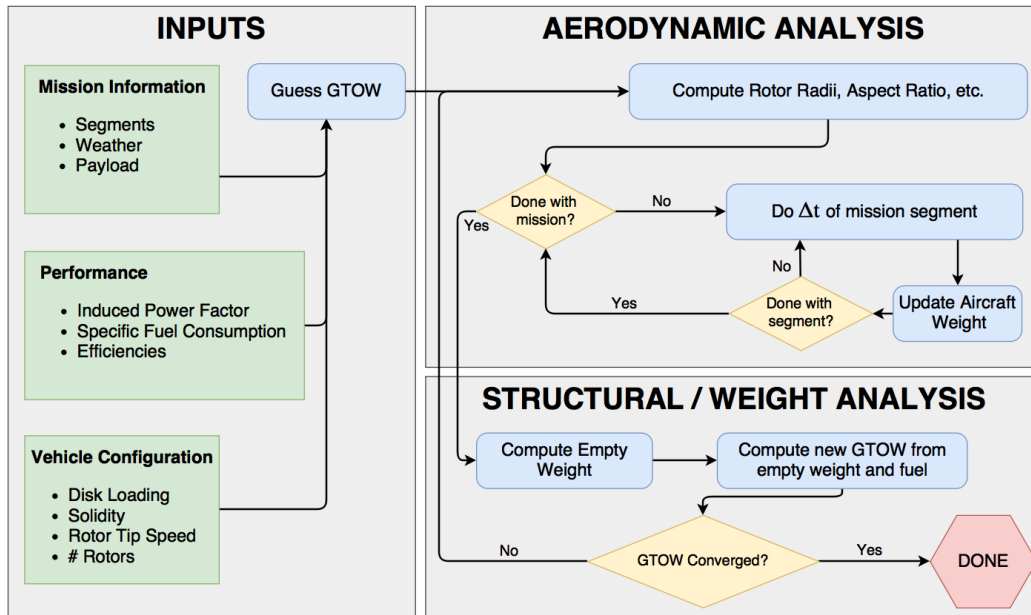
FIGURE 5.1: Team-developed flowchart showing sizing code convergence procedure

through with a small timestep to allow for variations in vehicle weight from fuel burn over time. This march (Δt) in time is especially important for a 24-hour mission where fuel weight is a substantial fraction of the aircraft weight. As noted, the developed structural and aerodynamic analyses are intricately coupled to the overall sizing algorithm.

5.1 Design Drivers

The inputs and outputs of the sizing code are a mathematical relationship that provide limited qualitative insight into one aircraft being better or more feasible than another. Restrictions on number of blades, disk loading, and rotor solidity have to be set to acceptable values when performing the sizing sweeps. Similarly, because the sizing code does not consider issues such as manufacturability or high angle of attack airfoil stall, such non-physical solutions should be filtered from the outputs. Other design drivers include looking at the benefit of lift-augmenting devices such as shrouds and weighing their benefits against weight penalties, which are explored in Section 5.1.4.

5.1.1 Blade Stall, Solidity, and Aspect Ratio

Rotor blade loading coefficient is defined as C_T/σ and is a measure of the non-dimensional lift on each blade. Through blade-element theory, a blade loading coefficient (C_T/σ) of 0.16 in hover can be directly related to the approximate stall region for a representative airfoil [1]. Considering that *Elysium* is not designed for high forward flight speed or complex maneuvers, the chosen maximum C_T/σ was 0.12, which provides sufficient stall margin for basic maneuvers and control authority against gusts.

For a rotor with constant tip speed, the profile power ($\sigma C_{d0}/8 \; \rho A V_{\text{tip}}^3$) remains constant over the entire mission. The weight of the aircraft, and consequently the induced power, is lower towards the end of the mission; thus, the profile power accounts for a significant fraction of the total power. It is therefore desirable to have a low rotor solidity σ to limit the profile power, which is
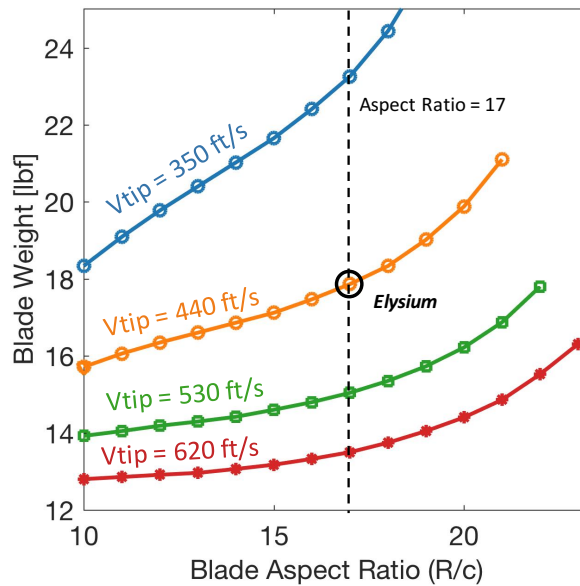
FIGURE 5.2: Variation of blade weight with tip speed and aspect ratio

related to the aspect ratio (via the solidity) of the rotor. *Elysium* was designed for a tip-speed of 440 ft/s (134 m/s) at take-off, described in more detail in Sections 5.1.3 and 5.4. This low tip speed limits centrifugal stiffening, resulting in the need for thicker, stiffer blade spars. Figure 5.2 shows the result of preliminary analysis into blade weight and blade aspect ratios for various tip speeds. For the selected tip speed of 440 ft/s (134 m/s), aspect ratios above 17 result in large changes in blade weight and, therefore, an aspect ratio of 17 was chosen as the maximum allowable limit for *Elysium*.

5.1.2 Number of Blades

Analysis of the effect of two and three blades on hover performance was conducted by analyzing a SMR in hover for 24 hours. The SMR was chosen as a baseline case and any aerodynamic differences between number of blades would extend to twin or other multi-rotor concepts.

Figure 5.3 shows required gross take-off weight vs blade loading for a two-bladed rotor of various solidity at different specified values of disk loading. Gross take-off weight should be minimized to reduce overall vehicle size and conserve fuel. The blade loading coefficient is a measure of blade stall and is limited to 0.12 to provide sufficient stall margin. As solidity decreases, blade profile drag is reduced resulting in a smaller vehicle carrying less fuel. Figure 5.3 shows the results for a two-bladed rotor. However, the trend for a three-bladed rotor is similar. Table 5.1 shows the comparison between the aspect ratios of two and three-bladed rotors of the same solidity. Even though two rotors may have the same solidity and therefore comparable profile drag, the high aspect ratios of the three-bladed rotor are more flexible and therefore more susceptible to aeroelastic issues. The limiting aspect ratio of 17 imposed in the previous subsection clearly motivates the use of two instead of three-blades for the *Elysium*.

5.1.3 Variable Radius and Tip Speed

When a large portion of the GTOW of an aircraft is fuel, the aircraft will operate in very different flight regimes with a full or empty fuel tank. Figures 5.4(a) and 5.4(b) show dimensional thrust for given rotor radii and rotor RPM respectively for an isolated rotor operating in the same
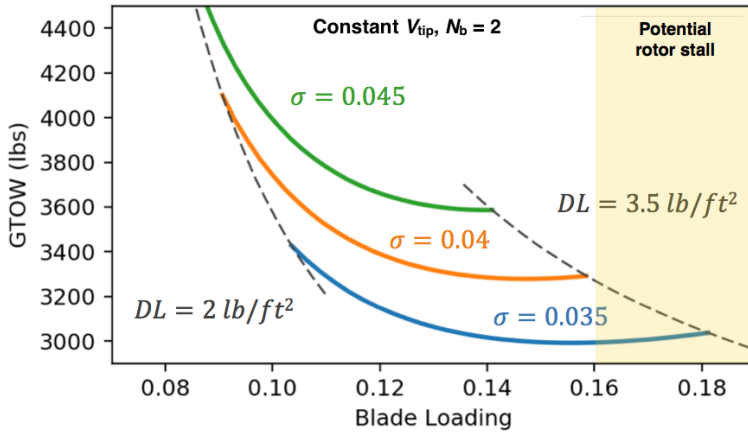
FIGURE 5.3: Variation of take-off weight with solidity and disk loading for a 2-bladed rotor.

TABLE 5.1: Solidity and aspect ratio for 2- and 3-blade rotors.

	Aspect Ratio	
	2 Blades	3 Blades
$\sigma = 0.035$	18.19	27.28
$\sigma = 0.040$	15.92	23.87
$\sigma = 0.045$	14.15	21.22

design space as the *Elysium*. From the analysis of RFP plots (Figure 2.1 in Section 2), it was shown that practical empty weight fractions at low disk loadings can be achieved if blade loading coefficient is held constant, thereby ensuring that FM is constant.

A constant blade loading line at $C_T/\sigma = 0.1$, slightly lower than the value chosen for the *Elysium*, is shown to highlight power savings that can be achieved by maintaining a constant blade loading over time. Operating at a constant C_T/σ also represents the optimal case for maintaining the same inflow distribution and hover performance for a selected blade geometry. Without a constant blade loading, the rotor would only operate at its ideal designed hover flight condition for a limited time over the 24-hour mission. Staying along a constant C_T/σ line by varying rotor RPM, shown in Fig. 5.4(b), results in 4× power savings for the shown case compared to the same variation made using variable rotor radius, Fig. 5.4(a). The benefit of variable RPM over variable radius is further highlighted by the mechanical complexity of a system that would allow variable solidity over time.
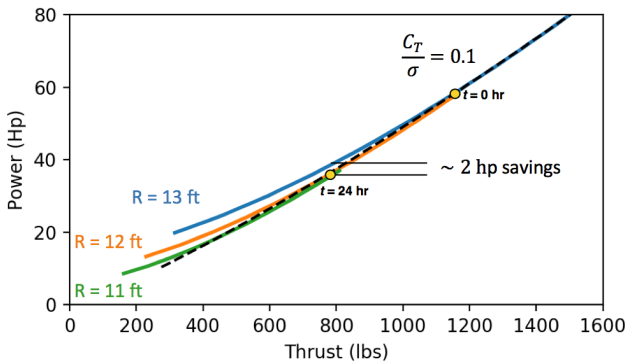
(a) Thrust variation with rotor radius, $\Omega = 318 RPM$
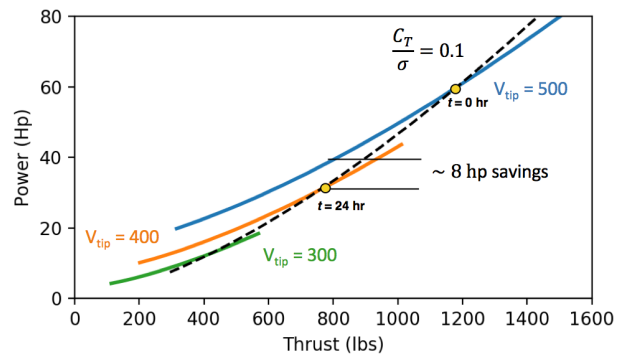
(b) Thrust variation with RPM, $R = 12ft$ (3.65m)

FIGURE 5.4: Comparison of design space for variable radius and variable RPM rotors

Figure 5.4(b) also provides insight into the effect of tip speed on hover performance. Vehicle weight and fuel consumption is directly related to the engine power through specific fuel consumption and engine power-to-weight ratios. For the same required thrust, a low tip speed with

high blade loading requires less power than a high tip speed with low blade loading. A well designed hovering rotor would therefore operate at the design blade loading, 0.12 for this mission, and minimum possible tip-speed satisfying the required thrust.

5.1.4 Shrouded Rotor

A "shrouded rotor" is a conventional rotor surrounded by a cylindrical shroud or duct used with the intention of enhancing the hovering performance. The shroud improves rotor performance by restricting the natural contraction of the rotor wake resulting in a decrease in the induced power. Theoretically, a shrouded rotor can consume 29% less power while producing the same amount of thrust [4]. Furthermore, a shroud enhances safety by protecting ground crew and blades from damage. However, there are also several shortcomings of the shrouded rotor. First, because of the fixed geometry of the shroud, rotor performance can be sub-optimal or even worse than the open rotor in forward flight (edgewise flow) because of flow separation over the duct resulting in large pitching moments and vibration along with an increase in power. In addition, the shroud adds weight to the system, which can overshadow the performance benefit from the shroud. Equation 5.1 shows the maximum allowable weight of a shroud based on momentum theory [5]

$$W_{\text{shroud}} < ((2\sigma_d)^{1/3} - 1)W_{\text{us}} \tag{5.1}$$

where W_{shroud} is the weight of the shroud, σ_d is an area ratio of diffuser exit to shroud throat (D_t), and W_{us} is the weight of an unshrouded vehicle. If *Elysium* were to be equipped with a shroud, the weight of one shroud should be less than 235.79 *lb* (=470.98/2) to reap the performance benefits from the shroud.
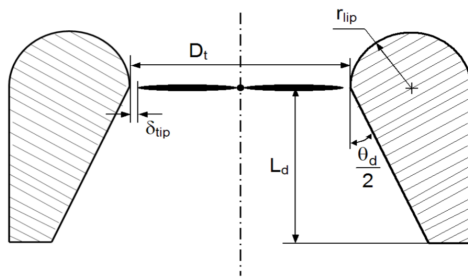
(a) Schematic of shroud. Reproduced from [4].
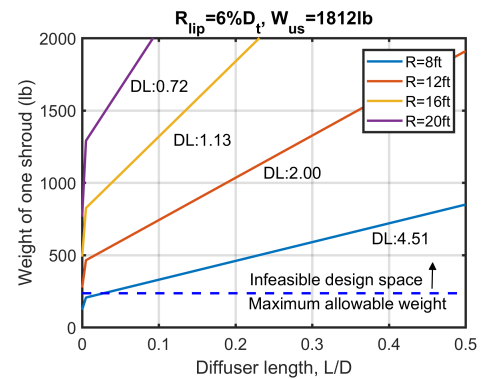
(b) Weight estimation of one shroud for different geometry

FIGURE 5.5: Weight estimation of one shroud for twin rotor.

Figure 5.5 shows the weight estimation of one shroud with an area ratio of 1 for different diffuser lengths. The outer structure of the shroud has thickness of 0.087 inches, consisting of 10 layers of carbon fabric laminates, and its internal structure is hollow. For simplicity, the rotor tip clearance (δ_t) is assumed zero, and the lip radius (r_{lip}) is 6% of the rotor diameter (D_t). In the figure, the maximum allowable weight of the shroud was added based on the Eq. 5.1 for the unshrouded twin rotor of 1812 lb. Also, the disk loading of the unshrouded vehicle was shown for the corresponding rotor diameter. Figure 5.5 shows that the shroud has performance benefits only when the rotor diameter is less than 8 ft for twin rotor. However, this rotor radius does not

meet the requirement of the sizing code, which has a much lower disk loading (1.9) as shown in Section 5.4. For this reason, the shroud was excluded in the present study.

5.2 Propulsion System

The RFP states that step-changes in propulsion technology are required to push the state-of-the-art and achieve a 24-hr hover mission. As a result, a large number of possible propulsion architectures were initially considered prior to final sizing including electric, chemical, and nuclear architectures, as shown in Fig. 5.6.

Figure 5.6 shows the architectures that were considered for the powerplant design of *Elysium*.
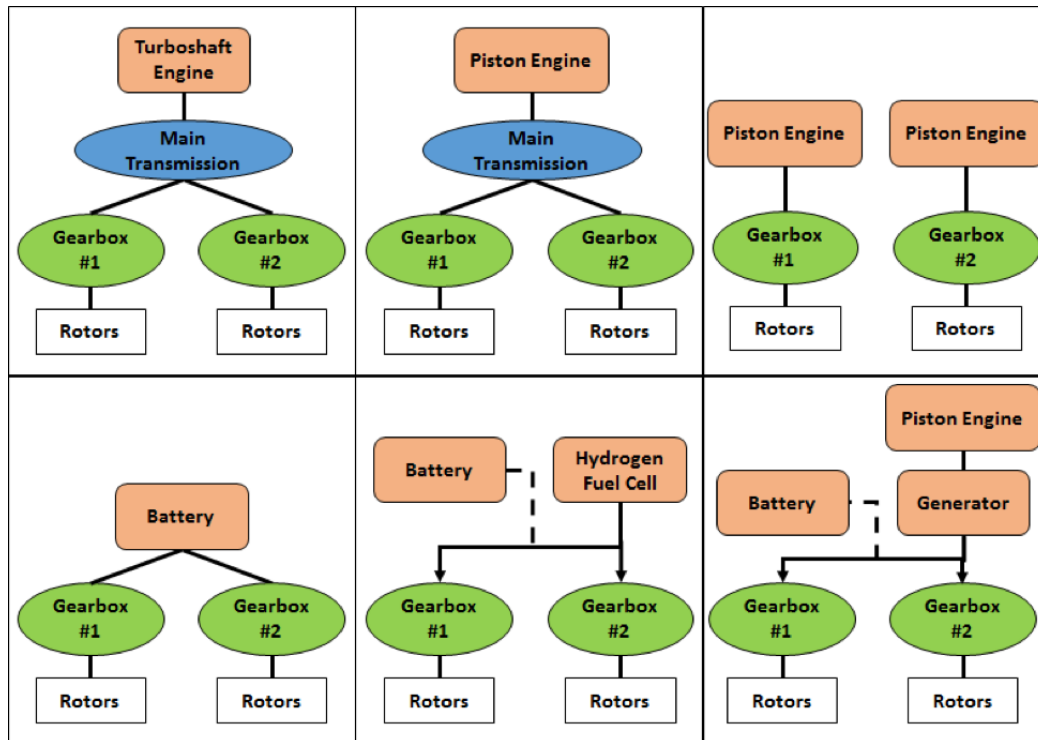
FIGURE 5.6: The gamut of powerplant options for *Elysium*.

5.2.1 Power Sources

The power sources that were examined are photovoltaic (PV) panels and paints, batteries, fuel cells, and compact nuclear reactors.

Solar energy: The conversion of solar energy into electricity is dependent on the availability of direct sunlight. Solar energy requires 500 ft^2 of PV surface to generate 5 kW power for 12 hours, assuming that the solar angle of incidence is normal to the surface. Given this best case scenario, it becomes apparent that use of solar energy as a primary power source at the expectedly large power requirements quickly becomes unattainable, not only due to the required surface area but also in terms of structural weight to support the PV surface. Therefore, the use of solar power as a sole source for *Elysium* was not considered.

Batteries: Modern electric and hybrid-electric vehicles typically use lead-acid, nickel, lithium-ion, or zinc-air batteries. Metal-air electrochemical batteries (e.g., zinc-air battery) have up to 6 times the energy density of the state-of art lithium-ion batteries which have an energy density

of 113.6 W/lb (250 W/kg). Therefore, only Aluminum-air batteries were considered for primary battery power sources since to-date they have the highest energy density of commercial metal-air electrochemical batteries at 590.9 W/lb (1,300 W/kg) [6]. Lithium-ion batteries were also considered as emergency power sources.

Hydrogen fuel cells: The Department of Energys hydrogen fuel cell research portfolio is primarily focused on polymer electrolyte membrane fuel cells (PEMFC) as a near term technology. Therefore, these cells were evaluated as possible power sources.

Nuclear: Lockheed Martin announced in 2014 efforts to develop a compact nuclear fusion reactor which could be suitable for aviation [7]. However, because of the lack of details about the reactor and published data this technology was not considered.

(a) Power vs Weight Sizing

(b) SFC vs Weight Sizing
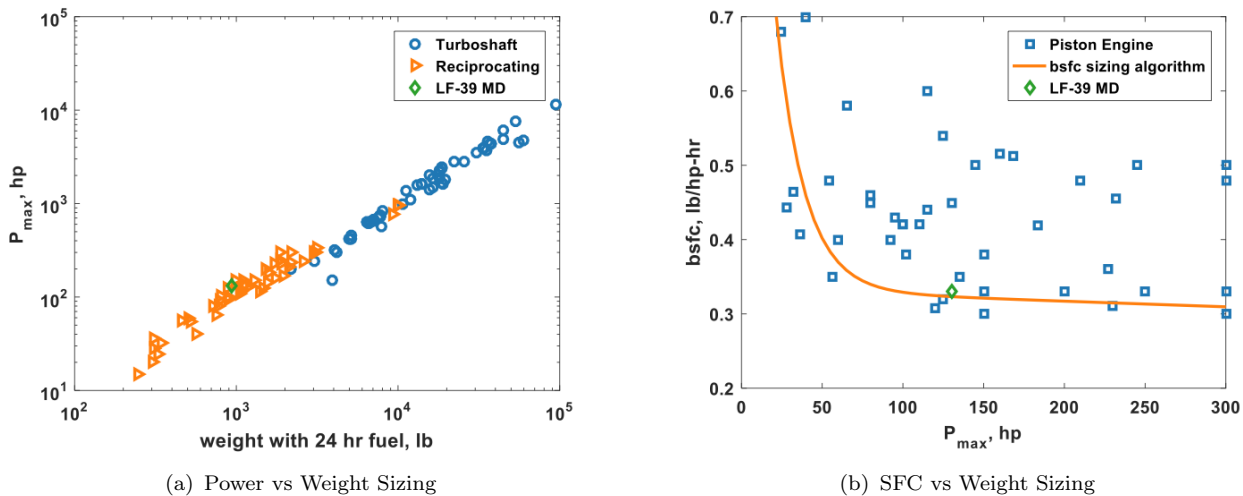
FIGURE 5.7: Comparison of Possible Propulsion Systems.

Internal Combustion Engines: Reciprocating engines and turbine engines were evaluated. Fuels were limited to MOGAS, AVGAS, diesel, and F-24.

5.2.2 Choice of Propulsion System Architecture

Six propulsion system architectures were considered for *Elysium* during the preliminary sizing process

Option 1: Turboshaft engine with direct mechanical power transmission: This system consists of a Jet-A-powered turboshaft engine connecting to a central transmission. The central transmission would distribute power to each rotor gearbox through a system of mechanical gears and drive shafts. The disadvantages of this system are: large number of rotating parts, complex central transmission and high fuel consumption.

Option 2: Reciprocating engine with mechanical power transmission: This system consists of a gasoline or diesel-powered reciprocating engine connecting to a central transmission. The central transmission distributes power to each rotor gearbox through a system of mechanical gears and drive shafts. The disadvantage of this system are: a large number of rotating parts and a complex central transmission.

Option 3: Dual reciprocating engine with mechanical power transmission: This system consists of a gasoline or diesel-powered reciprocating engine connecting to each rotor gearbox through a system of mechanical gears. This option suffers from a large number of rotating parts.

Option 4: Aluminum-air battery-powered DC Brushless (DCBL) motor with electric power transmission: This system consists of an aluminum-air battery connected by aluminum cabling to electric motors. The electric motors are connected to each rotor gearbox. The disadvantages of this system are the need to carry dead weight of the non-consumable battery weights and reduced efficiencies in power transmission.

Option 5: Hydrogen-fuel-cell-powered DCBL motor with electric power transmission: This system consists of a Proton-change-membrane-hydrogen-fuel-cell connected by aluminum cabling to electric motors. The electric motors are connected to each rotor gearbox. This system also includes an emergency battery for a powered landing in case of generator failure. The disadvantages of this system are: need to carry the dead weight of the hydrogen storage tank and reduced efficiencies in power transmission.

Option 6: Generator-powered DCBL motor with electric power transmission: This system consists of a gas- or diesel-powered reciprocating engine connecting to a DCBL generator. The electric power is then routed from the generator to electric motors are connected to each rotor gearbox via aluminum cabling. This system also includes an emergency battery for a powered landing in case of generator failure. The disadvantage of this system is the efficient of power transmission.

To compare the candidate systems, sizing equations for reciprocating engines, turboshaft engines, and DCBL motors in the 35 hp to 200 hp power class were developed from the data presented in Fig. 5.7(a). Specific fuel consumption data from Fig. 5.7(b) was used to develop SFC vs power curves for reciprocating and turbine engines. A generator sizing equation was developed by pairing DCBL motors to low-bsfc, high power-to-weight reciprocating engines. The hydrogen fuel cell was sized based on Department of Energy 2020 targets for fuel cell technologies [8, 9]. The batteries were sized based on commercially available high-energy batteries.
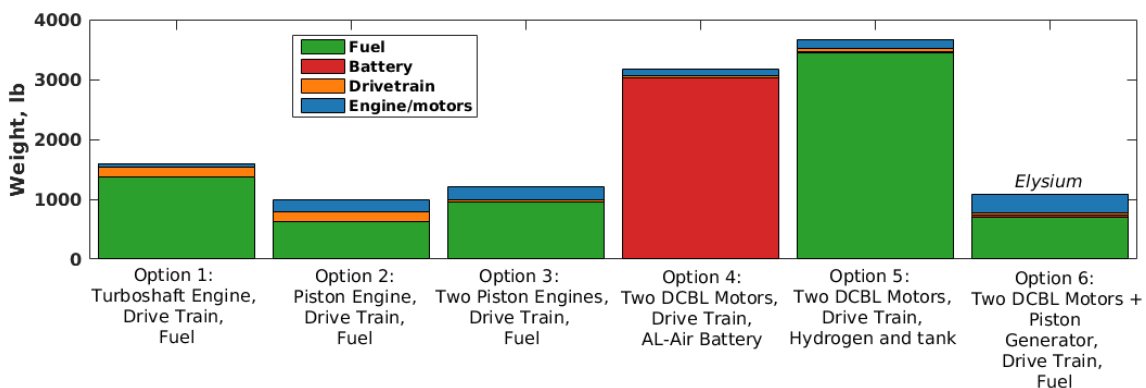
FIGURE 5.8: Propulsion Sizing

Figure 5.8 shows the results of a propulsion system trade study for a 100 hp, twin-rotor vehicle during a 24-hr hover mission. Option 1 was eliminated due to the excessive fuel consumption of the turboshaft engine. Option 3 was eliminated due to the increase in weight when compared to a single reciprocating system and increased maintenance added by a second engine. Option 4 was

eliminated due to the excessive weight of the batteries required. Option 5 was eliminated due to the excessive weight of the hydrogen storage tank required. Options 2 (piston engine drivetrain) and 6 (piston engine, generator drivetrain) have very similar fuel consumptions and system weights. In terms of maintenance, it is expected that option 6 will require less maintenance due to low maintenance of electric motors and the removal of a main transmission and drivetrain components. Additionally when the potential for future innovations are considered, possible step-change advances in electric technologies (e.g. batteries, fuel cells, and electric motors) can outpace advances in mechanical technologies. Therefore, option 6, a reciprocating-generator with DCBL motors was selected to emphasize system simplicity, maintainability, and potential for future innovations.

5.3 Multi-rotor Structural Weight

The AFDD weight model uses curve-fitted data points from real helicopters to give estimates of helicopter component weights based on simple criteria. While this works well for traditional single main rotor (SMR) and coaxial designs, such a model does not exist within AFDD to accurately estimate the structural arm weight for a multi-rotor vehicle. The proposed twin would also be an extrapolation of the AFDD curve fit since the *Elysium* is in a different weight class from conventional tandem aircraft. An in-house sizing algorithm was therefore developed by the team to provide a more detailed structural weight for multi-rotor designs. This algorithm was broken up into two phases: (1) defining the rotor spatial arrangement, (2) calculating the weight of the structure required to support the rotors.
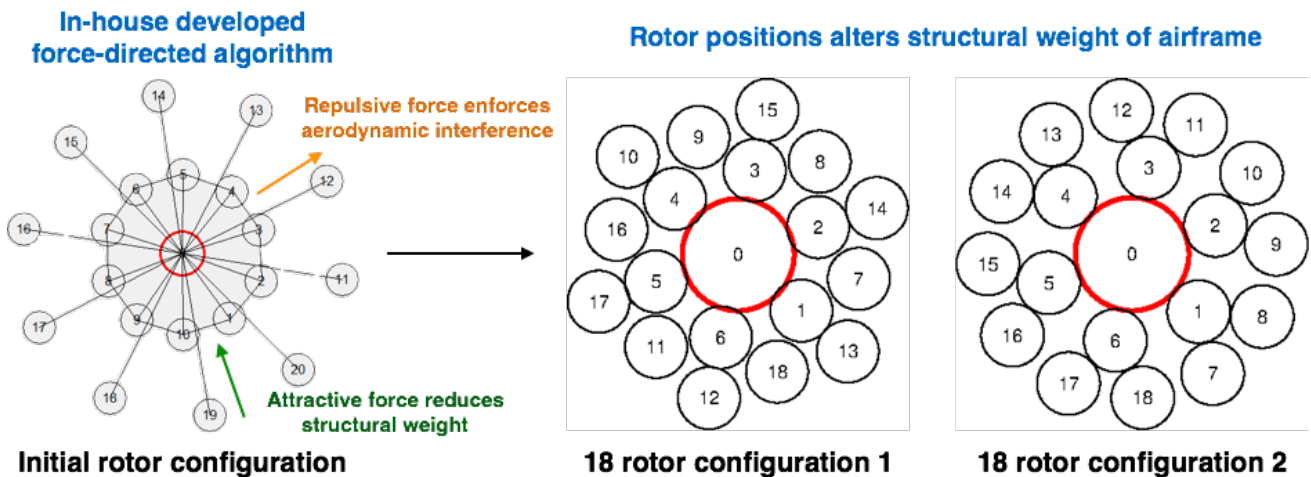
FIGURE 5.9: Schematic illustrating the in-house developed algorithm to define rotor layout.

For a given number of rotors, a significant number of rotor arrangements are possible. The rotors can be spaced far apart or packed tightly together, have various symmetric patterns, and be placed in a variable number of rings around the centroid of the vehicle. Minimizing the structural weights demands rotors that are packed tightly together; however, if the rotors are too tightly packed, aerodynamic interference can degrade the performance. Indeed, two rotors rotating in the same plane require a tip clearance of $0.2R$ for minimal aerodynamic interference [10]. Additional considerations were given to symmetric configurations, as these help simplify the vehicle controls and ensure that the center of gravity is at the centroid of the vehicle. A graphic layout, force-directed algorithm was therefore developed to generate possible configurations subjected to these metrics, a schematic of which is shown in Fig. 5.9.

The force-directed algorithm modeled each rotor as a point with both repulsive and attractive forces. The repulsive force existed between all pairs of rotors and, to enforce the aerodynamic interference, grew exponentially as two points became closer than $2.2R$. Additionally, selected rotors were drawn together by an attractive force which increased linearly with distance. Based on the number of rotors, initial rotor arrangement, and selection of rotors drawn together by the attractive force, the force-directed algorithm generated the arrangement which resulted in a low energy state. Artificial damping was added to the model to facilitate convergence. For a given number of rotors, as many as four possible rotor arrangements were generated.

Once the possible rotor arrangements were determined, the weight of the support structure required to support these rotors was calculated. Because this weight was used in the preliminary vehicle selection, it was necessary to have a structural weight model which was dependent on rotor size and number of rotors. A Timoshenko beam model was created, in which the rotor locations, structural support orientations, and rotor thrust and torque based on momentum theory were used to size the structure. As the AFDD weight model is primarily based off of legacy rotorcraft, the beams were circular tubes made of aluminum, so that the structural weight would be consistent with the other components in the AFDD model. With constraints that the beam have a maximum stress safety factor of 1.75 and that it does not fail due to buckling, the tube diameter and thickness were iteratively varied for a given set of inputs until the minimum weight structure was achieved. Parametric sweeps over the rotor radius and vehicle weight were then performed for each number of rotors. Structural weight equations, which were a function of the rotor radius, vehicle weight, and number of rotors, were therefore generated for use in the sizing code.

5.4 Results of Preliminary Sizing

The design of an efficient 24-hour hovering aircraft is an enormous challenge, requiring creativity to achieve the mission solely by incorporating existing technologies. Analysis of the design space for current technology and material weights from AFDD reveal that a specially-designed single main rotor could be outfitted to accomplish the mission; however, a high gross take-off weight and large percentage of stored fuel would make it an extremely inefficient design. A primary factor driving the design of an appropriate 24-hour hovering vehicle is choosing the lightest, most fuel-efficient vehicle.

5.4.1 Analysis of Single and Two-Rotor Systems

Figure 5.10 shows the comparison between one and two rotor aircraft for the full 24-hour sizing mission outlined in Section 5.1.2. For all vehicles, a disk loading of 1.9 lb/ft^2 (9.3 kg/m^2) was used with a rotor tip speed of 440 ft/s (134 m/s). These values were chosen from a parametric sweep to obtain the minimum gross take-off weight for a maximum C_T/σ of 0.12. In the first bar, a traditional single main-rotor is shown with 10% of the main rotor power used for the tail rotor. Over the 24-hour mission, this 10% power results in a 20% increase in GTOW, as shown in the second bar of the plot where the tail rotor power is neglected. The second bar is meant to represent an ideal hovering SMR where all power is used for the main rotor for thrust.

To avoid diverting power to the tail rotor, a coaxial rotor system instead uses counter-rotating rotors. Bar 3 of Fig. 5.10 shows the result of a coaxial rotor for the sizing mission. An interference factor $\kappa_{int} = 1.2$ is used to account for the lower rotor operating in the wake of the upper[1]. The interference factor between rotors may be negligible for many applications, however, for a

24-hour hover mission, the inefficiencies result in higher fuel consumption just as was seen for the SMR with tail-rotor. Intermeshing rotors also have an interference factor and can be rejected for the same reasons.
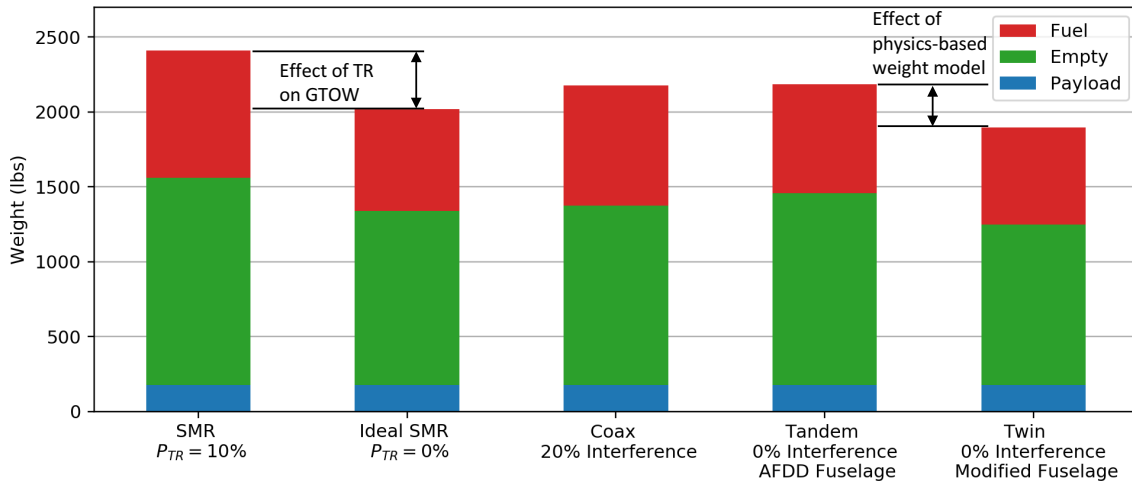
FIGURE 5.10: Comparison of one and and two-rotor aircrafts using rubber diesel engine and AFDD weight estimates

Interference between rotors can be mitigated by moving the rotors apart into a conventional "Tandem" configuration. The conventional tandem configuration is shown in bar 4, where a full tandem fuselage is approximated from AFDD models. While the interference factor between rotors no longer exists, the much larger tandem fuselage results in an aircraft that closely resembles the Coax for weight. Finally the right-most bar of figure 5.10 shows a "Twin" configuration where the rotors are not overlapping to avoid interference but the fuselage is small and compact with only support arms out to the rotors. This design highlights the benefits of using multiple, non-interfering rotors with weight-efficient structural support.

5.4.2 Analysis of Multi-Rotor Systems

The one and two-rotor comparisons from the previous section show a trend toward multiple rotors to reduce total aircraft weight and fuel. Especially with recent advancements in distributed electric propulsion and the success of multi-rotor micro air vehicles, further analysis must be made for a comprehensive overview of the design space.

The structural arm weight model, presented in Section 5.3, was used in combination with the AFDD model for other component weight estimates. Engine, generator, electric motor, and power distribution weights were used from the model presented in Section 5.2.

Figure 5.11 shows the GTOW result of many different multi-rotor configurations up to 18 rotors. The trend clearly shows an increase in aircraft and fuel weight as the number of rotors increases above two. The SMR result from Fig. 5.10 is included for a baseline comparison. So as to keep all multi-rotor configurations on a level field for comparison, the same rubber diesel generator was used and disk loading fixed at 1.5 lb/ft^2 (7.32 kg/m^2) with tip speeds of 440 ft/s (134 m/s). The blade loading is held constant over time by reducing RPM approximately 16% over 24-hours.

The sweep of rotor numbers uses momentum theory to model the aerodynamics and does not consider Reynolds number effects. The relatively low tip speeds of the blades result in the 75%
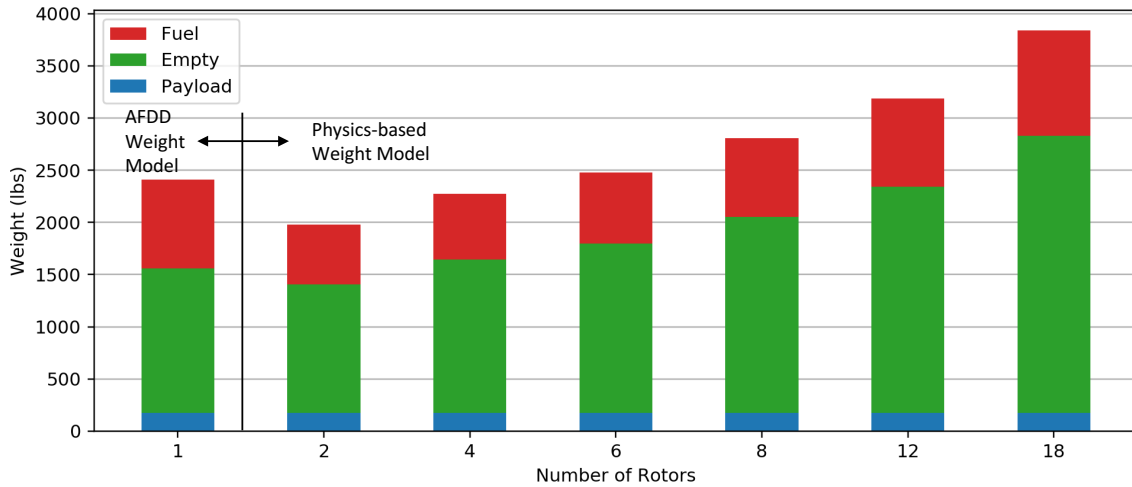
FIGURE 5.11: Comparison of multi-rotor configurations with same hybrid efficiencies, rubber diesel generator, and structural weight model using variable RPM to achieve constant C_T/σ.

span Reynolds number for the rotors to be below 1 million for configurations with more than four rotors. The four- and two-rotor aircrafts have $Re_{75\%} = 1.0$ and 1.4 million respectively, which is still much lower than for typical rotorcrafts. The trend in Fig. 5.11 is therefore likely under-predicting the weight as the number of rotors increases, further motivating the selection of the twin configuration for the *Elysium*.

5.4.3 Hybrid-Electric Twin-Rotor Design

Section 5.4.1 showed the twin-rotor design was superior to other single and two-rotor configurations and Sec. 5.4.2 also showed that the twin out-performs other multi-rotors using distributed hybrid electric propulsion. This section presents the convergence of the sizing code from a generic, rubber-engine twin-rotor design to the *Elysium* through detailed analysis of the design space. Chapter 11 presents in more detail the specific propulsion system and efficiencies used for the results of this section.

The relationship between disk-loading and tip speed is shown for the twin-rotor configuration in Fig. 5.12. Each point on the line represents a twin-rotor aircraft capable of completing the sizing mission defined in Section 3.2. The selected maximum blade loading of $C_T/\sigma = 0.12$ limits the domain of feasible points in the x-direction and the desire for a lightweight aircraft motivates the selection of the lowest possible point in the y-direction.

The selected design point, circled in black on Fig. 5.12, is approximately at the point where variations in disk-loading at $DL = 1.9$ lb/ft^2 (9.3 kg/m^2) and tip-speed at 440 ft/s (134 m/s) asymptote together. Zooming in on the region near the selected design point, obtaining decreased GTOW by further decreasing disk-loading would require significant reductions in tip-speed. Shown in red, the line for $V_{tip} = 390$ ft/s (119 m/s) is roughly tangent to the disk loading lines and continues parallel to lines of constant disk loading in the area of interest.

Whereas carpet plots for typical helicopter missions are generally more orthogonal, the 24-hour sizing mission reveals unintuitive trends, such as the asymptotic behavior of disk loading and tip-speed lines. The collapse of lines in the design space is directly a result of contradicting trends between the aerodynamics and structures. From an aerodynamic standpoint, for example,
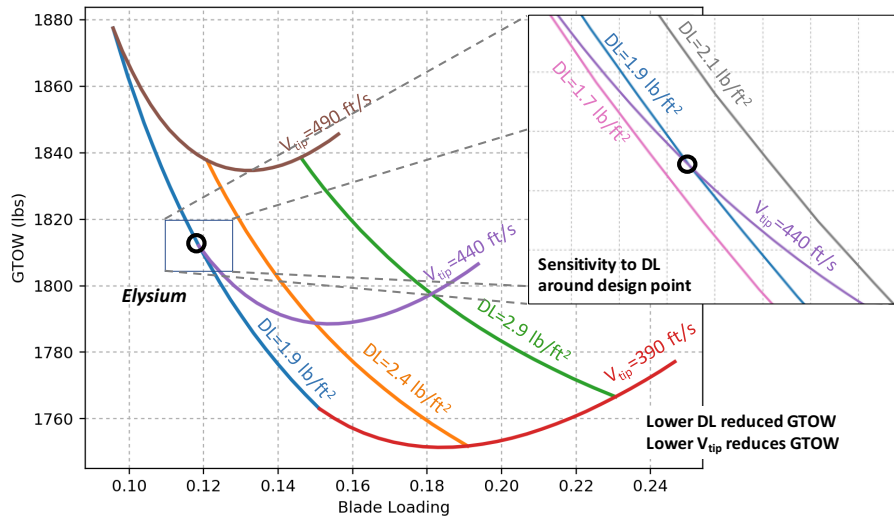
FIGURE 5.12: Carpet plot of takeoff weight and blade loading for various disk loadings and tip speeds. Selected design point at GTOW is shown in black.

reducing disk loading and tip speed together will result in a lower required power and lighter propulsion system. Structural concerns with the loss of centrifugal stiffening and large, heavy blades dictate the optimal configuration is in the opposite direction, where both tip speed and disk loading are high. The superposition of opposing trend lines leads to a saddle point in the design space.

6 Vehicle Specifications

Elysium is a twin rotor vehicle built to hover autonomously with a 210 lb (95 kg) payload, and capable of achieving the longest hover in history at over 24 hours. Vehicle specifications, summarized in Table 6.1, break convention and reflect the design's focus on hover efficiency.

7 Blade Aerodynamic Design

7.1 Design Goals

While the main rotor of a general helicopter is a compromise between hover and forward flight performance, *Elysium* was designed to maximize hovering efficiency. The rotor of *Elysium* employs a variable collective (for control) with varying RPM (to maintain constant FM) over 24 hour duration. This RPM scheduling allows the blade to operate at a constant blade loading (C_T/σ) at the best possible hovering efficiency during the mission. The blade geometry (twist, taper, airfoil section) was chosen such that the rotor has the best hovering efficiency at given blade loading (C_T/σ).

7.2 Design Methodology

The primary goal of the aerodynamic design of the rotor was to obtain maximum hovering efficiency over the entire 24 hour duration. The aerodynamic design of the rotor was carried out in two primary phases, each designed to extract the highest possible efficiency from the rotor blades.

TABLE 6.1: Summary of Vehicle Specifications

Parameter	Value	
	English	Metric
Takeoff Weight	1811.9 lb	821.8 kg
Empty Weight Fraction	0.60	0.60
Power Loading Fraction	0.10	0.10
Fuel Weight Fraction	0.28	0.28
Disk Loading DL	1.9 lb/ft^2	9.3 kg/m^2
Average Power Loading PL	26.6 lb/hp	87.3 N/kW
Blade Loading C_T/σ	0.12	0.12
Blade Radius	12.3 ft	3.75 m
Blade Aspect Ratio	17	17
Thrust Weighted solidity σ_e	0.0437	0.0437
Hover Tip Speed	440 ft/s	134.1 m/s
Power Installed	125 hp	93.2 kW
Number of Rotors	2	2
Number of Blades	4	4

1. The baseline geometry of the blade was obtained through an in-house Blade Element Momentum Theory (BEMT) code. An extensive parametric study of blade geometries (twist, taper and airfoil selection) was conducted while GTOW, radius, tip speed, and thrust weighted solidity were held constant. Note that *Elysium* varies the rotor RPM with time over 24 hours to ensure a constant blade loading coefficient throughout the mission. The targets were to maximize power loading and figure of merit (FM). Because the operating Reynolds number over the blade were in low to medium range (500,000 – 1,000,000), 2D CFD tables were created using an extensively validated in-house code [11, 12] for the various airfoils explored. Care was taken to include laminar-turbulent transition models [13] as the standard fully turbulent models can result in imprecise values of lift, drag and pitching moment.

2. The effect of tip shape on blade performance was investigated with an in-house 3-D computational fluid dynamics code [14]. Because the rotor of *Elysium* operates in subsonic flow, the compressible effects at the tip of the blade are negligible during the mission. Consequently, blade sweep was not considered at these low Mach numbers, since it adds primarily to the pitching moment about the feathering axis. Nevertheless, tip shape of the blade can still have an effect on blade performance, wake structures, blade-vortex interactions, and acoustics. Using the 3D solver, wake structures in the near field were analyzed for various anhedral tip-shapes and the resulting vortex structure.

3. The rotational direction of each rotor was decided based on the insights from existing results. Because *Elysium* employs twin rotors, rotational direction of two rotors can affect not only rotor performances, wake structures, but also flight performances. Through the analysis of existing coaxial rotors and paper study, the rotational direction of the rotor was determined.
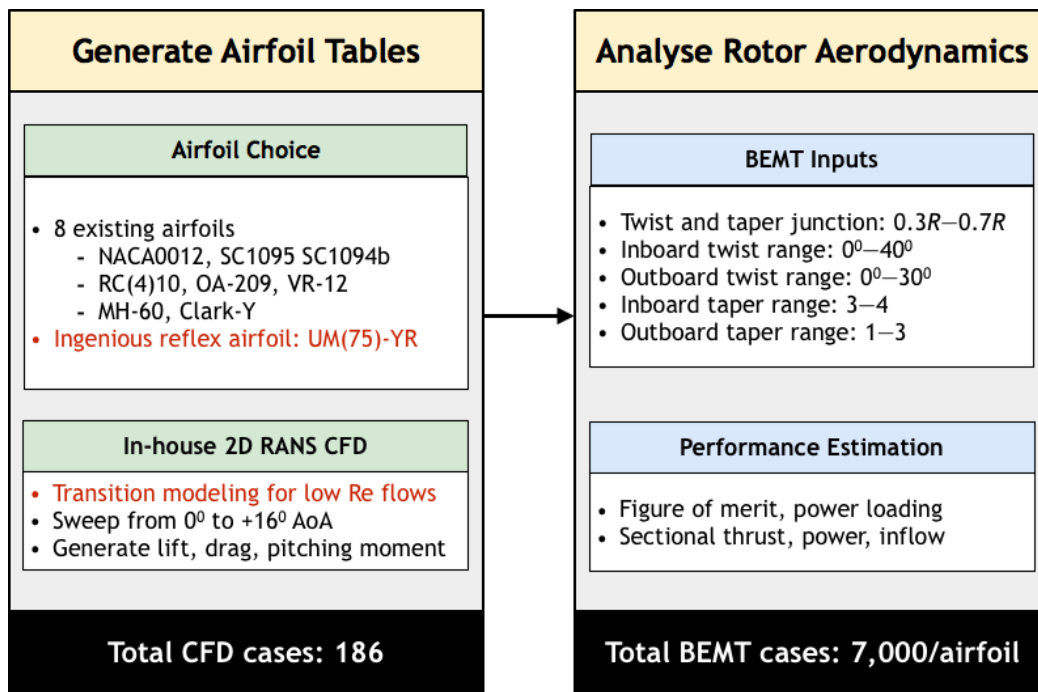
FIGURE 7.1: Schematic outlining the process for evaluating blade aerodynamic performance.

7.3 Blade Aerodynamic Design

An ideal hovering rotor predicts hyperbolic twist and taper distribution as being the geometric shape of the rotor for maximizing hovering performance. However, this formulation does not account for effects of tip-loss and Reynolds number on stall characteristics of the airfoil. Therefore, while the hyperbolic distributions serve as a guideline, an analysis that considers carefully the flow characteristics under the current operating conditions is required. Table 7.1 shows tip Mach and Reynolds number of the rotor over 24 hour duration. The maximum tip Mach number is about 0.4 and corresponding Reynolds number is 1 million. In general, the blade has lower lift-to-drag (L/D) ratio and smaller stall margin in this range of Reynolds number compared to helicopters in the heavier weight class.

Figure 7.1 shows the overall process used to determine the aerodynamic of the rotor blades. The first step consisted of generating airfoil tables for chosen airfoils to determine the variation of aerodynamic loads with angle of attack. An in-house two-dimensional Reynolds-Averaged Navier–Stokes solver (TURNS) was used for this purpose. A salient feature of TURNS is the inclusion of a laminar-turbulent transition model that is essential for the Reynolds number range of interest ($0.5 - 1$ million). The second step used a blade element momentum theory to analyze the performance of the rotor for different geometries. A total of 186 CFD cases and 7,000 blade designs per airfoil were analyzed.

TABLE 7.1: Tip Mach and Reynolds number of *Elysium*.

Rotor Radius	12.3 ft
Tip Mach	0.33–0.39
Tip Re	0.7–1 million

7.3.1 Baseline Airfoil Selection

The proper selection of airfoil is fundamental to maximizing the hovering efficiency of the rotor. For airfoil selection, the following aerodynamic characteristics are mainly required: (1) High lift-to-drag (L/D) ratio at medium Reynolds number, and (2) Broad range of angle of attack around maximum L/D. To choose the airfoil sections that have best performance at the operating conditions of *Elysium*, a total of eight airfoil sections were analyzed: NACA0012, SC-1095, SC-1094b, RC(4)-10, OA-209, VR-12, MH-60, and Clark-Y. The airfoil performance in terms of lift, drag and pitching moment were analyzed using an in-house 2D Navier–Stokes CFD solver [11–13] at the operating range of Reynolds number and Mach numbers. Lift-to-drag (L/D) coefficient for some of these airfoils are presented in Fig. 7.2.
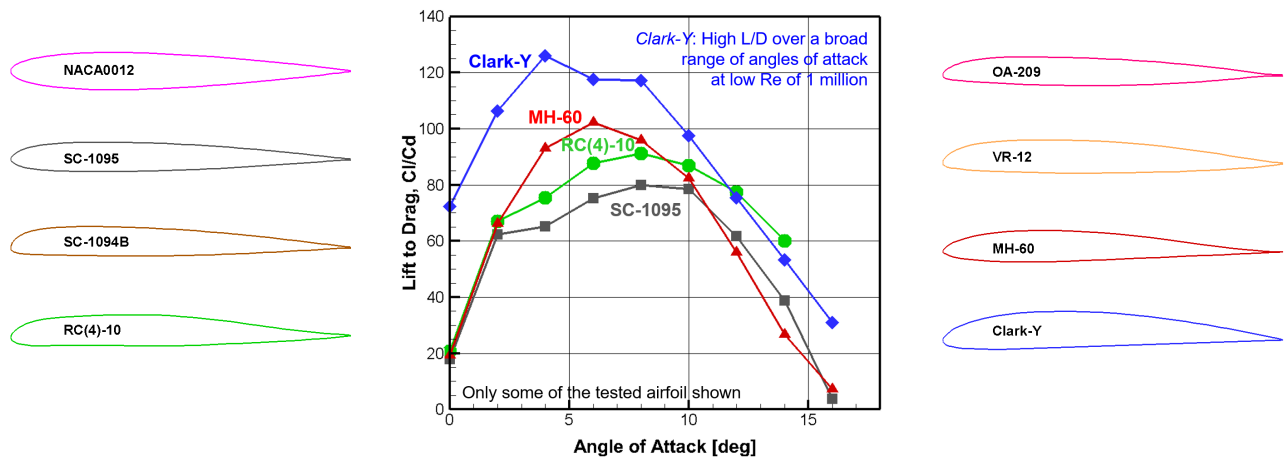
FIGURE 7.2: Outline of 8 airfoil sections and comparison L/D ratio for selected airfoils.

NACA0012 is a symmetric airfoil with low pitching moment, but is not desirable for the current mission because it has low lift capability and stall margin. Sikorsky's SC-1095 and SC-1094b airfoils have been validated in the field and widely used such as in the UH-60 main rotor. However, their operating tip Mach number is higher than that of *Elysium*, and these airfoils were designed to operate with moderate efficiency in both hover and forward flight. "High-lift" airfoil sections, such as NASA RC(4)-10, ONERA OA-209, and Boeing-Vertol VR-12, have good lift capability ($L/D \approx 120 \sim 140$), but they are not suitable for the *Elysium's* rotor because of their high operating Reynolds number compared to the requirement for the current design.

MH-60 and Clark-Y are airfoils for mid-range Reynolds number flow. Both airfoils have high L/D ratio at the operating conditions of *Elysium*. On one hand, MH-60 has a narrower range of operating angles of attack for maximum L/D and is less robust around the optimal angle of attack, as shown in Fig. 7.2. Furthermore, it has not been applied for real aircraft except for remote control aircraft. On the other hand, Clark-Y airfoil has a broader range of angle of attack around maximum L/D ratio (about 5°) and it has been widely used in general aviation aircraft for over 70 years [15]. Therefore, the Clark-Y airfoil was chosen as the primary airfoil for this blade.

7.3.2 Blade Twist and Taper

Incorporation of twist and taper into blade design improves hovering performance. On one hand, twist affects the inflow distribution on the rotor disk, which can be used to achieve the ideal uniform distribution. On the other hand, blade taper aims at reducing the profile by enabling the airfoil sections to operate at their angle of attack for best performance (max L/D). To find the optimal twist and taper distributions, an extensive parametric study was conducted. The following parameters were varied: (1) Inboard twist rate (0°/ft to 3.252°/ft), (2) Outboard twist rate (0°/ft to 2.439°/ft), (3) Twist junction (0.3R to 0.7R), (4) Inboard taper ratio (3 to 4), (5) Outboard taper ratio (1 to 3) and (6) Taper transition (0.3R to 0.7R). This sweep resulted in a total of 7,000 blade designs for a single airfoil.

TABLE 7.2: Comparison of best geometry for different twist and taper combinations.

Geometry	Single Twist Single Taper Single Airfoil	Bi Twist Single Taper Single Airfoil	Bi-Twist Bi-Taper Single Airfoil	Optimum Hovering Rotor
Inboard Twist	0.813°/ft	3.253°/ft	3.253°/ft	Hyperbolic
Outboard Twist	-	0.813°/ft	0.813°/ft	Hyperbolic
Twist Junction	-	0.4R	0.4R	-
Inboard Taper	4	4	4	Hyperbolic
Outboard Taper	-	-	2	Hyperbolic
Taper Transition	-	-	0.7R	-
Airfoil	Clark-Y	Clark-Y	Clark-Y	Clark-Y
Figure of Merit	0.848	0.852 (+0.5%)	0.852 (+0.5%)	0.889 (+4.8%)
Pitching moment [lb·ft]	-39.548	-39.452	-39.551	-46.195
Pitch link load [lb]	124.9	124.6 (-0.2%)	124.9 (0.0%)	145.9 (16.8%)

Table 7.2 shows different combinations of blade twist and taper which resulted in the best FM for each condition. All calculations were performed with the Clark-Y airfoil and all geometries had a taper ratio of 4. A study was conducted on the effects of a bi-tapered blade, but the performance benefits were not worth the additional complexity in design and manufacturing. The results show the blade with single linear twist and taper has a FM of 0.848 and the addition of bilinear twist improves the FM by 0.5% from the single linear twist and taper. Table 7.2 shows that the blade with single linear twist and taper has a FM that is 4.8% lower that the ideal scenario with zero induced losses (induced power factor, $\kappa = 1$). The current design has an induced power factor value of 1.06 across the 24 hour mission time.

7.3.3 New Reflex Camber Airfoil: UM(75)-YR

As shown in Fig. 7.2, Clark-Y airfoil has high lift capability in a medium range of Reynolds number, which has been used on various general aviation aircraft. However, the Clark-Y has relatively high negative pitching moment because of its flat lower surface, which can result in high pitch link loads as shown in Table 7.2. To offset this large pitching moment, a new reflex airfoil was designed based on the Clark-Y airfoil such that it has a positive pitching moment with minor reduction to the L/D capabilities. Figure 7.3 shows the geometry of the Clark-Y and newly designed UM(75)-YR airfoil. For the UM(75)-YR, the camber line of the baseline airfoil was reflected at 75% of chord and then interpolated with third-order polynomials to smooth the

camber line. Figure 7.4 shows 2-D CFD results of L/D ratio and pitching moment for Clark-Y and new UM(75)-YR airfoil at Reynolds number of 1 million with moderate Mach number. The new UM(75)-YR still has a good maximum L/D ratio, about 95, and generates positive pitching moment though all angles of attack.

(a) Clark-Y and New UM(75)-YR

(b) Exaggerated view of airfoil camber lines
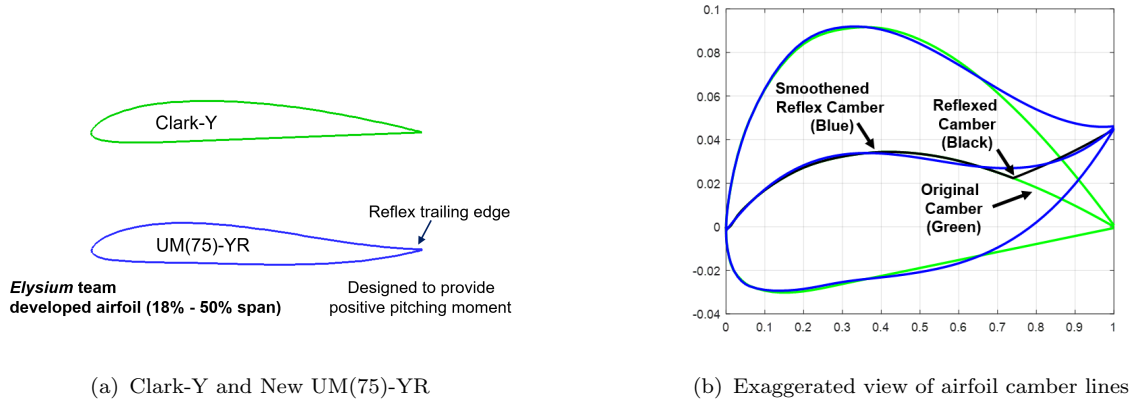
FIGURE 7.3: Geometric comparison of the Clark-Y and developed UM(75)-YR airfoil.

(a) Lift to Drag ratio

(b) Pitching moment
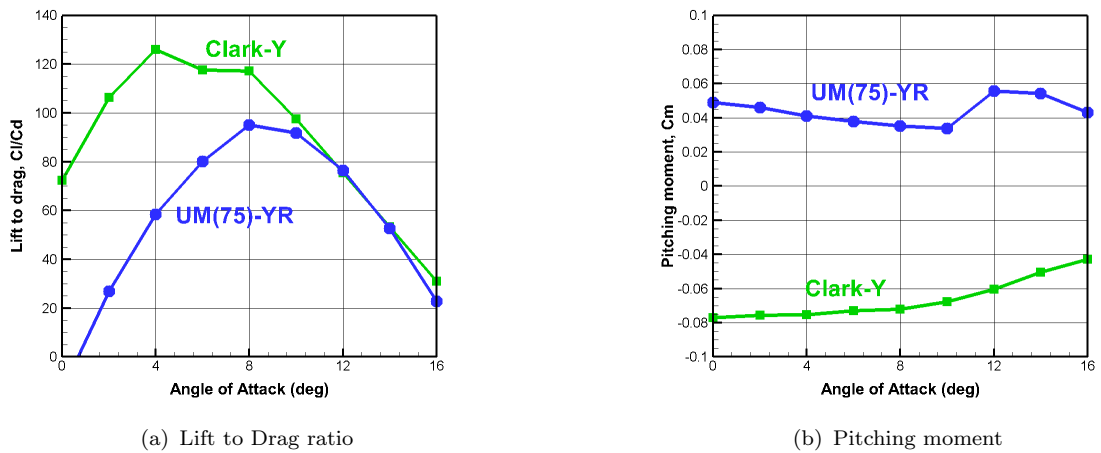
FIGURE 7.4: Aerodynamic characteristics of Clark-Y and New UM(75)-YR at Reynolds number of 1 million.

7.3.4 Bi-Airfoil Section

The UM(75)-YR was designed to reduce the pitch link loads, with minimal reduction to hovering performance. Therefore, this airfoil is used in the inboard sections, where the dynamic pressure is lower. To find the best location of airfoil junction between Clark-Y and UM(75)-YR, the airfoil junction was varied from $0.3R$ to $0.6R$ with a $0.1R$ airfoil transition. A parametric study of twist and taper was performed as discussed in Section 7.3.2. Table 7.3 shows the final output of twist, taper, airfoil junction for the bi-airfoil blade. The table shows that the current blade geometry, which has bilinear twist, single taper, and bi-airfoil of Clark-Y and UM(75)-YR airfoil, reduces pitch link loads by 60% with a reduction in FM of only 0.1% compared to the single airfoil baseline case, which will result in a lighter pitch link.
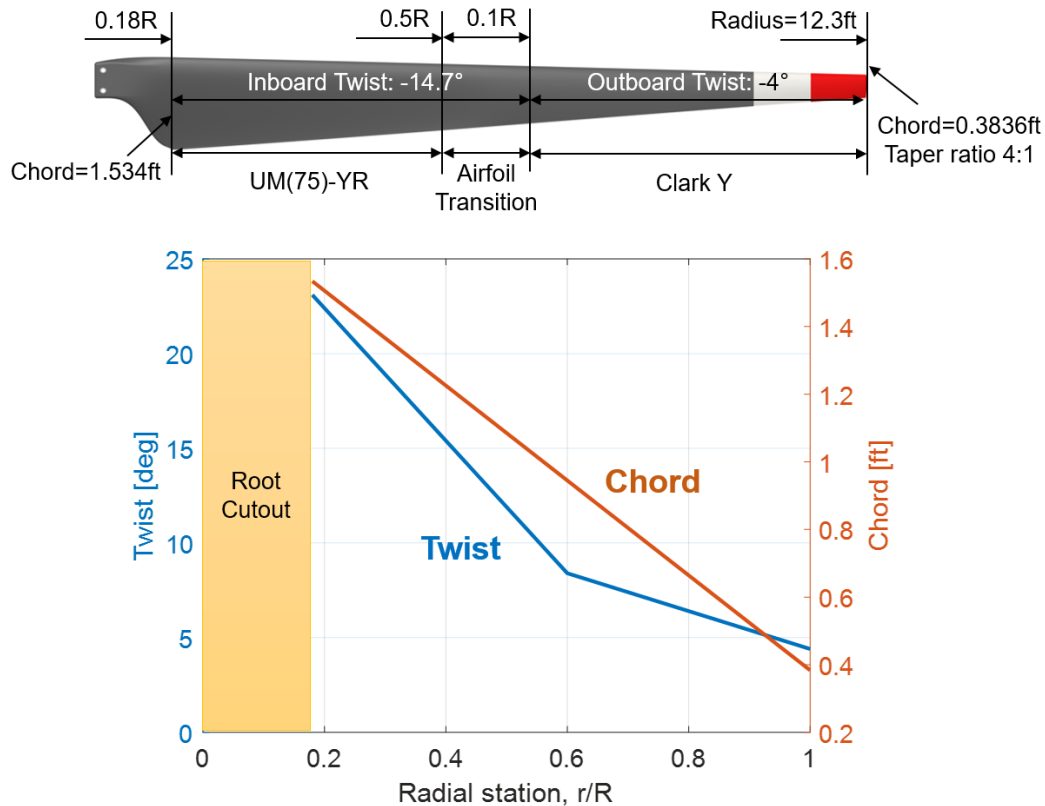
FIGURE 7.5: Geometry of *Elysium's* blade.

7.4   Blade Aerodynamic Performance

Figure 7.5 shows the final blade geometry of *Elysium*. The blade employs bilinear twist, single taper, and bi-airfoil section to optimize hovering efficiency, i.e., figure of merit and power loading. Induced power and profile power are governed by the spanwise variation in inflow and operating angle of attack of the airfoil, respectively. Figure 7.6(a) shows the spanwise variation of inflow, which is almost uniform across the span resulting in a low induced power factor of 1.06. The taper ratio was chosen such that the airfoil (UM(75)-YR inboard and Clark-Y outboard) operate close to the angle of attack for maximum L/D (which is close to the angle of attack for maximum $L^{3/2}/D$) as shown in Fig. 7.6(b). While the inboard sections operate at a higher than optimal angle of attack, the dynamic pressure in these sections is low and there is sufficient stall margin across the span. Additional performance plots are presented in Section 19.

8 Blade Structural Design

8.1   Structural Design

The blade sectional properties were determined using an in-house team-developed non-linear Euler-Bernoulli beam model. In hover, the blades experience only steady loading; however, gusts and the forward flight segments of the mission will introduce vibratory loads and both the steady and vibratory loading must be considered in the design. These aerodynamic and inertial loads were applied to the model and the blade was sized to withstand the stresses at all

(a) Inflow
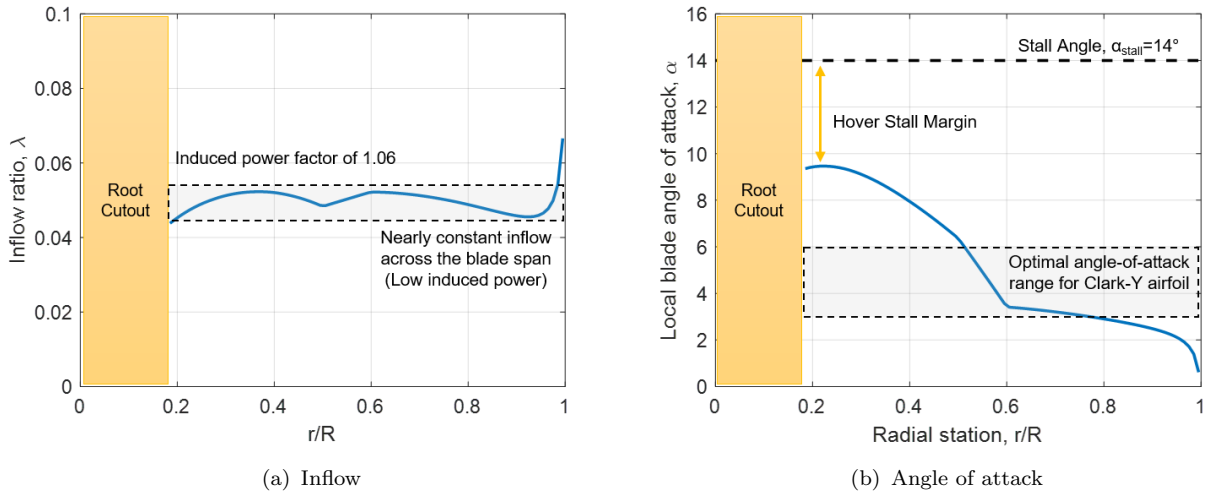
(b) Angle of attack

FIGURE 7.6: Spanwise variation of: (a) Inflow, and (b) Angle of attack, of *Elysium* during hover.

TABLE 7.3: Effect of bi-section airfoil.

Geometry	Single Twist Single Taper Single Airfoil	Bi Twist Single Taper Bi Airfoil
Inboard Twist	0.813°/ft	2.846°/ft
Outboard Twist	-	0.813°/ft
Twist Junction	-	0.6R
Inboard Taper	4	4
Outboard Taper	-	-
Inboard Airfoil	Clark-Y	UM(75)-YR
Outboard Airfoil	Clark-Y	Clark-Y
Airfoil Junction	-	0.5R
FM	0.848	0.847 (-0.1%)
PL [lb/hp]	22.447	22.428
Pitching moment [lb·ft]	-39.548	-16.369
Pitch link load [lb]	124.9	51.7 (-58.6%)

locations along the span. A specially developed cross-sectional analysis tool was used that took in the external blade geometry along the span, and calculated the spanwise mass and stiffness variations based on design variables including chordwise locations of the spar, spar thickness, and skin thickness. Parametric sweeps of these variables were conducted to determine values which resulted in minimal weight blade designs that were capable of withstanding the stresses. Leading edge masses were continually updated to ensure that the center of gravity was at 24.9% of the chord. The spanwise inertial and stiffness properties were then used as inputs to DYMORE to calculate the vibratory modes. The final blade structure was then tailored by adjusting the trailing edge tab and adding tuning masses until desired structural frequencies were achieved across the entire range of operational RPM.

Figure 8.1 shows the primary structural sections of the rotor blade. At 10% span, the blade

contains a titanium insert to prevent the blade from separating from the hub, primarily through assisting in transfer of the centrifugal loads to the hub. From 10% span to the root cutout at 18% span, the loads are carried by the spar with an aerodynamic fairing provided to limit the shank drag. The primary lifting surface runs from 18% span to the tip.
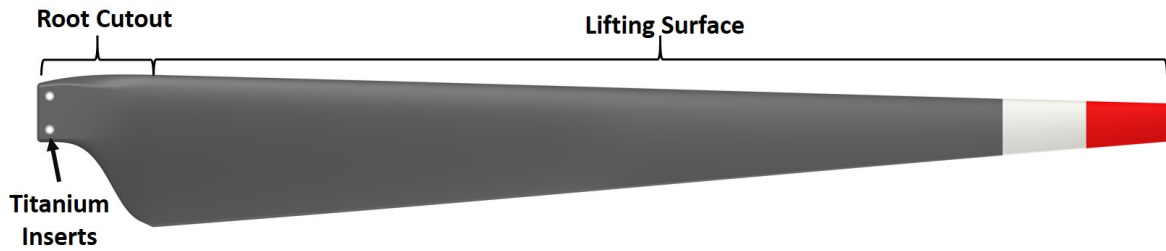
FIGURE 8.1: Main rotor sections.

8.1.1 Blade Internal Structure

The complete internal structure of the blade is shown in Fig. 8.2. The primary load carrying member is an elliptical spar, which runs from 9% to 35% of the chord and is composed of unidirectional T300 graphite/epoxy in a $[\pm45/0/90/0_2/90/0]_s$. The elliptical spar was selected due to its simple closed-section geometry that provides high flap and torsional stiffness, with the T300 graphite/epoxy chosen because of the higher specific stiffness and ultimate strength that it provides compared to other composite materials, such as glass fiber, while also having a lower density. The outer $[\pm45°]$ layers provide torsional stiffness, while the four layers of $[0°]$ were intermixed with the $[90°]$ plies to reduce the probability of delamination and prevent microcracks from coalescing [16].
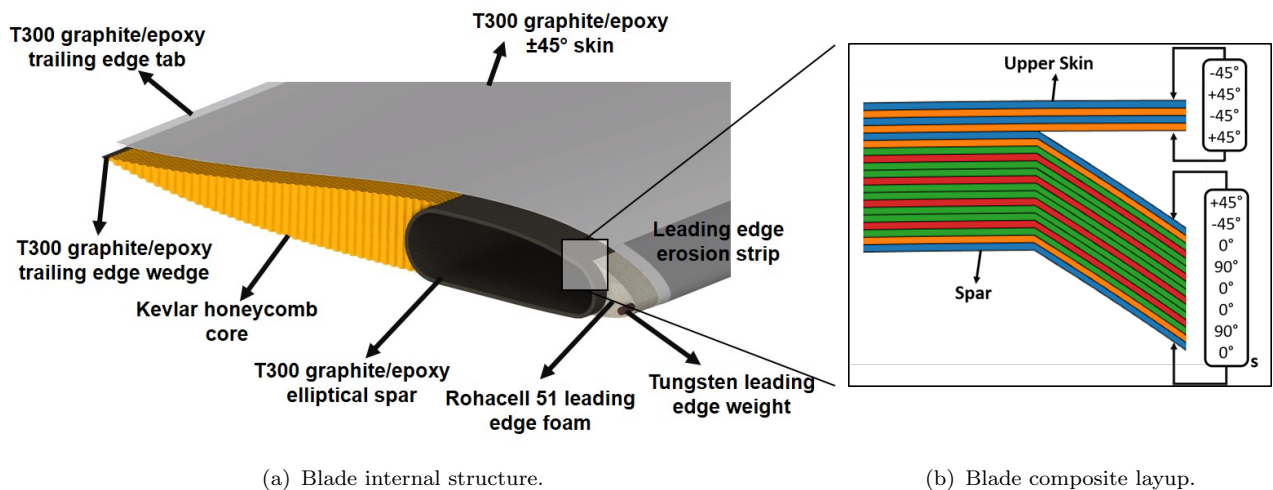
(a) Blade internal structure.

(b) Blade composite layup.

FIGURE 8.2: Internal structure of the blade.

The center of gravity was maintained at 24.9% of the chord through the use of tungsten leading edge weights. This places the CG ahead of the elastic axis, which ensures sufficient stability from pitch-flap flutter. Rohacell 51 foam is added at the leading edge of the blade to maintain the aerodynamic profile of the leading edge while also preventing chord-wise movement of the tungsten mass. A stainless steel strip forms the outer profile of the leading edge and protects the blade from abrasion and erosion.

The blade skin is constructed of four balanced [±45] plies of T300 graphite/epoxy to provide a high torsional stiffness. A trailing edge tab of 2% of the chord is formed by the upper and bottom skin surfaces to help prevent trailing edge de-bonding. A wedge of graphite/epoxy is inserted at the trailing edge to provide additional support against delamination as well as increase the lag stiffness. The remaining aft section of the blade is filled with a Kevlar honeycomb core to maintain the aerodynamic profile of the blade. Kevlar honeycomb was selected due to the 400% increase in stiffness that it provides compared to Nomex honeycomb while also maintaining excellent thermal and moisture stability [17]. More importantly, Kevlar honeycomb is extremely lightweight compared to typical foam cores, and therefore minimizes the amount of leading edge weights required for a proper chordwise center of gravity. Because *Elysium* is a technology demonstrator and will not be flying in extreme weather conditions, lightning protection and deicing systems were not included in order to minimize the structural blade weight.

8.1.2 Blade Manufacturing

A two step process is used for fabricating the blades. The first step is manufacturing the spar, for which a block of foam core is machined to the internal geometry of the spar and serves as a mandrel for fiber placement. The titanium insert is aligned with the foam core and continuous unidirectional composite tapes are laid up from the tip of the rotor, around the titanium insert, and back to the tip using automated fiber placement. Automated fiber placement can work with tape as small as 3 mm [16], and to account for the changes in the spar dimensions due to both the significant blade taper and increasing spar thickness, additional layers are started when moving inboard along the span. An additional five layers of carbon fiber are also included at the blade root to provide the strength necessary to prevent the blade from shearing off during operation.

The second step creates the aerodynamic surface of the blade. The trailing edge honeycomb and fiber glass insert are placed behind the spar and the leading edge weights and foam are added in front. This assembly is then wrapped with the [±45°] T300 graphite/epoxy prepreg to contain the structure and maintain the aerodynamic shape. This assembly is placed in a mold for the final cure. The mold introduces a small recess in the blade for the stainless steel erosion strip, which is added in a tertiary step.

8.1.3 Rotor Blade Sectional Properties

Based on the cross-sectional analysis, the final weight of an individual blade is 18.9 lbs (84.2 N). For the entire system of four blades, this accounts for 75.7 lbs (336.9 N). The individual component weights are summarized in Table 8.1. The spar, which serves as the primary load carrying member accounts for nearly half of the blade weight at 47.2%. The skin and leading edge weights also have significant contributions to the total blade weight at 26.6% and 13.6%, respectively.

The non-dimensional mass and stiffness distributions of the blade about its elastic axis are shown in Fig. 8.3. The hub connection begins at 10% span and the root cutout begins at 18% span, therefore the stiffness and mass properties within this region are dominated by the spar properties and titanium root insert. Outboard of the root cutout, the skin and leading edge weights contribute to the sectional properties and spanwise variations are observed due to the blade taper. Discrete changes in the sectional properties, which are most evident in the mass distribution, are a result of ply dropoffs from the root cutout to the blade tip. The slight increase in mass at the tip was a result of additional leading edge weights for tuning the torsional

(a) Mass distribution

(b) Flap stiffness distribution

(c) Lag stiffness distribution

(d) Torsional stiffness distribution
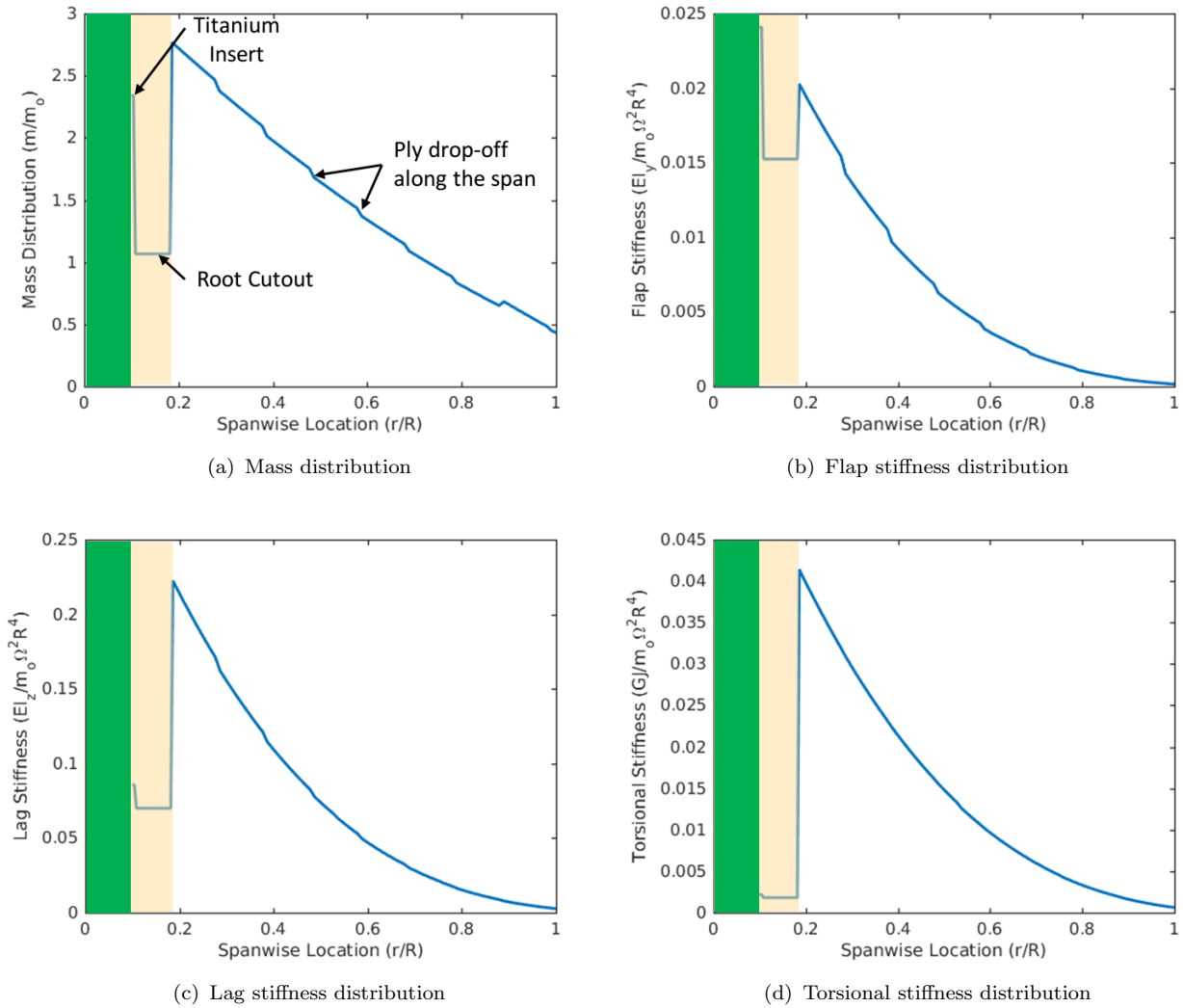
FIGURE 8.3: Sectional properties along the blade

frequency of the rotor.

Figure 8.4 shows the fan plot for *Elysium's* rotor. Because the blade is both highly twisted and highly tapered, significant coupling is observed between the lag and flap modes. The rotor is semi-articulated and soft in-plane with a first lag frequency of 0.618/rev. While stiff in-plane rotors alleviate concerns about air and ground resonance, they come at the expense of transmitting higher steady and vibratory loads and were therefore not selected. The first flap frequency of the rotor is 1.047/rev, which corresponds to an equivalent hinge offset of 4.4%. The first five frequencies are provided in Table 8.2. These modes are sufficiently far away from the operational RPM over the entire mission, thereby avoiding resonance. This allows the rotor to continuously vary its RPM throughout the entire mission without the need for discrete step changes in RPM to avoid resonance. All other rotor frequencies are above 10/rev.

8.1.4   Aeroelastic Analysis

Aeroelastic instabilities from pitch-flap and flap-lag coupling were considered during the rotor design by performing an eigen-analysis on the appropriate mass, damping, and stiffness matrices

TABLE 8.1: Individual component contributions to total blade weight.

Component	Weight, lb (N)	Weight %
Spar	8.94 (39.8)	47.2
Skin	5.03 (22.4)	26.6
Tungsten weight	2.57 (11.5)	13.6
Stainless steel strip	1.33 (5.93)	7.04
Honeycomb	0.84 (3.75)	4.46
Titanium Insert	0.12 (0.53)	0.63
Rohacell Foam	0.085 (0.38)	0.45

FIGURE 8.4: Fan plot showing rotor frequencies as a function of rotor rpm.
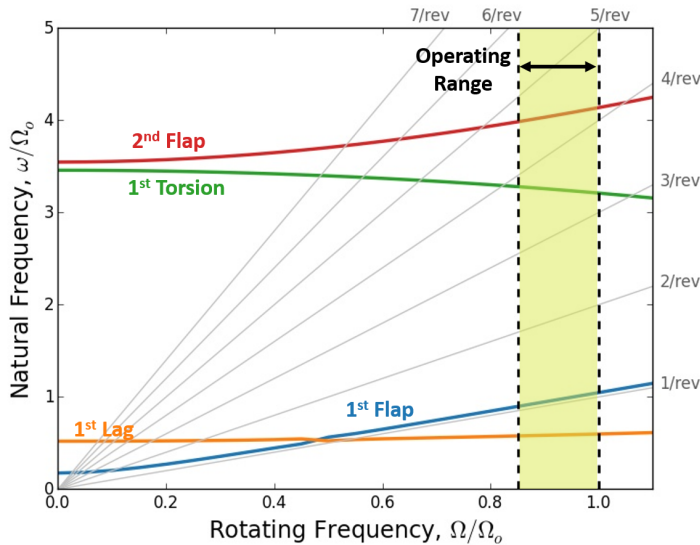
TABLE 8.2: First 5 rotor frequencies (/rev)

Mode	Time t = 0 hrs	Time t = 24 hrs
1st Lag	0.618	0.701
1st Flap	1.047	1.055
1st Torsion	3.21	3.86
2nd Flap	4.14	4.69
3rd Flap	9.09	10.43

to ensure sufficient stability margin. Pitch-flap instabilities are related phenomena that couple the pitching and flapping motion of the blade and are most effectively managed by placing the blade center of gravity at or in front of the quarter-chord. Figure 8.5(a) shows the stability boundaries for pitch divergence and pitch-flap flutter as a function of the c.g. location and torsional frequency. With a torsional frequency of 3.21/rev and a c.g. at 24.9% of the chord, *Elysium's* blades are stable from both pitch divergence and pitch-flap flutter.

Flap-lag flutter involves the undesirable coupling of the flap and lag motion resulting from limited aerodynamic damping in lag. An in-plane damper located on the hub provides sufficient damping to prevent this instability. The root loci for flap-lag flutter are plotted in Fig. 8.5(b), which shows that the rotor is stable.

8.1.5 Ground Resonance

Elysium is a soft in-plane semi-articulated design, so ground resonance is an important consideration. The support frequencies of the landing gear were analyzed using a specially developed in-house 3D beam model, in which the skid landing gear were treated as beam elements with rigid body mass and inertia properties for the fuselage. The landing gear frequencies were 4.65 Hz and

(a) Pitch-flap stability boundaries

(b) Flap-lag stability roots
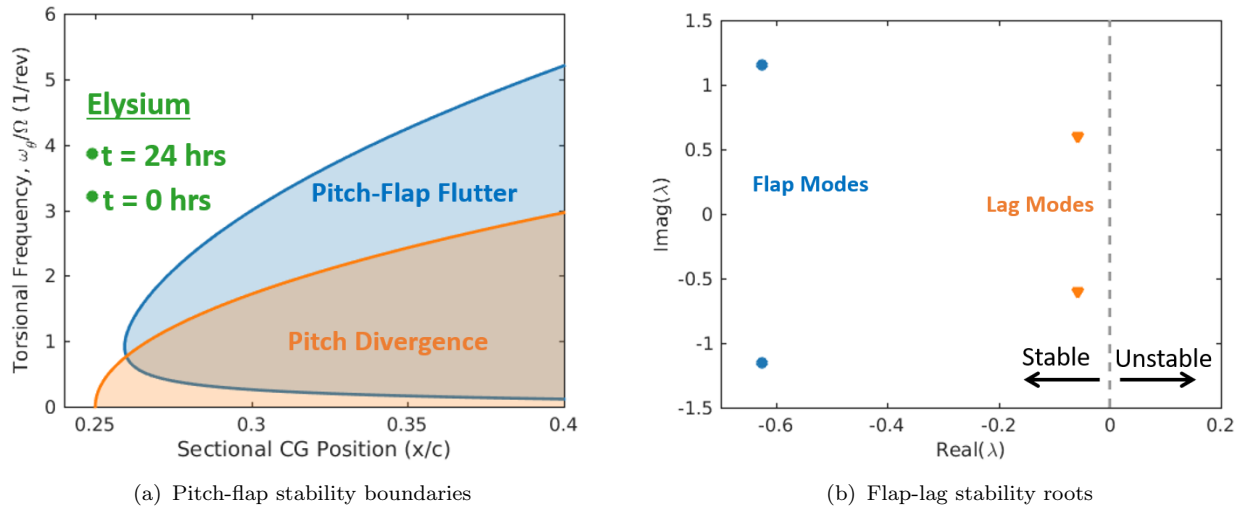
FIGURE 8.5: Aeroelastic Stability Boundaries
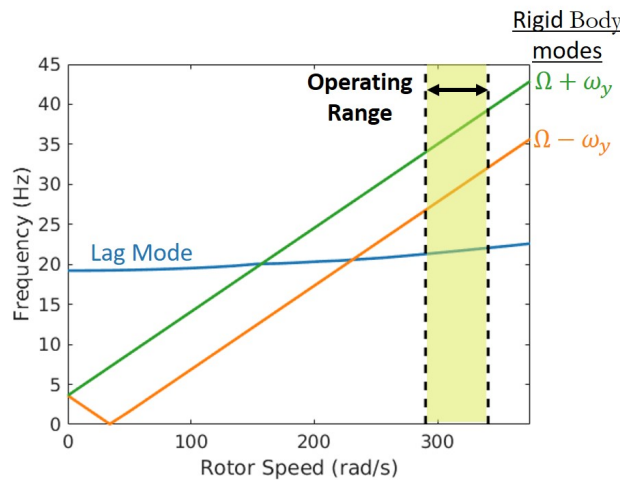
FIGURE 8.6: Stability analysis of ground resonance for the two-bladed semi-articulated rotor in the rotating frame.

3.61 Hz for body pitch and roll, respectively. The elastomeric dampers used on *Elysium's* semi-articulated hub have a relatively large damping ratio of 0.1 [18] and therefore only require a small amount of support damping to remain stable from ground resonance. Figure 8.6 shows the uncoupled ground resonance results for *Elysium's* two-bladed rotor, from which it can be seen that the rigid body modes and lag modes are sufficiently separated. Using the Deutsch criteria for two-bladed rotors, a more detailed ground resonance analysis was considered throughout the range of operational RPM, from which it was found that the inherent material damping of the skid landing gear was more than sufficient to prevent ground resonance. This material damping was also found to stabilize the shaft critical mode, which can only be stabilized by the support damping.

Main Rotor Assembly
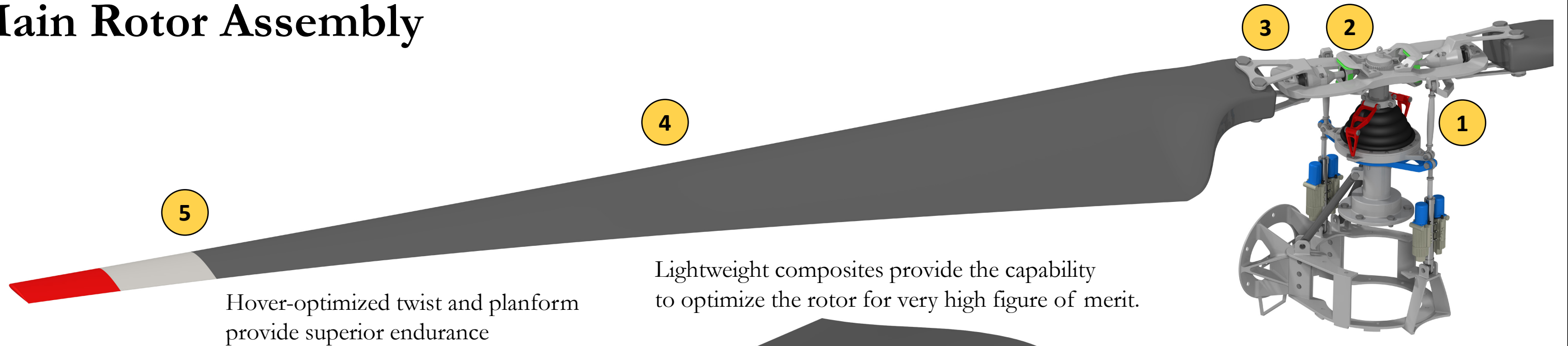
Hover-optimized twist and planform provide superior endurance

Lightweight composites provide the capability to optimize the rotor for very high figure of merit.

4 Bi-linear Twisted Blades

5 Blade Structure

Mono-cyclic swashplate provides mechanical simplicity

Simple attachment of blades to the hub through titanium bolts

1 Swashplate Assembly

3 Blade Attachment

Mechanically compact and eliminates the need for continuous maintenance of hinges

2 Hub Assembly

9 Hub Design

9.1 Hub Selection

For the design of *Elysium*, various rotor hub systems were considered. The 24 hours of continuous operation demands a rotor hub design that is mechanically simple, while still providing the control authority to respond to wind gusts. Ultimately, these constraints led to the selection of a semi-articulated rotor hub. The following qualitative assessments were used while comparing the different hub configurations.

Articulated: Articulated hubs utilize mechanical hinges in flap, lag, and pitch, which makes them mechanically complex with a high part count. These hubs also require continuous maintenance to ensure that the hinges are properly lubricated and free of contaminants, and are therefore not well suited for *Elysium's* 24 hour mission.

Teetering: In a teetering rotor, the two blades are rigidly connected and flap together about a teetering hinge. This eliminates much of the mechanical complexity associated with an articulated rotor, while still avoiding the transfer of vibratory flapping moments to the hub.

Semi-Articulated: Semi-articulated hubs use a flexure to control the flap motion of the blades and an elastomic bearing and lead-lag damper for the pitch and lag motions. These hubs are mechanically compact and eliminate the continuous maintenance associated with mechanical hinges.

Hingeless: Unlike semi-articulated hubs, hingeless hubs use the flexure to control both flap and lag motion while still using a bearing to control pitch. Because the flap and lag motion are both controlled by the flexure, these hubs often have significant flap-lag coupling and high vibratory loads.

Bearingless: Bearingless rotors are mechanically simple designs in which all three degrees of motion are controlled by the flexure design of the hub. However, because of redundant load paths, these designs add a significant level of complexity to the structural dynamics design and, because they have little in-plane damping, are more susceptible to aeromechanical instabilities.

The semi-articulated rotor provides a hub which can withstand the long duration of *Elysium's* mission with minimal maintenance. The elastomeric bearings and dampers used in the semi-articulated design provide a maintenance-free operation and are naturally fail-safe due to wear being gradual and visible [19]. While the teetering rotor was also an attractive option, it still uses a mechanical hinge which requires more maintenance than a semi-articulated rotor. Since the majority of the mission is spent in hover, during which the loads are steady, the teetering rotor will behave in the same manner as a semi-articulated rotor, such that the blades on both rotors would be subjected to the same loading. Finally, because the disk loading and therefore download of the rotors are relatively low, vertical gusts can place a teetering rotor into a low-g vertex ring state substantially increasing the possibility of mast bumping. Based on these considerations, the semi-articulated rotor is selected for *Elysium's* design.

9.2 Hub Design

A semi-articulated rotor can be categorized into one of two groups based on the location of its components and the transfer of loads. The first configuration, used most notably in Bell helicopters such as the 412 and 429, has the pitch-lag bearing and blade grip mounted within

an opening in the flap flexure. These are located outboard of the lag damper, and centrifugal load is transmitted through the flexure. The second configuration, used by Airbus Helicopters for the Dauphin and other models, has the pitch-lag bearing inboard of the flexure. The blade grip, which takes the centrifugal load, is composed of two beams above and below the flexure. In this configuration, the lag damper is mounted at the blade-end of the flexure within the blade grip.

The choice between the two semi-articulated layouts was driven by a desire to have smaller, lighter components with a low flap frequency, which led to the selection of the first configuration. This configuration has the advantage of a smaller blade grip and a flexure that begins closer to the rotor shaft, which reduces the virtual hinge offset and therefore the flap frequency. This also results in a reduction of the loads and vibrations experienced by the hub at the expense of maneuverability, which was not a main design driver for the *Elysium*. The final hub, shown in Fig. 9.1, is composed of the main components summarized below.
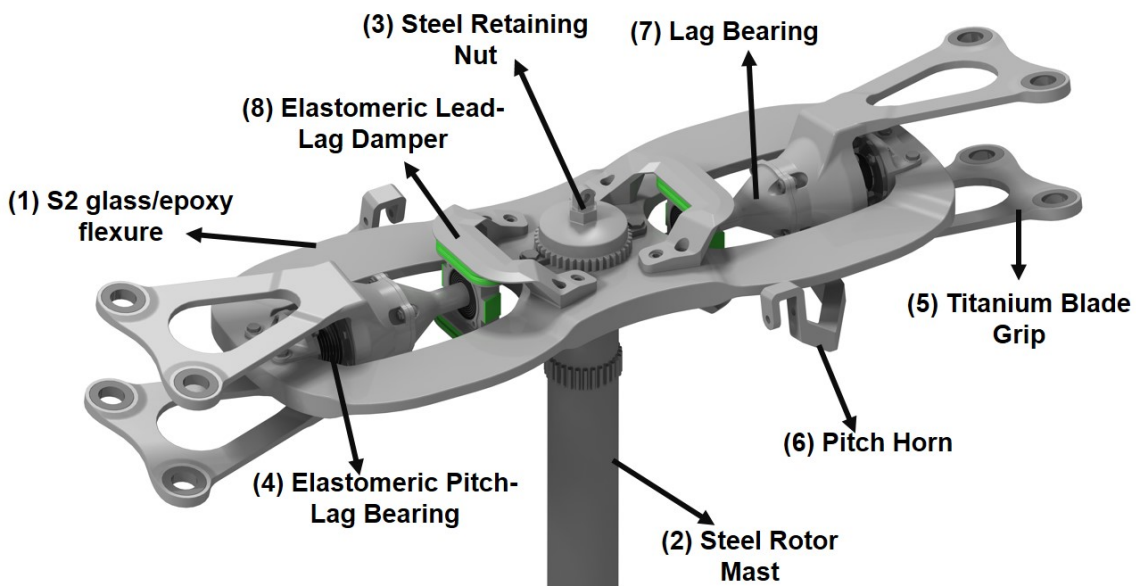
FIGURE 9.1: Rotor hub components.

Flap Flexure: The flexure (1) is essentially two parallel flat beams joined together and thickened at both ends where the mounting bracket and rotor shaft connect. At the center of the flexure and integral to the fiberglass layup is a splined cylinder that mates with splines on the main rotor shaft (2). The flexure is installed by sliding its splines and those of the shaft together until the flexure comes to rest on a flange extruded from the shaft. A retaining nut (3) is then torqued onto the flexure and locked in place with two locking tabs which bolt to the flexure to prevent the hub from detaching during flight. From the flexure, the rotor mast experiences flap and lead-lag forces from the blades as a bending moment and torsion, respectively, while lift is seen as an axial load.

Pitch-Lag Bearing: All of the pitch and lag motion as well as the centrifugal, lift, and drag loads are transferred through the blade grip into the pitch-lag bearing (4). The spherical bearing, similar to those manufactured by LORD, has alternating layers of thin metal shims and elastomeric material. It compresses from the centrifugal, lift, and drag forces, but shears due to torsion and lead-lag. Lag motion occurs about this bearing, at 6.2% span.

Blade Grip: The blade grip (5) has the rotor blade attachment points: two 0.75 in. (1.905 cm) diameter holes in flanges that slide over the blade. All the blade loads pass through these flanges: centrifugal, lift, and drag forces as well as pitch, lag, and flap moments. The forces and moments are transferred to a hollow casing where the pitch horn is joined and the pitch-lag bearing is bolted. The flanges have a void in the center to reduce weight and are thicker around the blade attachment points and casing connection where stress concentrations occur.

Pitch Horn: Integral to the blade grip, the pitch horn (6) passes under the flexure and has a mounting position for the pitch link ball joint. It experiences the pitching moments as bending stresses and transmits these loads axially into the pitch link. The pitch horn is mounted near the center of the flexure, which allows the pitch links to be mounted nearly vertically without increasing the size of the swashplate. The blade can experience up to 23° of pitch from its nominal position before the pitch horn contacts the flexure. The moment arm of the pitch horn is 5.19 in., therefore to achieve 1° of blade pitch, the actuator must stroke 0.091 in. (0.23 cm).

Lag Damper Bearing: Lag motion is transferred from the blade grip through a lever arm (7) into a spherical elastomeric bearing housed within the lag damper. Because the lag and flap hinges are outboard of the lag damper, this bearing will experience compression due to the lever action as well as rotation along both axes. Similar to the pitch-lag bearing, it has alternating layers of thin metal shims and elastomeric material.

Lag Damper: The lag damper (8), sometimes called a frequency adaptor, is connected to the lag damper bearing and experiences shearing due to lead-lag motion and compression due to flapping. Rather than connecting the lag damper to a separate plate floating over the flexure as seen on some hubs, the lag damper is bolted directly to the flexure to lower the weight of the damper housing. The lag damper is positioned close to the rotor mast to maximize the lever arm from the pitch-lag bearing and increase its damping effectiveness.

9.2.1 Flexure Design

The hub flexure must transmit all the loads, excluding the pitching moment, to the mast while remaining flexible to maintain a low flap frequency, therefore requiring a detailed design. To provide these characteristics, the flexure is made of S2 glass/epoxy, due to its improved fatigue and mechanical strength when compared to other glass/epoxy composites and its greater flexibility when compared to graphite/epoxy composites. The flexure was initially designed by modeling both strips of the flexure using the team-developed non-linear beam analysis coupled with the aeroelastic

FIGURE 9.2: Virtual flapping hinge of flexure.

analysis of the blades. This analysis led to each of the flexural strips being 1.7 in. wide by 0.36 in. thick (4.32 by 0.91 cm). The predominant loading in the flexure is axial, and to maximize its strength while also reducing the probability of coalescing of microcracks, a ply layup of $[(0)_2/90/(0)_2/\pm45/(0)_2]_{6s}$ was used.
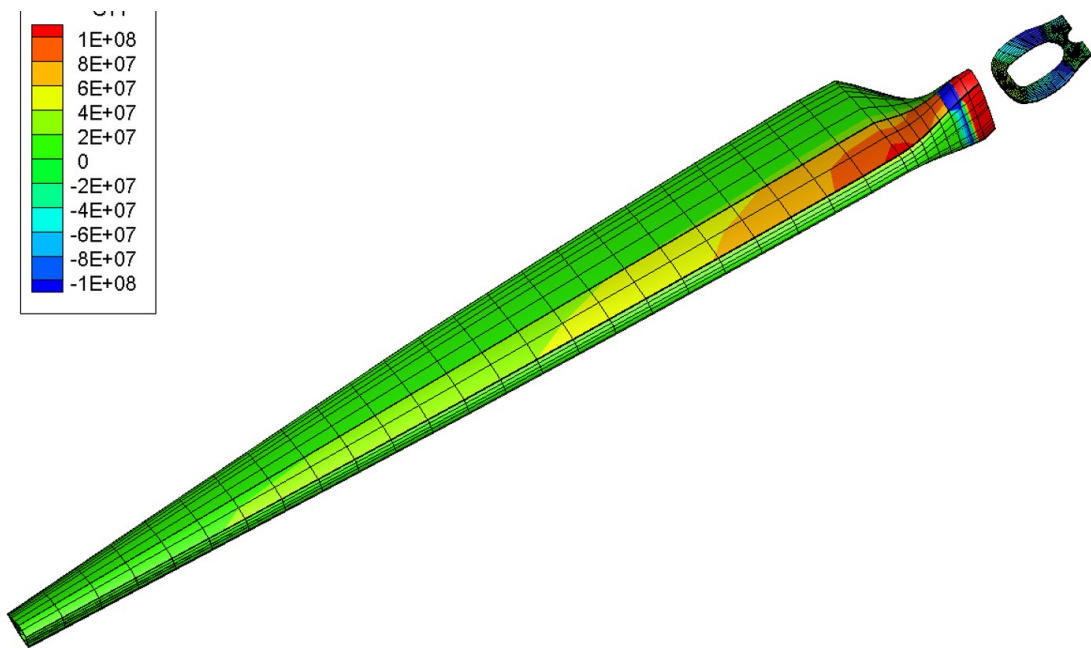
FIGURE 9.3: Full structural analysis in hover.

The final flexure design is stiff in lead-lag, allowing the rotor to lag primarily about the pitch-lag bearing, but flexible in flap, with a virtual flap hinge of 4.4%, as shown in Fig. 9.2. The desire to keep the pitch link vertical and also minimize the size of the swashplate resulted in the virtual flap hinge and pitch link not being coincident. While this introduces a small amount of positive δ_3 coupling, the aeroelastic analysis showed that this coupling had only a minor impact on the stability.

TABLE 9.1: Effect of blade pre-cone angle on maximum blade moment.

Blade pre-cone, β_p [deg.]	Max Flap Moment [ft-lb]	Max Flap Moment [N-m]
0	3081	4177
1	2107	2857
2	1073	1455
2.25	**948**	**1285**
2.5	1081	1466
3	1373	1862
4	2044	2771

Using the in-house, team-developed aeroelastic trim analysis, variations in the pre-cone angle were studied to create a design which minimizes the blade and hub stresses. The results of this analysis are summarized in Table 9.1, which shows that a pre-cone of 2.25° reduces the maximum flapping moment by 69%. A pre-lag of 1° was also designed into the flexure to reduce the lead-lag moment at the hub.

To substantiate the initial sizing of the hub, a 3D analysis of the hub and blade was performed using X3D, a finite element tool capable of generating a trimmed solution for a helicopter. The load case considered during the analysis was hovering, as this is the primary objective of *Elysium's* mission. The two components considered in the analysis were the hub flexure and the blade, with the other components being represented by flexible joints. For the analysis, the hub was considered fixed about the rotor shaft and the rotor was trimmed to the aerodynamic loads in hover. The maximum compressive stress in the flexure was 37.6 ksi (259 MPa) which when applying the Tsai-Wu failure criteria resulted in a minimum safety factor of 1.87, which agreed well with the initial beam calculations of 1.67.

(a) Axial stress.

(b) Axial strain.

FIGURE 9.4: Hub flexure detailed results in hover.

9.3 Swashplate Design

Elysium utilizes a specially-designed half-cyclic swashplate system, which tilts only in the direction of the longitudinal axis of the rotor tip path plane. The unique half-cyclic system was selected because, while longitudinal cyclic provides pitch control for *Elysium's* side-by-side rotor system, lateral control is achieved using differential collective. In a similar way, the Boeing CH-47 Chinook is a twin rotor that uses differential collective between its fore and aft rotors to alter the longitudinal pitch of the vehicle. Thus for simplicity, redundancy, and to minimize vehicle weight, the addition of lateral cyclic control was determined to be an unnecessary requirement for the swashplate.

A swashplateless design utilizing trailing edge flaps on each blade to achieve control was initially considered for its light weight and low part count; however, the use of trailing edge flaps also introduces a number of challenges that would negatively affect the simplicity and reliability of the vehicle. Trailing edge flaps, though beneficial in high speed forward flight, have a relatively low technology readiness level compared to typical swashplate drive systems and are not reliably capable of withstanding the high centrifugal loading of hover. For these reasons, a swashplateless hub was rejected in favor of *Elysium's* swashplate design, shown in Fig. 9.5.

The top of the swashplate system clamps onto the main rotor shaft via a splined collar that meshes with matching splines on the shaft, creating a solid connection to efficiently deliver the torque from the main rotor shaft into the swashplate. Pin joints on the clamp connect to two rotating scissor linkages; *Elysium's* swashplate design has two rotating scissors for additional redundancy during the extended operation of the design mission. Because these linkages are subjected to a great deal of wear from constant cyclic loading during flight, utilizing two scissors adds redundancy and safety to *Elysium's* design [20]. The lower half of the rotating scissors attach to the rotating swashplate via a ball joint that is held in place by two thin metal tabs, allowing the rotating swashplate to tilt freely about the lower half of the scissor linkage.

The rotating swashplate is divided into an upper and lower half that encases the outer race of an angular contact bearing, which serves as the bridge between the fixed and rotating swashplates. Similarly, the fixed swashplate surrounds the inner race of the contact bearing. In this way, the fixed and rotating swashplate components are able to rotate freely with respect to one another. Small extensions on the rotating swashplate, carefully sized to prevent any contact with the arms of the fixed swashplate extensions below, connect to the two pitch links via a ball-and-socket joint such that each pitch link is positioned parallel to the shaft.

The fixed swashplate clamps onto an aluminum spherical centering bearing in the center of the

(a) Swashplate Assembly.

(b) Internal view of the swashplate.
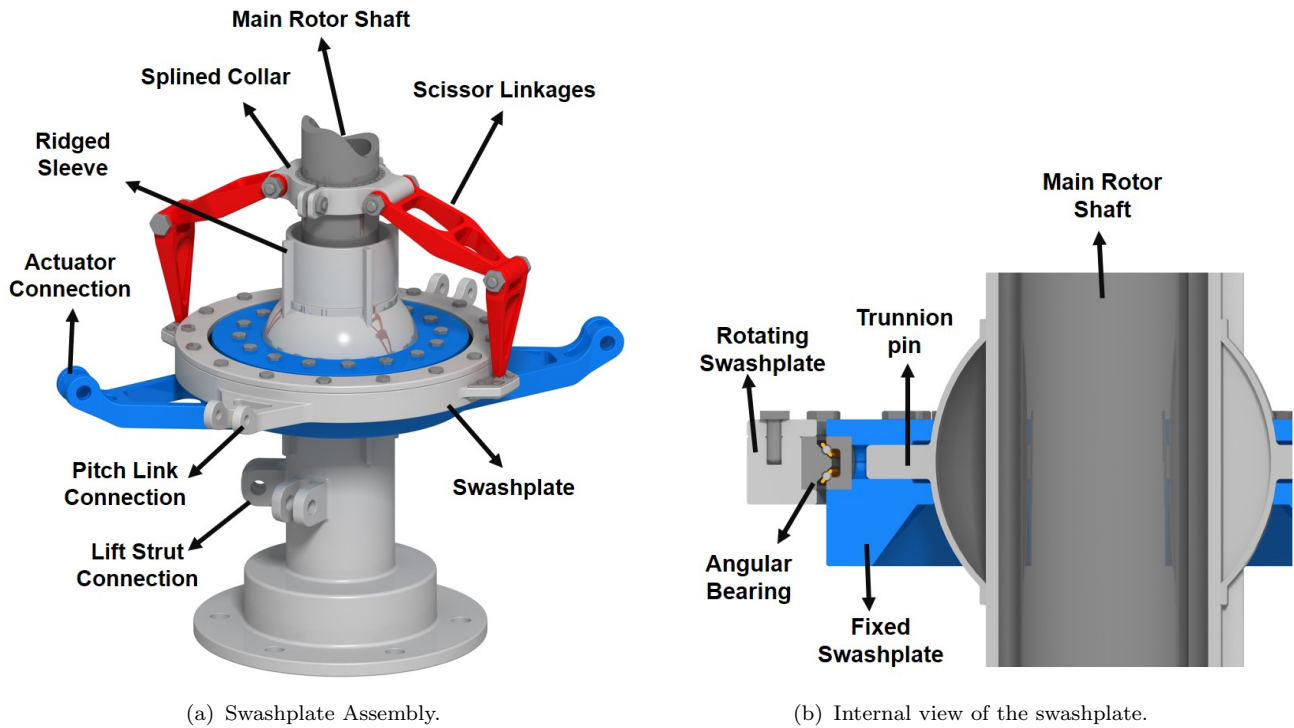
FIGURE 9.5: Components of *Elysium's* swashplate.

swashplate system, which supports both the fixed and the rotating swashplates and enables longitudinal tilting motion. The half-cyclic swashplate system does not require fixed scissor linkages to hold the fixed swashplate in place, and instead constrains its motion with pins and ridged connections. Two trunnion pins protruding from the spherical bearing restrict the swashplate to tilting about one axis, while ridges on the sleeve that encases the rotor shaft prevent rotation while allowing vertical translation. The inner diameter of the sleeve was sized to allow the shaft to slide into position before attaching the toothed clamp. At the bottom of the main rotor shaft, the sleeve fits over a set of bearings which allow the shaft to rotate while transferring the loads to the lift struts and the gearbox casing to which it is bolted.

10 Structural Design

Elysium's unique mission necessitates a structure that is both lightweight, to maintain a low empty weight, and durable, to withstand the dynamic loads of the 24 hour mission. Additional design considerations included the aerodynamic efficiency and transportability of the structure. The following sections outline the load path through the structural components of the airframe, starting from the nacelle and ending at the fuselage.

10.1 Nacelle Design

The nacelle is the main load-bearing structure that transfers the loads from the rotor into the arm and houses the gearbox, motor, electronic speed controller (ESC), radiator, fan, water pump, and coolant expansion tank. Though the nacelle skin is not load-bearing, it does have to withstand the vibration caused by the oscillatory rotor loads and the drag imposed on the vehicle during forward flight. The skin consists of four plies of high-temperature AS4 graphite-epoxy and is stiffened with four carbon composite stringers that run vertically from the top to the bottom

of the nacelle and five evenly spaced ribs that encircle the nacelle body. The stringers and ribs are positioned such that the inner components of the nacelle, such as the motor, radiator, or pump, can be removed. A panel with a clamshell door is secured with quarter-turn fasteners that enable quick access to the inner nacelle components. The skin is stiffened at the point where an aerodynamic fairing extends outward to envelope the arm, and fiberglass I-beams and vertical struts extend outward to secure the skin and stringers to the frame inside the nacelle.

(a) Nacelle structure with internal components.

(b) Nacelle structural components.
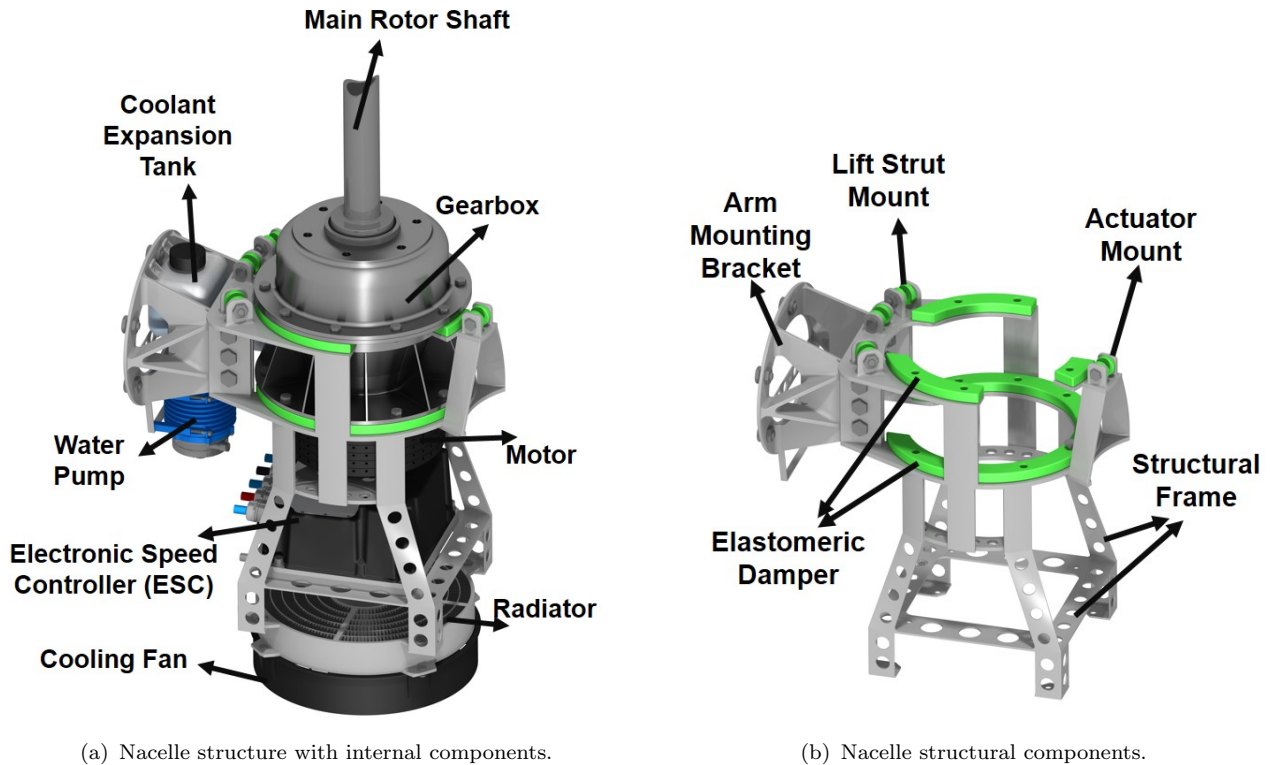
FIGURE 10.1: Nacelle structure with skin removed.

The frame is divided into two segments: the outer frame is a ring-like structure that houses the gearbox, motor, ESC, radiator, and fan, while the inner frame consists of an elliptical flange, brace plates, and supporting members that transfer the loads from the outer frame to the arm. In the portion of the outer frame that is not load-bearing, lightening holes are utilized to keep nacelle weight down. On the inboard section of the outer frame, there are three mount points where two lift struts and one actuator connect via pin joints. Damping pads are placed at the base of the gearbox and at the base of each strut and actuator to isolate vibration induced by the rotor.
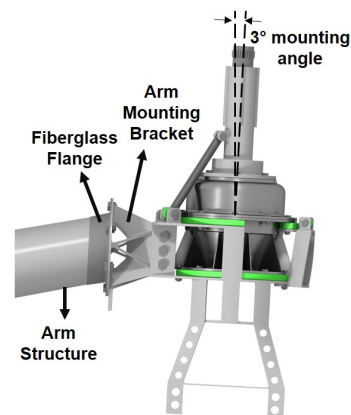
FIGURE 10.2: Attachment of the nacelle to the arm.

10.2   Nacelle to Arm Attachment

The nacelle and arm are connected through a fiber glass flange, which is bonded to the outer surface of the arm and bolts to the aluminum frame on the nacelle, as shown in Fig. 10.2. Fiber glass is chosen over graphite/epoxy composites to avoid corrosion of the aluminum frame, while the six bolts allow for easy disassembly of the structure during transportation. From the analysis of the arm structure, it was determined that the nacelle frame should be mounted to the arm at a 3° angle, such that the thrust generated by the rotor is used for generating lift, as opposed to producing side force.

10.3   Arm Structure Design

The twin rotor design of *Elysium* requires an arm structure capable of supporting the rotor loads in all flight conditions. Sizing the arm structure required careful consideration of both the structural and aerodynamic characteristics, both in hover and forward flight. Truss, stressed-skin, and wing structures were all considered in the initial design of the arms. Analysis of the truss structures, through a specially developed in-house 3D bar finite-element tool, showed that while the truss structure was the lightest option, it was also the largest structure in terms of cross-section and was most susceptible to critical failure modes, such as buckling. A wing structure provided the most aerodynamically efficient profile for forward flight, but was also the heaviest option because of the additional weight of the skin needed to form the aerodynamic profile. The stressed-skin structure provided a great balance of structural weight and aerodynamic performance, and was ultimately selected for the arm structure.

10.3.1   Cross Section Selection

While designing the arm structure, it was found that the deflection of the arm was a more critical constraint than the stress within the arm. An arm that was designed based on stress alone resulted in more than one foot of deflection at the tip of the arm; equivalent to more than 10° of rotation of the rotor plane, thereby reducing the hovering performance of the vehicle. Instead, the arms were sized by limiting the tip deflection to 0.45 ft (0.137 m), i.e., 3.8° of rotor plane rotation while maintaining the stress constraint. An elliptic cross-section was adopted and parametric sweeps were performed by varying the cross section geometry and taper ratio along the span of the arm, the results of which are shown in Fig. 10.8. Both the weight of the arm and the aerodynamic performance can be improved by increasing the beam taper, but manufacturing and assembly constraints limited the dimension at the tip, and therefore the possible taper to about 1.5. Because the primary load on the arm structure was due to the rotor thrust (along the b-axis of the ellipse), increasing the width of the ellipse (increasing a/b) resulted in a less weight efficient structure. However, lengthening the ellipse resulted in a lower drag coefficient due to reduced flat plate area, which significantly improved the forward flight capability with only a minor impact on the download penalty in hover. It was therefore decided that an elliptical cross-section, with a cross-sectional ratio of $a/b = 1.5$ and a beam taper of 1.54, provided the best balance of structural and aerodynamic performance.

10.3.2   Final Arm Design

Although global buckling of the structure was determined to be less of an issue, the large bending moments carried by the structure presented the possibility of localized buckling. Sheet and
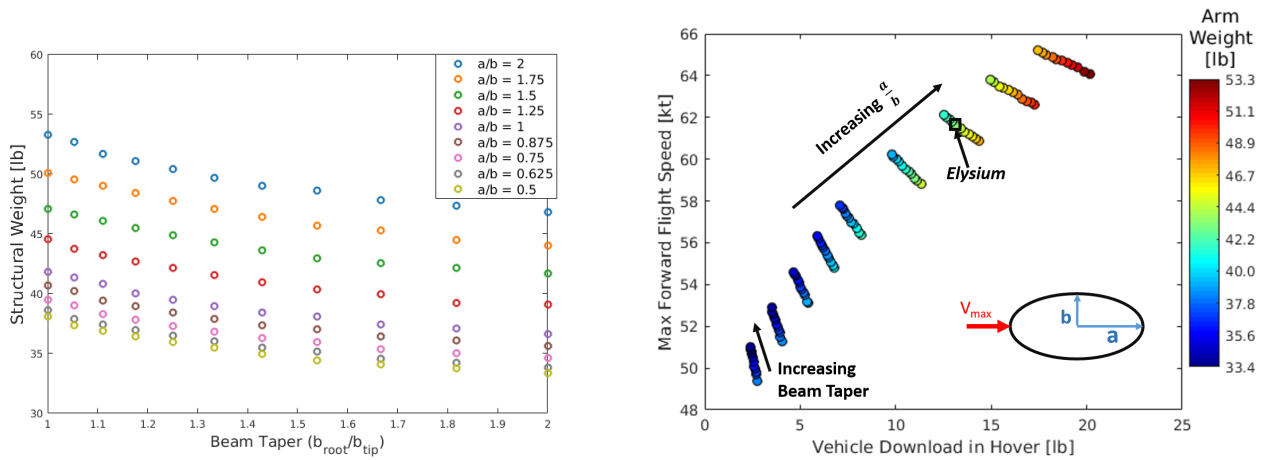
(a) Effect of beam taper and cross sectional geometry on arm weight.

(b) Effect of beam taper and cross sectional geometry on forward flight speed and download in hover.

FIGURE 10.3: Structural and aerodynamic performance of various arm geometries.

stringer as well as honeycomb sandwich designs are used to improve buckling resistance, with the honeycomb sandwich providing the same strength with an overall lighter weight [21]. A study of materials, including IM7, AS4, and T300 graphite/epoxies and S2 glass/epoxy, and ply layup was then performed to maximize the strength and stiffness of the arm, resulting in the structure shown in Fig. 10.4.
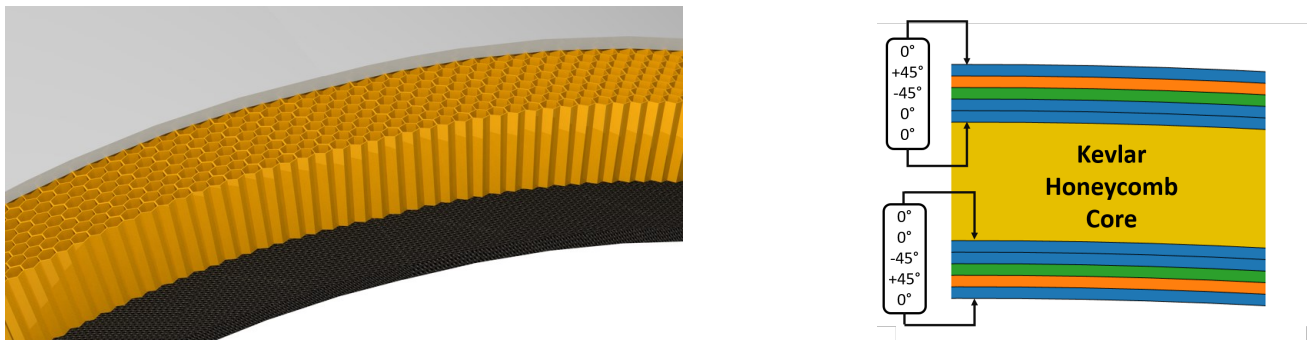
(a) Graphite/epoxy and Kevlar sandwich structure used for *Elysium's* arms.

(b) Arm composite layup (along top edge).

FIGURE 10.4: Arm structure of *Elysium*.

The arm's response to various load cases was evaluated using an in-house specially developed 3D finite element analysis, which provides the capability to analyze the static and dynamic responses of a composite structure with individual ply resolution. The specific conditions considered for this structure were hover at maximum weight, forward flight at maximum speed, response to a blade-out load in which one of the blades separates, a hard landing with a 3g vertical load, and a hard landing with a 1.5g lateral load. The response of the arm structure to each of these load cases is presented in Table 10.1. Because the arm is bolted directly to the bulkheads, the root of the arm is fixed in all degrees of freedom. For the hovering, forward flight, and gust response cases, the hub forces and moments are applied as distributed loads across the tip of the arm. For the hard landing, the rotor is considered to be non-operational to represent the most extreme case. Figure 10.5 shows the full stress distribution in the vehicle during hover, while Fig. 10.6

show the detailed stress distribution during maximum forward flight speed, hard landing with a 3g vertical load, and blade-out loading. Each of these detailed stress distributions are one foot sections of the arm starting from the arm-fuselage connection. The detailed analysis showed that the worst loading case was that of a blade-out loading, during which the safety factor was still 1.79.

TABLE 10.1: Arm Response to various load cases.

Load Case	Hover	60 kt Forward Flight	Blade-out Load	3g Vertical Load	1.5g Lateral Load
Max Tip Deflection [ft (m)]	0.629	0.815	0.874	-0.281	0.073
Max Tip Rotation [deg]	4.65	6.07	6.37	-2.08	0.045
Minimum Reserve Factor	2.10	1.82	1.79	4.71	25.9
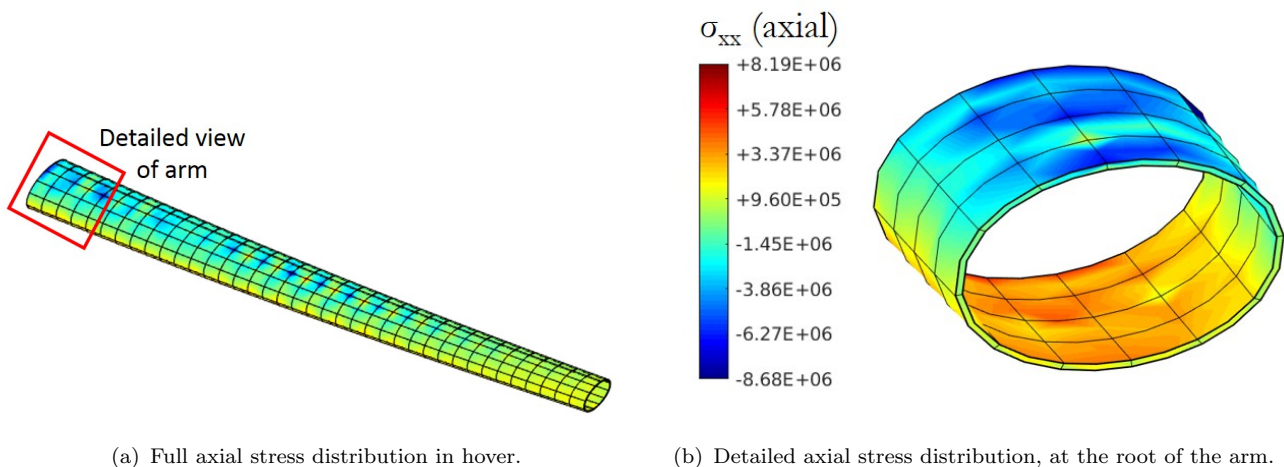
(a) Full axial stress distribution in hover.

(b) Detailed axial stress distribution, at the root of the arm.

FIGURE 10.5: Axial stress distribution in hover.

10.4   Arm to Fuselage Attachment

The arm structure supports all of the rotor loads during flight, which ultimately must be transferred to the main fuselage bulkheads. A wing box, as shown in Fig. 10.7, was designed to assist in transmitting the loads to the fuselage. The two main bulkheads form the sides of the wing box, through which the bending moments due to the rotor torque and the shear force from the rotor thrust are transmitted. The top of the wing box is a honeycomb sandwich structure with the fuselage skin forming the top of the sandwich structure and a horizontal plate forming the

(a) Axial stress at maximum forward flight. (b) Axial stress at 3g hard landing. (c) Axial stress in blade-out loading.
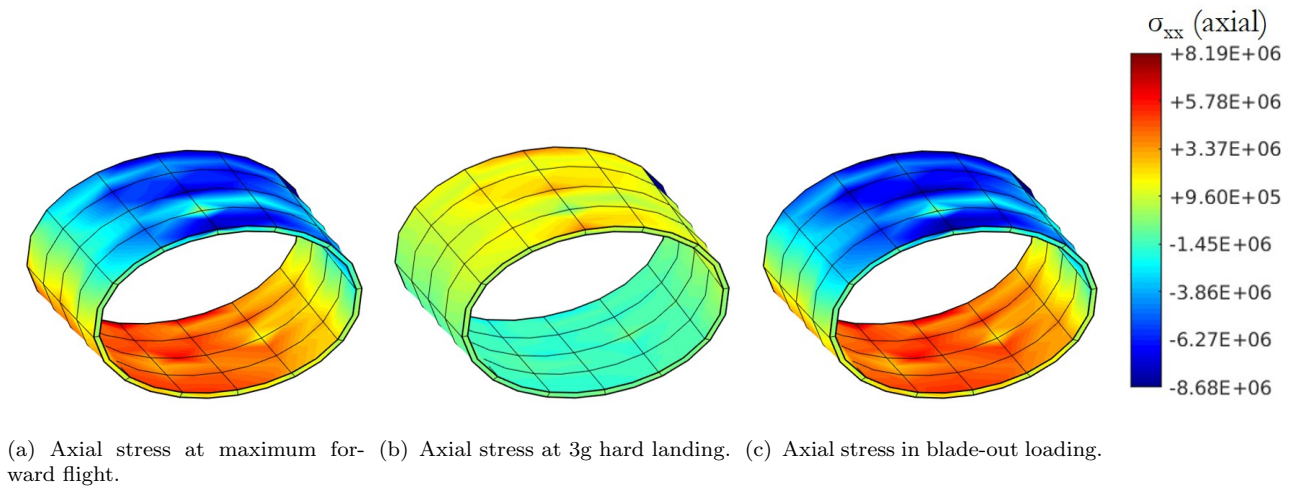
FIGURE 10.6: Axial stress distribution for various flight conditions.

bottom. Due to the large compressive force resulting from the bending moment from the rotor thrust, horizontal stiffeners run along the plate to increase axial stiffness and prevent buckling. The bottom plate of the wing box is also a honeycomb sandwich structure. Horizontal stiffeners run along this panel to provide additional axial stiffness required for withstanding the tensile force from the bending moment due to the rotor thrust.

(a) Detailed view of the wing box.

(b) Arm being attached to the fuselage.
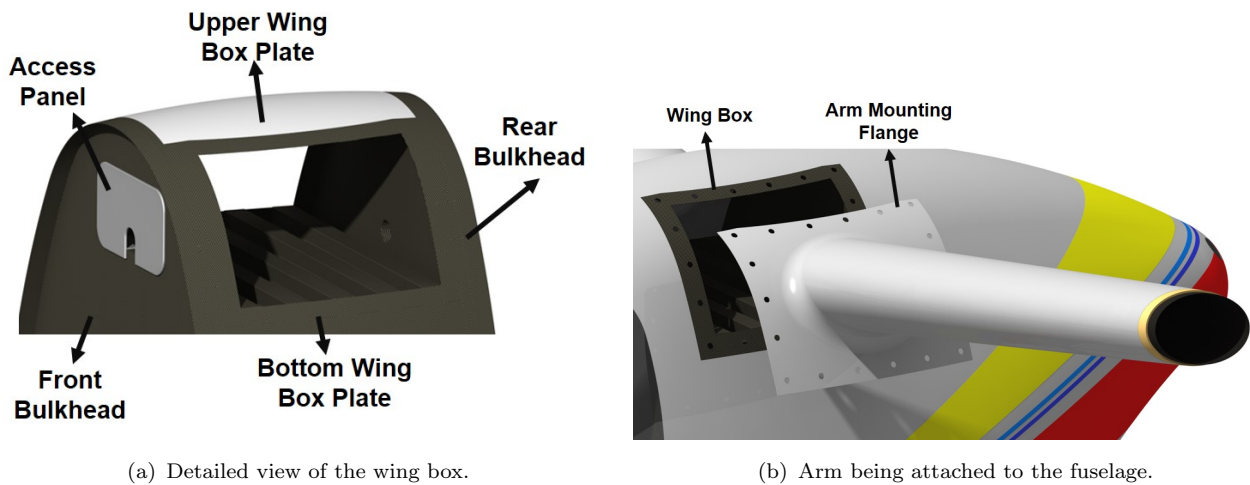
FIGURE 10.7: Wing box for mounting *Elysium's* arm to the fuselage.

The bottom plate of the wing box and the two main bulkheads are co-cured as separate parts and then co-bonded during the assembly of the fuselage. The top of the wing box is co-bonded to this structure afterwards with additional bolts provided for redundancy. *Elysium* has a relatively large longitudinal span of 51.7 ft (15.8 m) from rotor tip to rotor tip and, to ease in the transportation of the vehicle, each arm is connected to the wing box with 20 bolts; five along each of the edges of the wing box. The 12 in. by 6 in. (30.5 cm by 15.2 cm) access panel on the front bulkhead provides access to these bolts for purposes of assembly and dis-assembly of the structure.
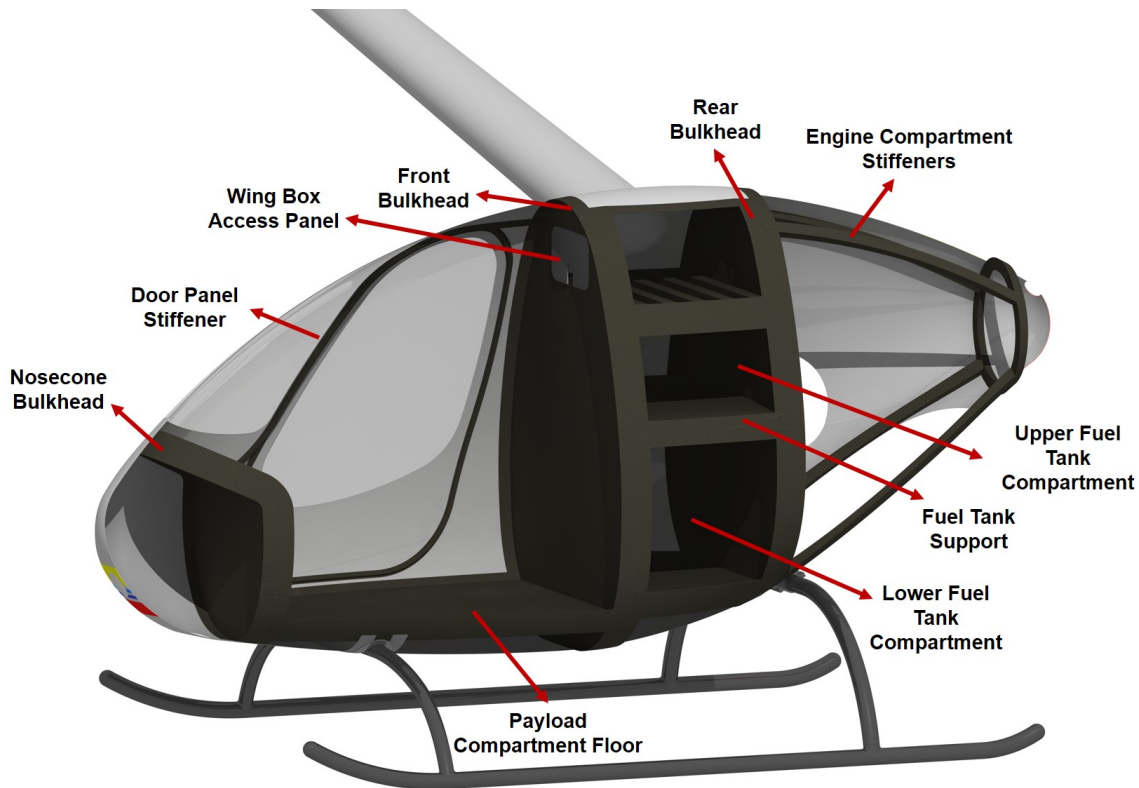
FIGURE 10.8: Main airframe structural components.

10.5 Fuselage Design

Elysium's airframe is a semi-monocoque design, composed of a composite frame with a honeycomb sandwich skin, with the main structural components highlighted in Fig. 10.8. Based on the requirements of this mission, the main drivers of the fuselage size were housing the simulated pilot, the fuel storage, and the propulsion system while supporting the loads from the rotors.

The primary load-bearing members of the fuselage are the two bulkheads that make up the fore and aft segment of the wing box, which carry the shear loads and bending moments from the two arms. The front bulkhead isolates the passenger from the fuel tanks, while the rear bulkhead separates the engine compartment from the fuel tanks. A removable 12 in. by 6 in. (30.5 cm by 15 cm) access panel in the fore bulkhead allows for easy maintenance of the fuselage-arm connections while maintaining the structural integrity of the bulkhead, and small openings in both the fore and rear bulkhead allow electrical wiring from the avionics suite and generator, respectively, to pass through the wing box to the arm structures. In addition to the protections provided by the fore bulkhead, the bottom of the wing box also acts as a firewall that separates and isolates the fuel tanks below. In accordance with Part 121, Section 247 of the FAR, the access panel and other apertures are sealed with fire-proof fittings such that no hazardous quantities of air, fluids, or flame can pass from the engine compartment to other parts of the vehicle. A 4 in. (10 cm) flange circumnavigating the two bulkheads forms the attachment point for the skin of the fuselage, and HI-LOK fasteners, commonly employed in commercial and military aviation, are utilized across the entire fuselage to provide consistent and uniform torquing requirements.

Four box-beam stringers form the frame of the engine compartment and terminate at a circular rib in the tail of the aircraft. Because the given mission will require 24 hours of hovering in place

with no significant airflow or downwash created by the twin rotors, a robust cooling system is required. Two circular radiators, one of which cools the engine while the other cools the generator, are mounted via brackets to the rear bulkhead. A fan attached to each radiator pulls in outside air to cool the system. A cutout 38 in. (96 cm) in length in the underside of the engine compartment and the two fans mounted on the sides of the fuselage allow for sufficient cooling by enabling the heat produced by the engine and accessory components to freely convect out of the fuselage. In the rear of the aircraft, the entire portion of the skin panel below the top stringers and between the rear bulkhead and the circular rib is a removable panel to allow unobstructed access to the engine compartment. The rear crosstube from *Elysium's* raised landing gear mounts to the rear bulkhead via brackets in the engine compartment, and the tail rib routes engine exhaust from the catalytic converter up and out of the rear of the fuselage; both features help to protect ground personnel from the fumes and prevent fire hazards that could be started by hot exhaust dispersed after landing the vehicle following the completion of a 24 hour mission.

Because this is such a high-endurance mission, a large quantity of fuel was needed to power the rotorcraft. The fuselage was designed such that the three fuel tanks (one fixed, two auxiliary) are located at the same fuselage station as the arm attachment points, ensuring that the thrust continues to act through the center of gravity (CG) of the vehicle as the fuel is depleted over the duration of the mission. Similarly, the other components in the aircraft were carefully positioned to keep the CG at precisely the same fuselage station; thus, as fuel is depleted, the CG range of the aircraft does not change more than 0.14 in. (0.36 cm) over the entire duration of the mission.

The skin of the nose cone, which is not load-bearing, is made of the same graphite-epoxy composite as the nacelles and the rest of the fuselage. The nose cone, which is hinged on one side, has quarter turn fasteners on the other for quick access and easy maintenance. The nose cone is separated from the passenger compartment by a fire-proof bulkhead, which insulates the inner components of the nose cone, including the batteries and avionics, from the rest of the aircraft. The avionics in the nose cone are carefully positioned to maintain an overall desirable CG location of the aircraft. The gimbal-mounted camera and LIDAR systems at the front of the nose cone are positioned out of the way of the landing gear, and allow unimpeded visibility in all directions.

In the event that *Elysium* were to be used for a passenger-carrying mission, the passenger compartment could be easily modified for passenger comfort. Interactive readouts could be mounted to the nosecone bulkhead and relay information to the occupant, and a large front window, positioned to give maximum visibility to the simulated occupant, would enable more than 180 degrees of lateral visibility.

11 Propulsion System

Based on the results of the vehicle sizing algorithm, *Elysium's* propulsion system was designed to provide each rotor with a maximum continuous power of 47.8 hp (35.7 kW) and an intermediate power of 51.6 hp (38.5kW). This section details the primary components, including the piston powerplant, DC brushless generator, rotor drive system, battery power system, thermal management system, and fuel management system, Fig. 11.1. *Elysium* utilizes separate DCBL controllers for the generator and rotor drive motors, to minimize electromechanical coupling. Additionally, *Elysium* has an emergency backup battery.
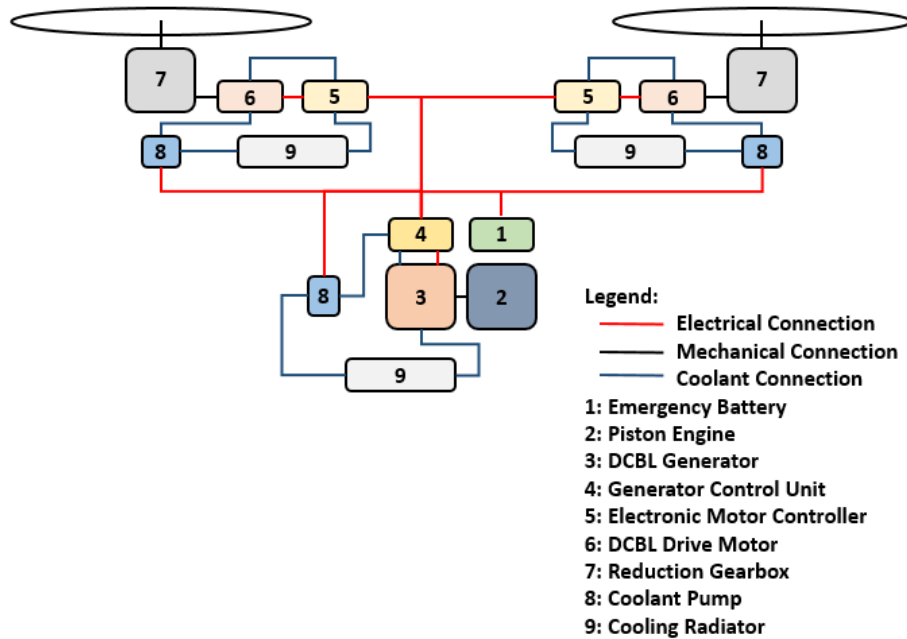
FIGURE 11.1: Conceptual layout of *Elysium's* propulsion system.

TABLE 11.1: Summary of Otto- and Diesel-cycle engine characteristics.

Feature	Diesel-Cycle Engines	Otto-Cycle Engines	Relative Advantage
Com-pression Ratio	12:1 to 16:1	8:1 to 12:1	High compression ratio increases efficiency work utilization, high compression ratio increase weight due to higher stresses
Throttle	Fuel regulation	Butterfly valve	Butterfly valves increase pumping losses by restricting air flow
Fuel	MOGAS, AVGAS	Jet-A, Diesel	Jet-A and diesel can gel at cold temperatures, diesels require glow plugs or heated fuel at low ambient air temperatures
Fuel Con-sump-tion	0.30-0.35 lb/hp-hr	0.31-0.5 lb/hp-hr	Use of electronic-control-and-fuel-injection systems have resulted in low fuel consumption for both types of engines

11.1 Piston engine trade study

An investigation of Otto- and Diesel-cycle engines and configurations is summarized in Table 11.1 and 11.2.

Table 11.1 compares four critical design differences between Diesel-cycle and Otto-cycle engines. With a high compression ratio, engines can utilize combustion energy more efficiently. Otto-cycle engines can not achieve the compression ratios of diesel engines due to premature ignition and knocking risks. Additionally, Otto-cycle engines throttle by restricting airflow which increases the pumping losses of the engine compared to diesel engines. Diesel-cycle engines with common rail direct fuel injection technology have better efficiencies than legacy Otto-cycle engines and

TABLE 11.2: Summary of investigated aviation engine configurations.

Feature	Side-valve	Overhead Cylinder/ Valve	Opposed Cylinder, Opposed Piston	Wankel
RPM	Low	Moderate	Moderate	High
Fuel compatibility	MOGAS, AVGAS	MOGAS, AVGAS, Diesel	MOGAS, AVGAS, Diesel	MOGAS, AVGAS, Diesel
Complexity	Low	Moderate	High	High
Technology Readiness Level	9	9	7	9

have brake specific fuel consumption (bsfc) values lower than 0.35 lb/hp-hr (0.213 kg/Kwh). The use of electronic fuel injection and ignition in Otto-cycle engines has resulted in bsfc lower than 0.35 lb/hp-hr (0.213 kg/Kwh) and specific powers approaching 0.8 hp/lb (0.49 kW/kg).

Engine configurations can greatly influence the performance parameters of an engine. The friction between a piston and cylinder accounts for approximately 10% energy input into the engine. As a result, friction losses of the engine increase as rpm increases [22, 23].

- Engines with overhead cylinders and valves operate at higher RPMs and compression ratios compared to earlier side-valve engine to achieve higher power. This configuration adds complexity and weight to the engine.

- Wankel engines have fewer reciprocating parts and a higher power-to-weight ratio than piston engines while operating at higher RPMs. However, Wankel engine technology has issues with maintenance and reliability.

- The sidevalve engine is a compact, low-rpm engine that has decreased sensitivity to low-octane fuels. Unlike the previously discussed configurations, side-valves has increased reliability as a valve failure will not result in an inoperable engine.

- Opposed-piston, opposed-cylinder (OPOC)engines are claimed to be up to 30% more efficient than modern Diesel-cycle and 50% more efficient than Otto-cycle engines. Achates Power has been developing OPOC technology since 2004 and has announced that the light-duty prototype would be produced by 2018 for testing [24]. At the present, OPOC engine technology is not ready for an aircraft required to be designed, built, and tested in the next 3-5 years.

Based on a comparative analysis of modern aviation engines, The LF-39 engine, produced by D-motor in limited rate production, was selected as the baseline engine for *Elysium*. The LF-39 was selected due to its low bsfc, high specific power (0.687 hp/lb)(including all engine accessories), low cost, increased safety, and its innovative application of existing technology to reduce fuel consumption. This engine is a six-cylinder, 4-stroke, direct-drive, side-valve engine with a liquid cooling system, electronic fuel injection. The LF-39 also has an integral starter, alternator, oil pump, and water pump with a wet weight of 189.2lb (86kg). The power ratings of this engine are:

- Maximum Power: 130 hp (97 kW)

- Intermediate Power: 125 hp (93 kW)

- Max Continuous Power (at 2,850 RPM): 117hp (87kW) Dynamometer tests show that this engine has a bsfc of 0.312 lb/hp-hr (0.19 kg/kWh)[25].

11.2 LF-39 MD

The LF-39 MD engine, shown in Fig. 11.2, is a modified D-motor LF-39. In addition to being resized to increase power to a maximum power of 140hp (104kW) and a maximum continuous power of 125hp (93kW) at 2850 rpm, the engine has been modified to reduce emission and improve bsfc.
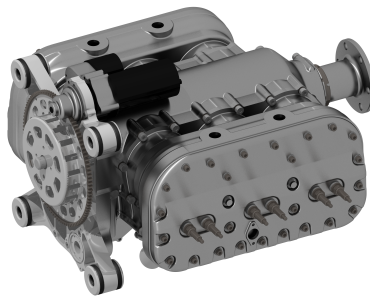
FIGURE 11.2: LF-39 MD engine.

With a wet weight of 203.5lb (92.5kg), the LF-39 MD includes the following technologies to increase performance and reduce sfc:

- Pop-up cylinders to increase compression ratio,

- An optimized combustion chamber with turbulence grooves to increase fuel-air mixing,

- An ultralow-friction cylinder surfacing, expected to reduce fuel consumption by 3% [26].

The LF-39 MD is capable of using 98 Octane MOGAS and includes a catalytic converter system to reduce emissions. Figure 11.3 shows the bsfc as a function of power for the LF-39 MD engine. This figure has been generated by averaging the bsfc for the LF-26, Rotax 912 ULS, and Rotax 912 IS engines[27–29]. An installation loss of 10% and bsfc reliability factor of 1.05 has been included in power and fuel consumption calculations to account performance losses not considered.

11.3 LF-39 MD Lubrication

The engine uses a dry-sump lubrication system. According to 14 CFR Part 27 Section 1011, it is necessary to provide a usable oil capacity of one gallon for every 40 gallons of fuel. Therefore the usable oil capacity is 2.5 gallons (2.1 required, 0.4 margin) with a 10% tank expansion margin.

The engine-driven pressure and oil scavenge pumps circulate oil between the engine and the oil tank. An engine mounted oil-filter provides particulate removal. Conical screen filters are placed on each scavenge line to protect the pumps from failure, and chips detectors are located downstream of the dry sump scavenge pump.
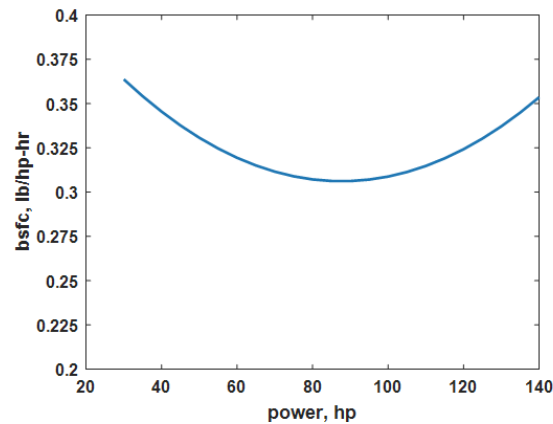
FIGURE 11.3: Brake specific fuel consumption from idle to maximum rated power.

TABLE 11.3: Summary of DCBL configurations.

Feature	Joby Motor JM series	Launchpoint Halbach arrays	Compact Dynamics	EMRAX electric motors
Efficiency at 2,800 RPM	<90%	<90%	<90%	>95%
Technology Readiness Level	7	7	8	9
Cost	>\$5,000	>\$5,000	>\$5,000	<\$5,000
Maximum Power of Expected Product Line	19 hp	134 hp	65 hp	200 hp
Cooling Options	Air-cooled Only	Air-cooled Only	Liquid-cooled Only	Air-cooled and/or Liquid-cooled

11.4 Electric motor and generator trade study

While selecting a DCBL generator, it is necessary to match generator characteristics to power-plant characteristics. Similarly it is necessary to match the motor characteristics with the rotor characteristics. Since the LF-39 operates at 2,850 RPM, the ideal DCBL motor and generator would have peak efficiency near 2,800 RPM and have a specific mechanical power greater than 1.0 lb/hp-hr. Table 11.3 gives a comparison of the Joby Motor JM series, the Launchpoint Halbach arrays, the Siemens/Compact Dynamics aviation prototypes, and EMRAX electric motors.

The Joby JM series motors and Launchpoint Halbach arrays, are air-cooled DCBL motors, which operate most efficiently at speeds greater than 5,000 rpm. Both have efficiencies below 90% at 2,800 rpm which make them unsuitable for pairing with the D-motor L-39 engine from a fuel consumption and thermal management viewpoint. Compact Dynamics offers 33.5hp (25kW) and 73.7hp (55kW) motors based off of the Siemens motors. The motors are liquid-cooled so they do not have the cooling issues at lower rpms like the Joby and Launchpoint motors. These motors also operate most efficiently above 5,000 RPM and have efficiencies below 90% at 2,800 RPM which make them unsuitable for pairing with the D-motor L-39 engine. The EMRAX motors are low-cost motors that were originally designed for aviation. While the motors produce maximum power at 5,500 RPM, maximum efficiency occurs between 1,500 and 3,500 RPM. The EMRAX

Power Systems

The novel hybrid power system uses a 98 octane MOGAS 125 hp piston engine coupled to a 110 hp electric generator, which powers two 51 hp electric motors in the rotor nacelles

The low fuel consumption engine and high efficiency electrical system allow Elysium to achieve 24 hours of hover

Coolant Tanks

Fuel Filter

Fuel Pump (hidden)

Engine

Generator

Exhaust

Water Pump

Engine Control Unit

Fan

Radiator

Catalytic Converter

Generator Control Unit

Oil Tank

Coolant Expansion Tank

Main Rotor Shaft

Gearbox

Water Pump

Electronic Speed Controller (ESC)

Electric Motor

Cooling Fan

Radiator
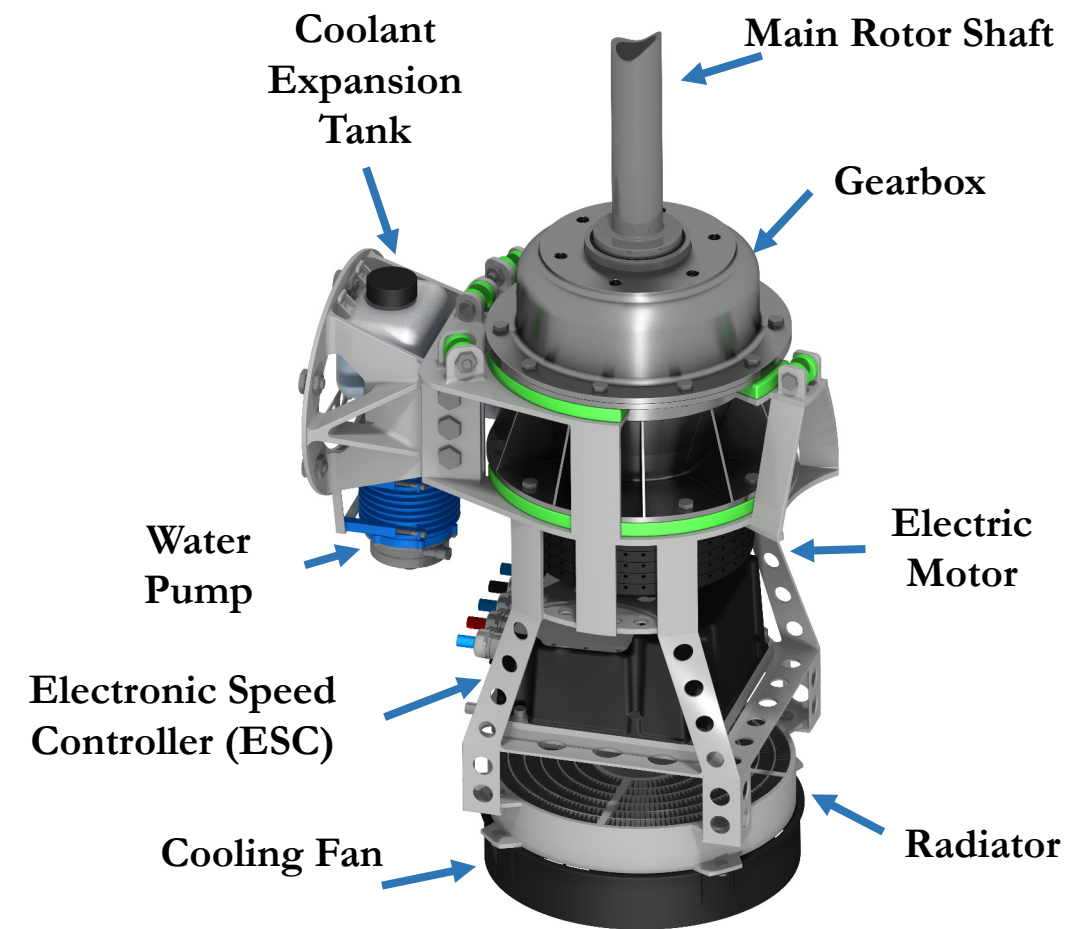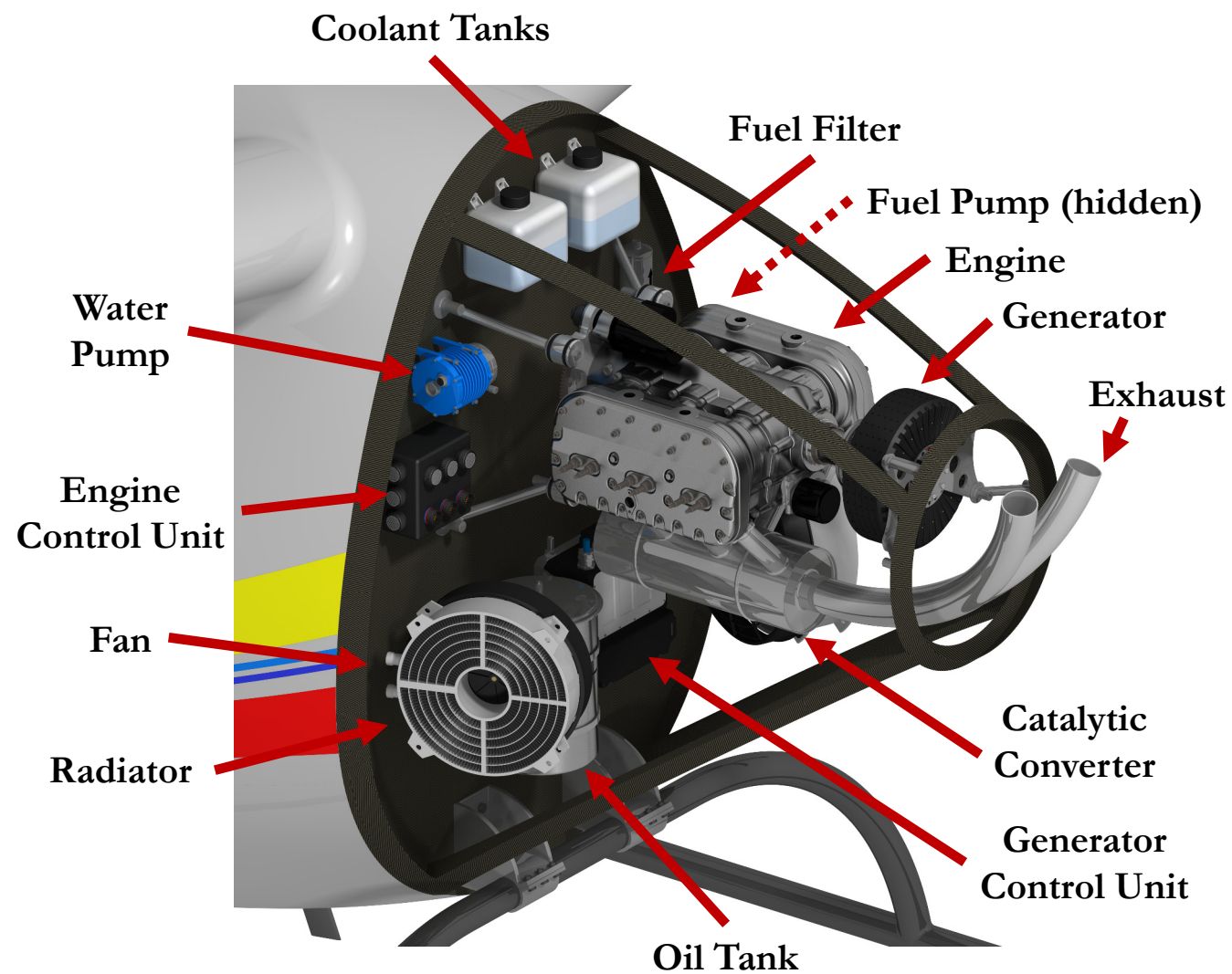
Auxiliary fuel tanks, made of rigid carbon fiber and holding 75 lb of fuel each, can be removed when 24 hour endurance is not required

268 is a liquid-cooled motor capable of producing a continuous power of 100 hp (74.6kW) at 2,800 rpm with 96% efficiency, while the EMRAX 348 is a liquid-cooled motor capable of producing a continuous power of 240 hp (180kW) at 2,800 rpm. Because the peak efficiencies of the EMRAX motors match the LF-39 MD operating RPM, the EMRAX motors were selected as the baseline product series.

The EMRAX motors have a low- (130VDC), medium- (460VDC), and high-voltage (670VDC) option. The low-voltage option allows for the use of a controller that is 11 lb (5 kg) but requires 63 lb (28.7kg) of wiring. The transmission efficiency of the low-voltage wiring is approximately 0.99. The medium-voltage option allows for the use of controller that is 15.4 lb (7kg) but requires 24.3 lb (11.1kg) of wiring. The transmission efficiency of the Medium-voltage wiring is approximately 0.99. The high-voltage option allows for the use of a controller that is 18.7 lb (8.5kg), but requires 12.2 lb (5.6 kg) of wiring. The transmission efficiency of the high-voltage wiring is approximately 0.99. The medium-voltage option was selected due to its weight.

11.5   EMRAX-274 MD Generator

The EMRAX-274 MD is a rubberized EMRAX generator that weighs 47.5 lb (21.6 kg) and has a continuous power of 110 hp (82kW) at 2,800 RPM. It is controlled by an Emsiso emDrive H300 liquid-cooled drive, shown in Fig. 11.4.
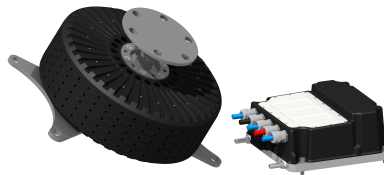
FIGURE 11.4: EMRAX 274-MD Generator with EMsiso emDrive H300.

The Emsiso H300 provides generator field control, and AC/DC power conversion for all medium voltage EMRAX motors and weighs 15.4 lb (7kg). It is capable of a continuous current of 300 Amps, and an intermediate current of 450 Amps at voltages between 100-450 V. The Emsiso H300X is a solid-state diode device it has a high electrical efficiency above 97% efficiency in expect mission power range from manufacturer test data (Fig. 11.5).
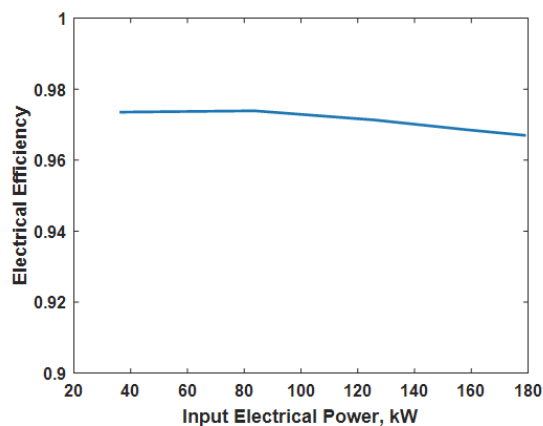
FIGURE 11.5: Emsiso emDrive 300 Efficiency data.

11.6 EMRAX-234 MD Drive Motor

The EMRAX-234 MD is also a rubberized EMRAX motor that weighs 29.5 lb (13.4 kg) and has a continuous power of 50 hp (37.3kW) at 2,800 RPM. It is also controlled by an Emsiso emDrive H300 liquid-cooled drive, Fig. 11.6

FIGURE 11.6: Drive motor placement.

11.7 Power distribution

Power from the EMRAX-274 MD Generator is transmitted to the rotor drive motors via electric cables. MCM-300 thermoplastic heat- and water-resistant nylon coated (THWN) Aluminum wire, with an current capacity of 230A and internal resistance of .0579 mOhm/ft, transmits power from the generator to a junction box. The junction box, located in a bay between the rotor arms, contains the electronic circuits to enable the system to be powered from the generator and/or emergency battery power. From the junction box, 4/0 THWN aluminum wire, with a current capacity of 180A and internal resistance of .0812 mOhm/ft, transmits power to the DCBL motors in each rotor nacelle. The expect power loss due to wire transmission is less than 1% at maximum continuous power.

11.8 Reduction Gearbox

To achieve the required rotor torque and RPM in hover and cruise, a planetary gearbox with a total gear reduction of 8.12:1 was integrated with the motor system to reduce drive motor rpm (Fig. 11.7). Because planetary gear reduction is limited to approximately 5:1 due to sun gear geometry and load constraints, a two-stage planetary (2.923:1 and 2.8:1) was used for *Elysium*. Tables 11.4 details the properties of the planetary gear sets. Power from the electric motor is transmitted through a splined shaft attached to the sun gear of the 1st planetary stage.

The 1st stage has a stationary ring gear, with four planets that are attached to a carrier set which transmits the torque to the sun gear of the second stage. The sun and planet gears are AISI 9310 carburized steel, grade 2. The ring gear is Nitralloy 135M, grade 2.

The 2nd stage has a stationary ring gear, with four planets that are attached to a carrier set which transmits
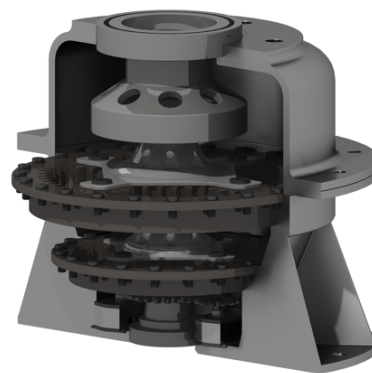
FIGURE 11.7: Reduction gearbox cut-away.

TABLE 11.4: First and second stage gear characteristics.

	First stage			Second stage		
	Sun Gear	Planet	Ring	Sun Gear	Planet	Ring
Number of Teeth	26	12	50	30	12	54
Lewis Form Factor	0.346	0.245	0.409	0.359	0.245	0.395
J	0.335	0.21	0.405	0.34	0.21	0.4146
Face width (in)	0.625	0.625	0.625	0.8	0.8	0.8
Diametral Pitch (teeth/in)	10	10	10	7.5	7.5	7.5
Pitch Diameter (in)	2.6	1.2	5.0	4.0	1.6	7.2
Reliability	0.995	0.995	0.995	0.995	0.995	0.995

the torque to the sun gear of the second stage. The sun and planet gears are AISI 9310 carburized steel, grade 2. The ring gear is Nitralloy 135M, grade 2.

The gears of both stages are superfinished to decrease surface wear. The gearbox housing is made from a Elektron 21 magnesium alloy. A combined centrifugal/sprag clutch is used for the rotor and fully engages the rotors at 225 rotor RPM to ensures that the electric motor start-up torque will be adequate when the rotor engages. The clutch disengages the geartrain for the rotor to overrun the electric motor allowing for autorotation.

The clutch is placed at the high-torque, gearbox output to decrease the likelihood of catastrophic failure. If a gear failure results in jamming of the rotating assemblies, this clutch will continue to spin freely, allowing for autorotation. The gearbox incorporates a wet sump lubrication system with dual oil pumps, chip detectors, and an oil cooler to maintain proper lubrication of the gears, bearings, and clutch.

11.9   Batteries

Elysium's propulsion system includes two batteries for use during vehicle operation (Fig. 11.8). The first is a 12V nickel-cadmium (NiCad) battery located in the nose cone. This battery is used to start the engine and to redundantly power the critical avionics and controllers within the aircraft. Should a main power loss occur, this battery would enable the pitch actuators and avionics to continue working during the emergency landing. Use of a NiCad battery, allows for the engine to start at -4°F (-20°C) ambient air temperature.

A Solar Impulse 2 battery, manufactured by in Air Energy, was selected for use in *Elysium*, due to its favorable energy density of 0.16 hp-hr/lb (260 Wh/kg). The battery weights 30.5 lb and was sized to allow for a three minutes of hover at

FIGURE 11.8: *Elysium's* battery placement.

maximum takeoff power in the event of engine failure. If the engine fails, *Elysium* locates an emergency landing zone and safely lands using the battery power. The battery is cooled by the avionics cooling system to prevent overheating.

11.10   Thermal management

One of the most common causes of electric motor failure is a low-resistance insulation failure due to overheating the motor. Overheating the motor can quickly degrade motor life. For example, a common rule of thumb is that for every 18°F (10°C) above the insulation temperature rating motor life is reduced by 50%. Conversely, operating 18°F (10°C) below the insulation temperature rating doubles motor life. Therefore, designs incorporating electric motors must consider thermal management to certify feasibility.

The EMRAX generators and motors selected for this configuration have a maximum winding and magnet temperature of 248°F (120°C). In order to properly cool the motor, the EMRAX motors require an airflow of 65.6 ft/s (20 m/s) at 77°F (25°C), or a liquid-coolant flow of 2.11 gal/min (8 L/min) at 120°F (50°C).

Figure 11.9 show a flowchart of the algorithm developed in house for sizing the cooling system. For the electric motor and generator cooling system, an off-design point of reduced controller and motor efficiencies (90%) and ambient air temperature of 27°F (15°C) above ISA was used to ensure sufficient cooling capabilities. For the reciprocating engine cooling system, a coolant heat dissipation requirement of 33% maximum power and ambient air temperature of 27°F (15°C) above ISA was used.
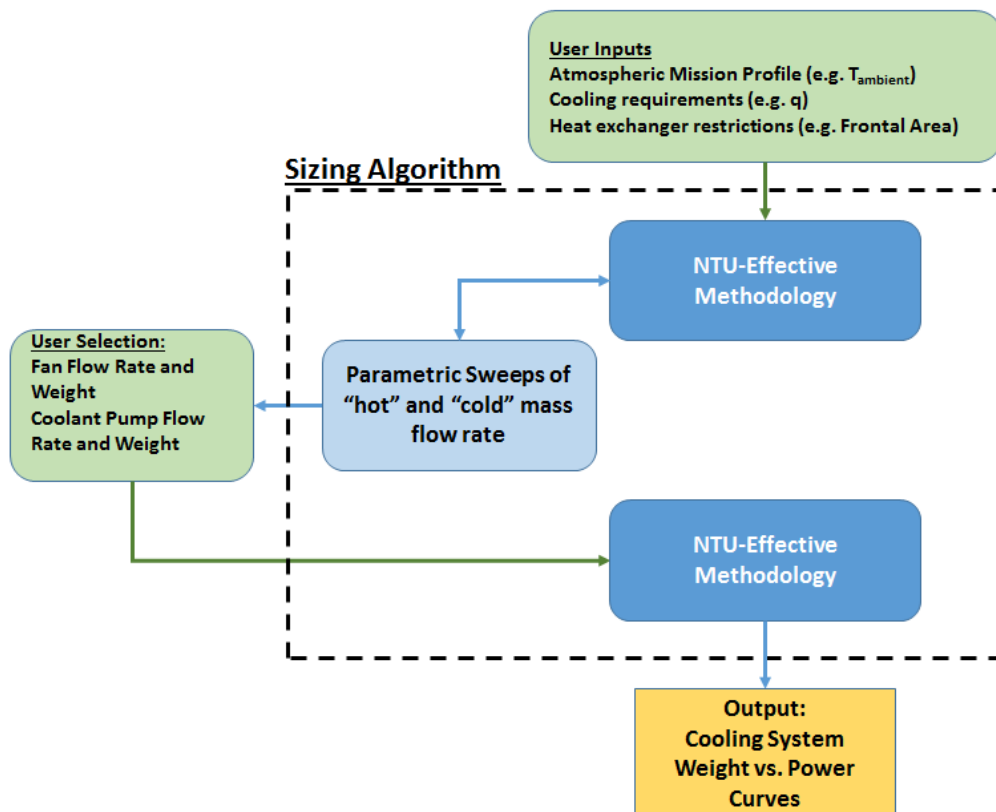
FIGURE 11.9: Conceptual flowchart of the thermal management sizing algorithm

The electric motor and generator cooling system consists of:

- An International Water-Guard aircraft water circulation pump (P/N 9-31001-01)

- 3 ft (0.91m) of flexible steel braiding

- A 12V Spal electric fan (P/N 30101522) capable of over 1,000 ft^3/min (28.3 m^3/min) at 10,000 ft (3048 m) above sea level

- A 9.68-0.87 flat tube-fin compact heat exchanger. At sea level the system is capable of removing 7.58 BTU/s (8 kW) of waste heat. The volume for the rotor electric motor radiator is 114 in^3 (0.00187 m^3), and the volume for the generator radiator is 294 in3 (0.00482m3).

The reciprocating engine cooling system consists of:

- The integral engine mounted water pump

- 3 ft (0.91 m) of flexible steel braiding

- A 12V Spal electric fan (P/N 30103202) capable of over 1,500 ft^3/min (42.5 m^3/min) at 10,000 ft (3048 m) above sea level

- A 9.68-0.87 flat tube-fin compact heat exchanger. The volume for the engine radiator is 396 in^3 (0.00650 m^3). At sea level the system is capable of removing 17.1 BTU/s (18 kW) of waste heat.

11.11   Fuel Management

Consumable fuel accounts for 27.6% of the GTOW. *Elysium's* fuel system includes a main tank which holds 58.4 U.S. gallons (221.1 L), and two removable auxiliary tanks that each hold 12.5 U.S. gallons (47.4 L), Fig. 11.10. The main tank and auxiliary tanks incorporate a series of baffles designed to mitigate fuel sloshing without trapping fuel.

FIGURE 11.10: Main and auxiliary fuel tank placement.

The main fuel tank is located at the lateral and longitudinal CG location of the helicopter to minimize CG travel during the duration of the flight. The auxiliary fuel tanks are mounted above the main tank and feed into the main tank. The connection between the auxiliary tanks and the main tanks is sized to account for a fuel flow 150% of the fuel consumption during maximum continuous power, in accordance of 14 CFR, Part 23, Section 955.

TABLE 11.5: Estimated endurance of alternative power sources.

	Li-ion Battery	Al-Air Battery	H2 PEMFC
Power Management	43.8 lb	43.8 lb	23.3 lb
Fuel Cell	Not Applicable	Not Applicable	69.7 lb
Fuel/Battery	831.2 lb	831.2 lb	54.5 lb
Endurance at 85 hp	1. hr	7.7 hr	6.8 hr

In addition to the engine driven fuel pump, an Airflow Performance auxiliary fuel pump with a relief bypass valve assembly is installed for engine startup and as an emergency backup.

The fuel system also incorporates a Bosch in-line fuel filter, digital fuel level indicator system, digital fuel flow rate indicator, lightning strike mitigation system, and fuel tank vents in accordance to 14 CFR Part 23, Section 951 to Section 1001.

11.12   Alternative powerplants

One of the primary benefits of an electric architecture is the electric power source can be replaced with one of similar voltage and current with minimal impact to the system characteristics. This vehicle is poised to serve as a testbed for multiple future innovations in electric power technologies. Currently the fuel system, engine, and generator (weighing 875 lb) can be replaced with a battery system or a hydrogen fuel cell. By conducting an analysis similar to the preliminary propulsion sizing analysis, the hover endurance of these systems can be estimated, as shown Table 11.5.

12 Avionics System

12.1   Mission Requirements

The avionics suite incorporates lightweight, power-efficient, and high-performance sensors designed for autonomy and robustness. *Elysium's* specific mission requires take-off and landing, hovering for an extended period of time, and flying short distances between hover stations, all of which require knowledge of system states, as well as an autopilot capable of controlling the vehicle. The specific requirements for each section are:

- **Takeoff and Landing:** *Elysium* will take-off from a prescribed location, where system health checks will be performed to ensure proper performance of each sensor. Ascending to the desired altitude requires altitude tracking as well as a knowledge of the surroundings in order to sense and avoid obstacles. Landing proves a greater challenge, and requires knowledge of the desired landing site, or the ability to identify a suitable site, as well as accurate attitude and altitude tracking measurements.

- **Hover:** Precise hover, which will comprise the vast majority of our mission, requires very accurate position information, as well as disturbance rejection capability.

- **Forward Flight:** Flight between hover locations requires knowledge of the desired waypoints and the ability to sense and avoid obstacles.

12.1.1 Avionics Tasks

- **State Identification:** One of the most important roles of the sensor suite is identification of the system states. With knowledge of the system states, *Elysium* implements an estimator to provide full-state feedback and stabilize the system. An inertial navigation system (INS) provides 3-axis attitude measurements through a compass, 3-axis attitude rate measurements through a gyro, and 3-axis acceleration measurements through accelerometers. The compass and gyro provide six of the system states directly, and the accelerometer measurements can be integrated to provide velocity and position measurements, in conjunction with velocity probes. The process of integrating accelerometer data suffers from drift, where the estimated position measurement drifts from the actual position measurement over time such that the error continues to grow. To correct drifting integration, *Elysium* carries out periodic updates of inertial position using GPS. In *Elysium's* mission where precision hover is required, a standard GPS with an accuracy of several meters is insufficient. Real-time kinetic (RTK) and precise point positioning (PPP) GPS units use a differential GPS approach, in which multiple GPS units are used on the ground in order to improve the positioning accuracy. The more accurate RTK approach allows for single-digit centimeter accuracy, and relies on a second ground-based GPS provided by the user, where the range of the RTK GPS is dependent on the range which the second GPS signal can be transmitted. The PPP approach facilitates slightly lower decimeter accuracy, but uses existing reference GPS towers across the globe, allowing for world-wide operation with no more hardware than required for a standard GPS. *Elysium* relies on PPP GPS due to the reduced operator workload and greater range, at a similar payload compared to an RTK system.

- **Autonomy:** The avionics has sufficient computational power to support autonomy for *Elysium*. Feedback control, sensor fusion, collision avoidance algorithms, and health and usage monitoring systems are all processed on board. Use of a ground control station allows for off-board data processing and long-term data-logging, though all tasks are onboard in case of an autonomous mission or communication failure. Computer redundancy is provided to ensure safety for the duration of the mission.

- **Height Above Ground Level:** For autonomous landing, *Elysium* has precise measurement of height above ground level. Using a radar altimeter for longer range readings and a Lidar for readings close to the ground, the vehicle accurately assesses its height for safe landing.

- **Collision Avoidance:** While the mission is not very aggressive, it remains important to avoid obstacles and prevent accidents. Identifying obstacles using cameras and Lidar allows the autopilot to change course to avoid them. Vehicle-to-vehicle communication through a mode-S transponder allows for both location sharing and mutual collision avoidance maneuvers.

- **Ground Communication:** A ground control station (GCS) is necessary to give operators on the ground the ability to monitor and pilot the vehicle remotely, giving an equivalent level of control as a pilot in the cockpit. The GCS is the link for data collection, which is extremely valuable, particularly as a technology demonstrator.

12.1.2   Sensors

- **UAV Navigation VECTOR Autopilot:**   The autopilot is required to handle the computational workload of autonomy, communicate with the rest of the avionics, and operate the control algorithm to drive the feedback algorithms and stabilize the vehicle. The *Elysium* is outfitted with the UAV Navigation VECTOR autopilot [30] shown in Fig. 12.1, as it satisfied the requirements for the mission, has a history of success in autonomous flight, and is forward compatible with upgrades to the vehicle. It has two powerful CPUs capable of meeting the demands of autonomous flight, with built-in redundancy. Five serial communication ports and an ethernet port allow the autopilot to monitor all of the sensors on the vehicle and control the gimbal. A joystick can be controlled at the GCS or plugged directly into the VECTOR for optionally manned operations. The VECTOR also includes the POLAR INS, which contains a GPS with 7 ft (2 m) horizontal accuracy, altimeter accurate to 50 ft (15 m), inertial measurement unit with a 1 kHz sample rate for 3-axis accelerometer, 3-axis rate gyro, and three axis magnetometer with roll and pitch error less than 0.5 degrees, all of which will provide data to the flight control system in order to stabilize the vehicle. *Elysium* uses **UAV Navigation's TELEM05** [31] for communication to the GCS, built to work with VECTOR and with a possible 60 mile (97 km) range. In addition to being very capable, the weight and power required for the autopilot are modest, at just 0.4 lb (180 g) and less than 2.5 W, and an additional 0.4 lb (180 g) and 6.5 W peak for the TELEM05. While *Elysium* includes a more accurate GPS, the secondary GPS in the autopilot serves as a failsafe. The GPS antenna is the **Comant CI-401-220**, which weighs 0.4 lb (170 g) and requires 0.16 W.

FIGURE 12.1: UAVN VECTOR Autopilot

- **Novatel FlexPak6 Precise Point Positioning Global Navigation Satellite System:**   The FlexPak6 PPP Global Navigation Satellite System (GNSS) receiver [32] provides *Elysium* with the precision position accuracy required for hover requirements of the mission, which are beyond that of a traditional GPS. Using the TERRASTAR-C infrastructure of global, precisely located GNSS reference stations, the FlexPak6 can achieve 1.6 in (4 cm) position accuracy. The FlexPak6 receives the GNSS signal using the Novatel GPS-702-GGL antenna. The combined weight and power of the PPP system are 1.8 lb (830 g) and 2.1 W.

- **UAV Vision CM160 Gimbal:** The CM160 gimbal [33] is a gyro-stabilized, multi-sensor unit capable of 360 degree azimuth and 120 degree pitch for two-degree-of-freedom rotation for full field-of-view. A Lidar, infrared (IR) camera, and optical camera mount inside the gimbal, allowing for varying field of view depending on mission scenario. In forward flight, the gimbal can angle for obstacle detection; in landing, point downward to assess height

above ground and suitability of landing site; in hover, monitor the ground or track a specific target; and in case of emergency, scout a suitable landing site. The CM160 is equipped with the **Renishaw ILM-150-R Lidar**, with a maximum measuring range of 490 ft (150 m) in high reflectivity (90%) and 246 ft (75 m) at low reflectivity (18%). The Lidar achieves 4 in (10 cm) accuracy, allowing for safe and precise landing maneuvers. At a greater range than the Lidar is capable, less accurate measurements of height above ground are taken with the radar altimeter to guide landing. The Lidar also provides distance measurements to objects in the path during forward flight, aiding in obstacle avoidance. The **Hitachi DI-SC120R Optical Camera** provides daylight imaging for *Elysium*, which is processed for obstacle detection, landing site suitability and any scouting or target tracking requirements. Similarly, the **FLIR Tau 2 IR camera** provides images in low or no light conditions, aiding in safe flight and landing for the duration of the *Elysium*'s 24 hour mission. The weight and power of the CM160 with all mounted sensors is 3.7 lb (1.7 kg) and 12 W.

FIGURE 12.2: UAV Vision CM160 Gimbal

- **Freeflight RA-4000 Radar Altimeter:** The Freeflight RA-4000 Radar altimeter [34] provides *Elysium* with height above ground level, a crucial metric when landing autonomously. The RA-4000 has a range of up to 2500 ft (760 m) and an accuracy of 3% up to 100 ft (30 m), 3% from 100 to 500 ft (152 m), and 5% from 500 to 2500 ft (762 m), giving sufficient accuracy as *Elysium* approaches the ground, and augmented by the Lidar close to the ground for improved accuracy.

- **Sagetech MXS ADS-B Transponder:** The MXS [35] facilitates Mode-S ADS-B communication between *Elysium* and other aircraft, sending and receiving location data, and working in tandem with nearby vehicles to calculate safe trajectories.

- **UAV Navigation GCS-03 Ground Control Station and Visionair Software:** The UAV Navigation GCS-03 and Visionair software [36] connect to the TELEM05 modem to receive and display information from *Elysium*. The GCS-03 includes the same 60 mile range and 115.2 Kb/s baud rate as the TELEM05. The Visionair software features a mission directed interface, a UAV mission planning and execution application. Flight modes include autonomous, manual using a joystick, waypoint navigation, hover, and return to base, including autonomous take-off and landing algorithms. The gimbal is also controllable through Visionair, giving the operator full authority over the eyes of the vehicle.

- **Whelen Parmetheus and Orion 650 lights** Whelen offers lightweight, efficient, and powerful lights that are used on *Elysium*; Parmetheus for landing and Orion 650 [37] in Fig. 12.3 distributed across the aircraft for anti-collision purposes. The Parmetheus light weighs 0.5 lb (0.23 kg) and requires 19 W, and the Orion 650 lights each weigh 0.26 lb (0.12 kg) and require 4.3W.

FIGURE 12.3:   Orion 650 anti-collision light

12.1.3   Additional Considerations

- **Power Distribution:**   The **CorePower 1162-4 electronic circuit breaker unit** [38] (ECBU) is used for power distribution to the avionics and basic health monitoring of the avionics. The ECBU can connect 24 separate devices between 2.5 A and 15 A, and offers current protection and voltage monitoring.

- **Electromagnetic Interference:**   Electromagnetic interference (EMI) is a problem for any avionic system, especially one with a hybrid-electric powertrain. In order to reduce EMI, avionics are located far from the powertrain on the aircraft, and contained inside a conductive enclosure. Wiring is also routed to reduce EMI, first by separating wires when possible, then twisting those that cannot be separated in order to cancel magnetic fields.

- **Cooling:**   Cooling of the avionics is performed using the **Sandia Aerospace ACF 328** [39] three-port blower fan into the avionics enclosure, allowing for direct cooling of the autopilot, telemetry unit, and PPP GNSS receiver.

13 Health and Usage Monitoring System (HUMS)

Health and Usage Monitoring Systems (HUMS) continuously monitor and analyze aircraft conditions to determine the status of flight critical components. In addition to increasing safety, the inclusion of the HUMS can reduce the number of mission aborts, increase mean time between failures, improve mission reliability, and provide performance increases to flight control feedback [40]. Because of the long duration of the expected mission, it is important to diagnose any problems effectively in real time during flight.

The HUMS aboard *Elysium* is comprised of two elements; on-board monitoring and off-board diagnostics and maintenance. The on-board monitoring system gathers and relays information directly to the autopilot. This data, such as engine oil temperature or electric motor current draw, is critical to the proper operation of the vehicle and does not usually require large bandwidth or computational power. This data can be streamed to the ground station for use by an operator or integrated on-board for autonomous control, as shown in Fig. 13.1. The off-board operator saves pertinent data from the various sensors onboard the aircraft to the ground station's

TABLE 12.1: Avionics Breakdown

Component	Model	Qty	Power (W)	Weight (lb)	Cost (USD)
Autopilot	UAVN VECTOR	1	2.5	0.4	10,000
Telemetry	UAVN TELEM05	1	6.5	0.4	1,200
GPS Antenna	Comant CI-401-220	1	0.2	0.4	600
PPP Receiver	Novatel FlexPak6	1	1.8	0.7	1,700
PPP Antenna	Novatel GPS-702-GGL	1	0.3	1.1	1,400
Gimbal	UAV Vision CM160	1	2	2.1	52,000
Lidar	Henshaw ILM-150-R	1	3	0.7	Included in Gimbal
Optical Camera	Hitachi DI-SC120R	1	6	0.6	Included in Gimbal
IR Camera	FLIR Tau 2	1	1	0.3	Included in Gimbal
Radar Altimeter	Freeflight RA-4000	1	11	2.3	8,000
ECBU	CorePower 1162-4	1	0	3.2	10,000
ADS-B	Sagetech MXS	1	15	0.3	1,200
Landing Light	Whelen Parmetheus	1	19	0.5	300
Anti-collision lights	Whelen Orion 650	3	11	0.9	1,500
Cooling	Sandia ACF 328	1	13	1.2	300
GCS system	UAVN GCS-03 and Visionair	1	-	-	7,700
Total			92	15	96,000

flight data recorder. This data is interrogated automatically with software that tracks the physical and temporal limits of the components. This information allows for real-time residual-life analysis, which improves the safety of the vehicle. The HUMS system also creates a diagnostic report for ground personnel and will flag possible failures before they can happen.

Proper design and implementation of HUMS can help in identification of faults prior to catastrophic or hazardous failure and help to take corrective actions during flight. This will minimize risks associated with failures in flight and significantly reduce risk of emergency landings.

13.1 Rotor System

Continuous monitoring of the rotor system health is vital to the operation of any autonomous aircraft. A series of strain gauges and accelerometers are located in the rotor system to continually provide vibration and loads data to the HUMS system. Data collected during component certification and initial flight testing will be used to create a database against which inflight data is compared. If the sensor data exhibit characteristics that indicate imminent failure modes or life-cycle limits, the system immediately alerts the ground control unit and transmits updated instructions to the autopilot. Additionally the system creates a diagnostic report for the ground crew. Track and balance is performed using an infrared (IR) camera in conjunction with the data from the strain gauges and accelerometers to ensure optimal rotor performance.

13.2 Engine

The engine performance software monitors the engine operating conditions through fuel flow, torque output, intake air temperature, exhaust air temperature, oil temperature, oil pressure, coolant temperature, and exhaust oxygen and oxides of Nitrogen. The system also records the time spent above operational torque limits, oil chip warnings, temperatures, average flight performance data, and fault monitoring. The HUMS also monitors the health of the electronic control unit and can override the electronic fuel injection and ignition system in case of fault.
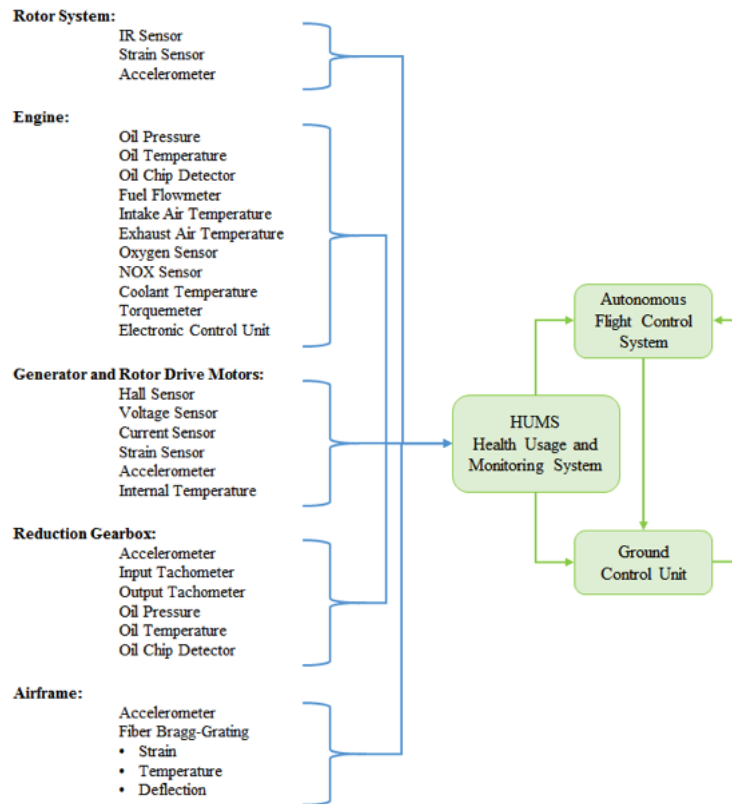
FIGURE 13.1: HUMS-Flight Control-Ground Control Unit interactions.

13.3 Generator and Rotor Drive Motors

Internal thermocouples and Hall sensors are installed in the generators and rotor drive motors to monitor motor temperature and RPM. In addition, current and voltage input to the controller is monitored to identify any electric faults. The diagnostic and fault data from the controller is directly streamed to the ground control unit. Strain gauges and accelerometers are used to record vibrations at the motor and stresses on the motor mounts.

13.4 Reduction Gearboxes

Each reduction gearbox is equipped with accelerometers and tachometers to monitor input RPM, output RPM, and vibration levels. The vibrations will be examined against the tachometer pulse trains. Any anomaly will be recorded and preventative action will be taken if required. The oil temperature, pressure, and chip detectors will be monitored for oil leaks and debris.

13.5 Airframe

Accelerometers are embedded into the airframe to monitor lateral and vertical accelerations to ensure acceptable levels of vibration and determine faults within the avionic attitude sensors. Optics fibers along with fiber Bragg-gratings will be used to determine strain, temperature, and deflections of critical airframe components. Since mechanical damage to the airframe damages the fibers, this anomaly can be quickly isolated using the optic fiber/grating network.

14 Weight Analysis

TABLE 14.1: *Elysium* Weight Estimates

	Component	Weight			x_{cg}		z_{cg}	
	Description	(lbs)	(kg)	(%$_{empty}$)	(ft)	(m)	(ft)	(m)
1	Rotor Group	102.1	46.3	9.4 %	6.75	8.63	2.06	2.63
	Blades	77.4	35.1	7.1 %	6.75	8.67	2.06	2.64
	Hubs	24.7	11.2	2.3 %	6.77	8.50	2.06	2.59
2	Airframe Group	217.4	98.6	20.0 %	5.95	2.76	1.81	0.85
	Fuselage	174.2	79.0	16.0 %	5.75	2.08	1.75	0.64
	Support Arms	43.2	19.6	4.0 %	6.75	5.50	2.06	1.68
3	Landing Gear Group	42.3	19.2	3.9 %	5.58	-0.50	1.70	-0.15
4	Propulsion Group	409.1	185.5	37.6 %	8.09	3.54	2.61	1.01
	Engine	265.3	120.3	24.3 %	9.00	3.58	2.74	1.09
	Cooling System	29.4	13.3	2.7 %	7.63	7.63	4.32	1.32
	Accessories	56.8	25.8	5.2 %	7.95	2.65	2.42	0.81
	Backup Battery	33.3	15.1	3.1 %	1.17	1.33	0.36	0.41
	Support	17.0	7.7	1.6 %	8.28	3.58	2.52	1.09
	Air Induction	7.3	3.3	0.7 %	9.25	2.75	2.82	0.84
5	Fuel System Group	68.7	31.2	6.3 %	7.72	3.04	2.35	0.93
	Tanks and Support	12.1	5.5	1.1 %	6.77	2.06	2.06	0.63
	Plumbing	56.6	25.7	5.2 %	7.92	3.25	2.41	0.99
6	Power Distribution	63.0	28.6	5.8 %	6.25	3.33	1.91	1.02
7	Flight Controls Group	117.6	53.3	10.8 %	6.77	6.60	2.06	2.01
	Actuators	57.6	26.1	5.3 %	6.77	7.27	2.06	2.21
	DCBL Motors	39.0	17.7	3.6 %	6.77	6.17	2.06	1.88
	Electronic Speed Controller	21.0	9.5	1.9 %	6.77	5.58	2.06	1.70
8	Drive System Group	56.6	25.6	5.2 %	6.77	6.98	2.06	2.13
	Gearboxes	41.1	18.6	3.8 %	6.77	6.75	2.06	2.06
	Rotor Masts	15.5	7.0	1.4 %	6.77	7.58	2.06	2.31
9	Avionics	15.1	6.3	1.4 %	1.82	1.86	0.56	0.57
	Gimbal	3.7	1.7	0.3 %	1.17	0.42	0.36	0.13
	Autopilot	0.4	0.2	0.1 %	0.75	2.17	0.23	0.66
	Telemetry	0.4	0.2	0.1 %	1.00	2.08	0.30	0.64
	GPS with Antenna	2.2	0.8	0.2 %	5.14	4.01	1.57	1.22
	Lighting	1.4	0.8	0.1 %	3.54	3.75	1.08	1.14
	Broadcasting	0.3	0.1	0.1 %	1.67	1.92	0.51	0.58
	ECBU [1]	3.2	1.5	0.3 %	0.58	1.33	0.18	0.41
	Altimeter	2.3	1.0	0.2 %	1.42	2.08	0.43	0.64
	Cooling	1.2	0.5	0.1 %	1.21	2.08	0.36	0.64
	Empty Weight	1091.9	495.2	100.0 %	7.02	4.06	2.14	1.24
	Simulated Passenger	210.0	95.0		4.92	2.00	1.50	0.61
	Fuel	510.0	226.3		6.77	2.06	2.06	0.63
	Gross Weight	1811.9	394.4	100.0 %	7.02	4.06	2.14	1.24

[1]Electronic Circuit Breaker Unit

(a) CG locations at MTOW

(b) CG locations for empty weight
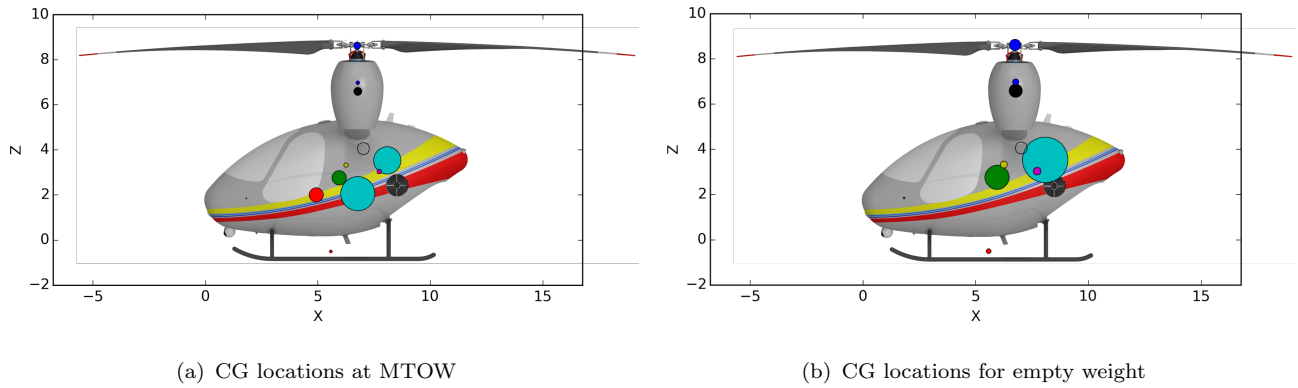
FIGURE 14.1: Center of gravity locations for *Elysium*.

15 Flight Dynamics and Controls

Elysium is required to precisely hold hover, with only a modest forward flight requirement, as opposed to modern helicopter designs that mostly pursue high speed flight. This allows *Elysium* to focus more on improved gust tolerance and hover performance instead of forward flight performance. The open-loop dynamic response of the vehicle contains unstable phugoid and dutch roll modes comparable to other helicopters, but the twin architecture provides inertial and kinetic symmetry about the x-z plane that eliminates couplings with pitch and thrust. The vehicle is controllable using collective and a single cyclic pitch actuator at each rotor, removing the need for full traditional swashplate control at each rotor. Heave and roll are achieved primarily through collective input, and pitch and yaw are achieved primarily through cyclic input. Because of the side-by-side twin rotor configuration, there is a large roll authority available to the system. The controller is developed by linearizing the system about given trim conditions, and then applying perturbations to verify the effectiveness and robustness of the controller, particularly in the presence of wind gusts. Gust tolerance is important for *Elysium* in order to hover precisely and remain inside each of the 66 ft (20 m) radius Hover Stations prescribed by the mission plan for the full duration of the 24-hour mission. While most vehicles that fly in a side-by-side configuration include horizontal and vertical stabilizers for forward flight stability, these large, passive control surfaces are very susceptible to gusts. With an effective control design, *Elysium* does not need to be outfitted with rear stabilizers for the mission profile, yielding reduced gust susceptibility, while still allowing for sufficient forward flight performance.

15.1 Dynamics

A nonlinear dynamics model of the *Elysium* vehicle is used to evaluate performance, perform stability analysis, and develop control architectures. The nonlinear model was developed in-house by the team, and includes rigid body dynamics, blade flapping dynamics, and the Pitt-Peters linear inflow model to evaluate the rigid body, rotor, and aerodynamic interactions in the system. The equations of motion of the system are

$$m\mathbf{a} + m\boldsymbol{\omega} \times \mathbf{v} = \mathbf{F}_g + \mathbf{F}_{rotors}$$
$$\mathbf{I}\dot{\boldsymbol{\omega}} + \boldsymbol{\omega} \times \mathbf{I}\boldsymbol{\omega} = \mathbf{M}_g + \mathbf{M}_{rotors},$$
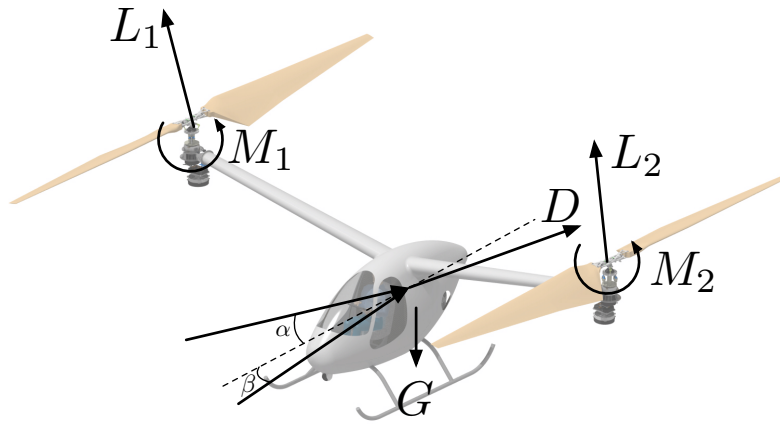
$$(15.1)$$

FIGURE 15.1: Helicopter forces and moments

where m, $\mathbf{a}$, $\boldsymbol{\omega}$, $\mathbf{v}$, and $\mathbf{I}$ are the mass, acceleration, angular velocity, translational velocity, and moment of inertia of the vehicle. The right hand side of the equation describes the forces and moments acting at the center of gravity and rotors of the vehicle.

15.1.1 Rotor Model

Multi-body dynamics analysis is used to incorporate rotor-body couplings. Rotor blades are assumed rigid with a hinge offset and hinge spring yielding $\nu_\beta = 1.05$, and harmonic balancing is performed for the first harmonic. Blade section aerodynamics are modeled using look-up tables with quasi-steady and non-circulatory corrections for airfoil pitch and plunge motions. The look-up tables span over all angles of attack and a pre-defined Reynolds number range. The Pitt-Peters linear inflow model computes non-uniform rotor inflow over the range of flight conditions. Rotor trim is solved by averaging rotor loads over one revolution and substituting into vehicle trim equations.

15.2 Vehicle Control

The *Elysium* is controlled through collective and a single cyclic at each rotor. Half cyclic provides the required control authority over all twelve vehicle states $[u, v, w, p, q, r, \phi, \theta, \psi, x, y, z]^T$ such that linearization yields a full-rank controllability matrix. Figure 15.2 shows the method of actuation on the vehicle. Roll is achieved through differential thrust using collective, pitch through cyclic, yaw through differential cyclic, and heave through collective. Coupling between

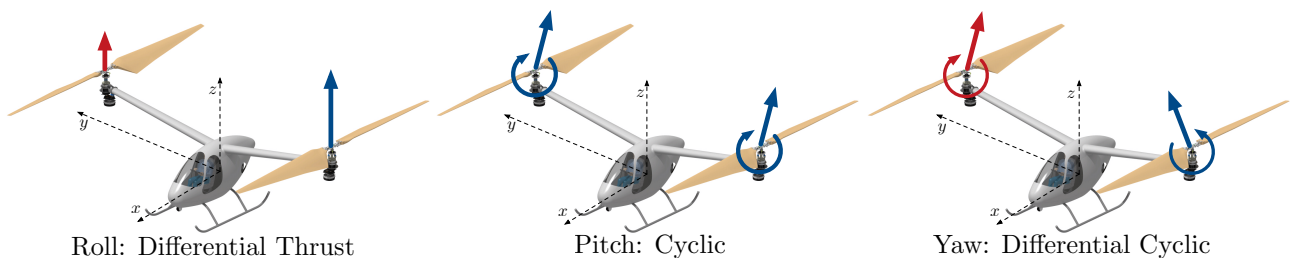| Roll: Differential Thrust | Pitch: Cyclic | Yaw: Differential Cyclic |

FIGURE 15.2

control inputs is reduced as compared to a single main rotor helicopter (SMR) due to the inherent

symmetry in the system. Identical increases in collective and cyclic on *Elysium* yield equal and opposite torques, decoupling heave and pitch, and the coupling between yaw and roll can be mitigated with appropriate roll/yaw mixing. Additionally, yaw authority is increased compared to most multirotor designs with four or more rotors. Differential cyclic tilts the rotors in opposite directions and provides a large moment arm relative to the center of gravity on which the yaw moment can act, compared to differential torque used on most multirotor helicopters, which is inherently weak as it relies on the aerodynamic drag of the rotors, and efficient rotor blades have high lift to drag ratios and reduce the drag force as much as possible.

15.3 Control Architecture

A simple and well-tested control architecture is possible for *Elysium* due to the well understood actuation and dynamics of the vehicle. Linear controllers designed for gain scheduling are sufficient and more robust than nonlinear controllers for these vehicles, where failure to sense fast rotor states at adequate sampling frequencies can result in critical failure. Using a linear quadratic regulator (LQR), *Elysium* is able to fly autonomously between waypoints, hover precisely, and remain inside the hover sphere under the influence of gust disturbances. The controller uses a cascaded control system with an inner and outer loop allows for rapid measurement and control of fast attitude dynamics, while maintaining the overall goal of achieving a desired position using the slower outer loop. The control architecture is shown in Fig. 15.3.
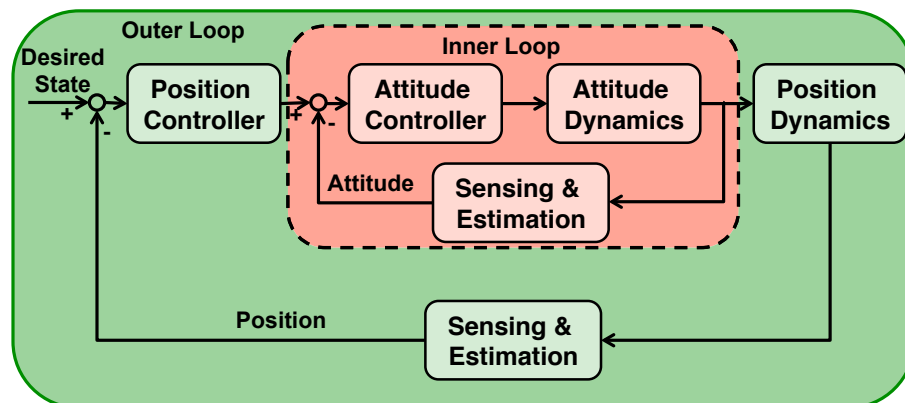
FIGURE 15.3:   Control Architecture: fast inner loop controls rapid attitude dynamics while slower outer loop controls translational dynamics

The LQR controller achieves a stable, optimal system response based on weighing control effort against state error. Each state and input are given an individual weight based on overall desired performance and flight condition. The flight conditions throughout the mission and the respective controller for each can be seen in Fig. 15.4.

- **Autonomous Hover:** *Elysium*'s autopilot stabilizes all states, both translational and rotational, for stable flight and return to the center of the Hover Station in case of disturbance. All states are stabilized, with relative input weight magnitude dependent on actuator and aerodynamic limitations.

- **Autonomous Waypoint Navigation:**

FIGURE 15.4: Control switching architecture throughout the mission

(a) Open loop

(b) Closed loop
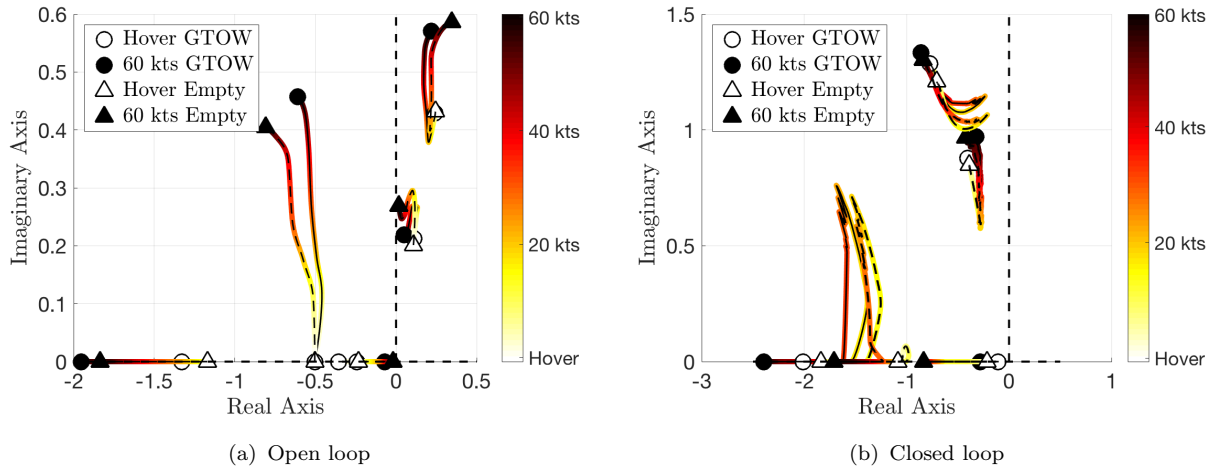
FIGURE 15.5: Root locus over velocity range

- – Outer Loop: Position commands drive the outer loop of the controller, and translational velocities initially propagate based on angles, and are commanded to zero as *Elysium* reaches the target.
- – Inner Loop: Heading angle is prescribed to point toward the desired location, and fuselage pitch is controlled to achieve a desired flight speed. Attitude rates are commanded to zero.

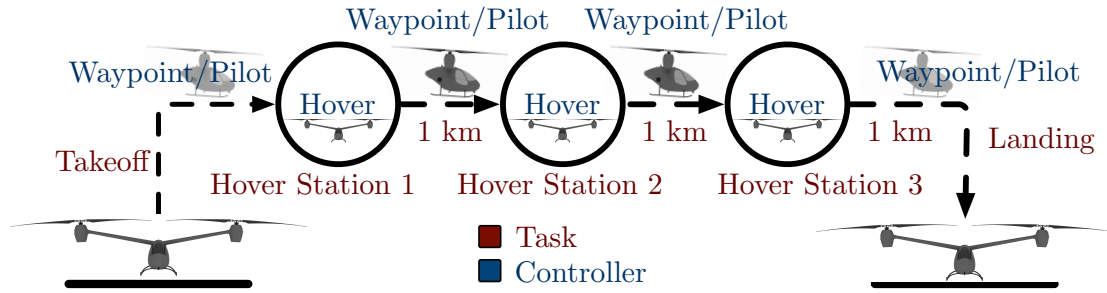- **Pilot Control:** The only non-autonomous control mode, a pilot in the loop may control either the attitude of the vehicle or the angular rates, depending on experience. Attitude control stabilizes angular rates to zero and stabilizes angles about the reference joystick inputs; translational states are not stabilized by the controller. Attitude rate control stabilizes angular velocities about joystick inputs, attitude and translational states are not stabilized by the controller.

15.4 Stability Analysis

A root locus approach was used to perform stability analysis, in which vehicle weight and flight speed were varied to capture the full mission envelope. Figure 15.5 shows the system with and without closed loop control from hover up to 60 knots, comparing gross-take-off-weight (GTOW) and empty weight. Modes at GTOW and empty weight show very similar characteristics across the flight envelope, justifying the use of a controller developed for GTOW for the duration of the

mission. In open loop, phugoid and dutch roll modes are unstable for the entire flight envelope, necessitating feedback control for stable flight. The short period mode is critically damped in hover, then becomes underdamped as the flight speed increases. When closed loop feedback is applied to the dynamics, all poles remain in the left-half-plane for the duration of the mission, showing system stability.

15.5   Gust Tolerance

Effective gust rejection is a key component of *Elysium*'s design in order to maintain stable flight, especially when flying in each of the Hover Stations. Distributed accelerometers are added to *Elysium* so that forces and moments can be estimated using a static observer, following [41]. The amplitude of the gust is simulated by applying a step wind input to the nonlinear time marching simulation and monitoring the forces and moments experienced by the vehicle. In practice, control actuators rotate the tip-path-plane about the y-axis, actively reducing the moment transmitted to the hub. This phenomena is taken into account through a decay of the moment about the y-axis to a constant value 25% of the original force, determined by solving the moment in a trim procedure on the vehicle under the same steady wind conditions. Without active control to directly mitigate the forces due to wind on any other axis, only the y-axis moment loads decay. The forces and moments are then multiplied by a $[1 - \cos]$ profile to match a typical gust disturbance [42]. The time-marching simulation uses the linear representation of the system dynamics, trimmed about a sweep of conditions and interpolated to identify the dynamics of the vehicle at any time. Dynamics are simplified by bringing the inflow and flapping states into the 12-state rigid body model under the assumption that inflow and flapping stabilize significantly faster than rigid body states. By sectioning the state matrix into four parts

$$\dot{x} = \left[\begin{array}{c|c} A_{1,1} & A_{1,2} \\ \hline A_{2,1} & A_{2,2} \end{array}\right] x + \left[\begin{array}{c} B_1 \\ \hline B_2 \end{array}\right],$$

the blade-flapping and inflow dynamics are brought into the 12 state A_{eff} and B_{eff} matrices using $A_{eff} = A_{1,1} - A_{1,2}^{-1} A_{2,2} A_{2,1}$ and $B_{eff} = B_1 - A_{1,2}^{-1} A_{2,2} B_2$ yielding a 12-state linear model representing *Elysium*. Controls are saturated based on the blade pitch limits established through aerodynamic analysis. Figures 15.6 and 15.7 show the vehicle translational response to gust perturbation with gusts of 49.2 ft/s (15 m/s) in longitudinal direction (x-axis), and 65.6 ft/s (20 m/s) in lateral direction (y-axis), respectively. Gust magnitudes were chosen as the worst case scenario for each direction based on control and aerodynamic limitations. In each case, *Elysium* remains controlled and returns to the equilibrium hover condition at the center of the Hover station sphere prescribed by the mission in under 20 seconds, with all deviations well within the 65 ft radius of the hover sphere. Gust response from perturbations in the negative direction are not shown as the response is of similar magnitude.

Additional gust response analysis is performed through analysis of the eigenvectors and eigenvalues of the controllability Gramian. Eigenvectors and eigenvalues define the axes of an ellipsoid, which describes the maneuverability of the aircraft when using control inputs, and describes the vehicle's susceptibility to disturbances when using disturbance inputs. The Gramian is found using the 12-state linear model. This is performed for *Elysium* and shown in the vertical direction in Fig. 15.8, indicating that with a collective range of four degrees, *Elysium* will overcome gusts of over 16 ft/s (5 m/s).
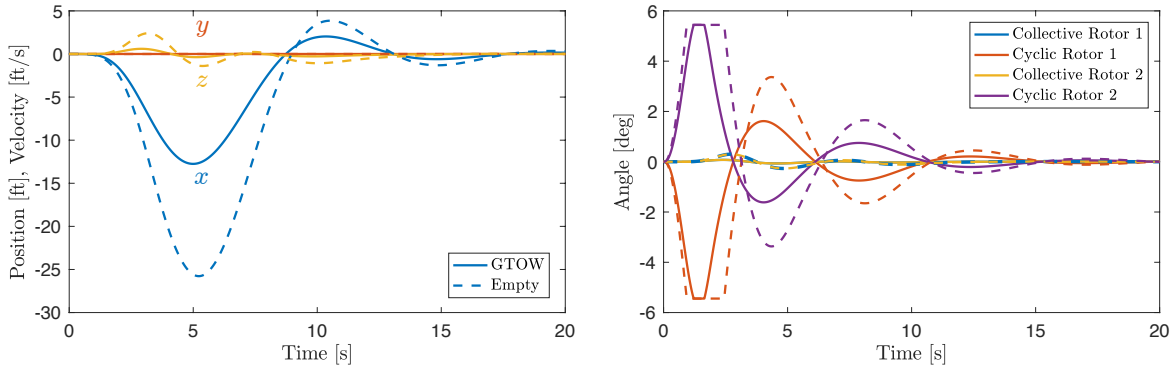
FIGURE 15.6: 49.2 ft/s gust in x direction; solid: GTOW, dotted: empty weight
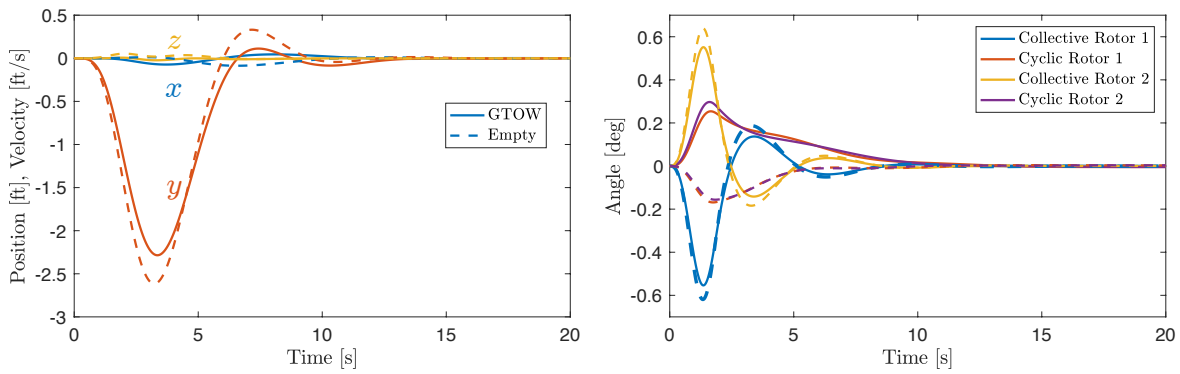

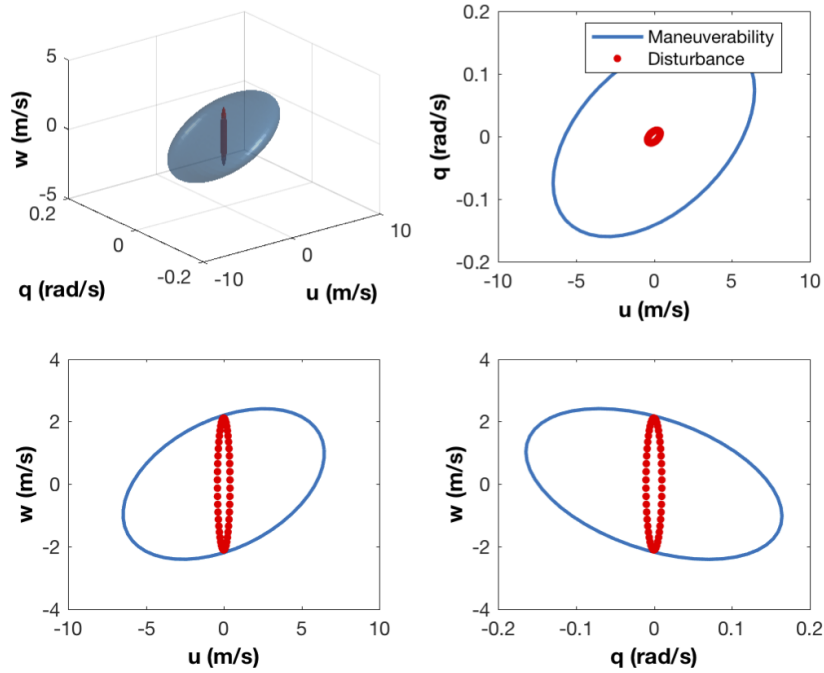FIGURE 15.7: 65.6 ft/s gust in y direction; solid: GTOW, dotted: empty weight

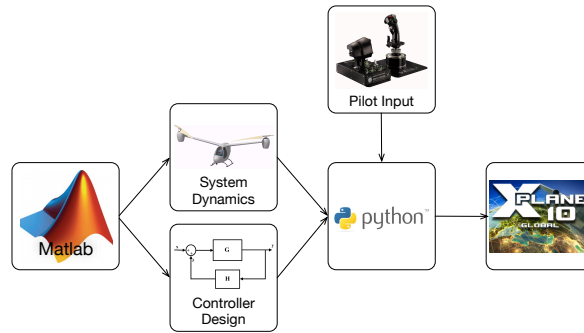FIGURE 15.8: Gust response in z direction

FIGURE 15.9: Connection to X-Plane

15.6 Simulation and Visualization Using X-Plane

The vehicle simulation process described above is used to develop a vehicle simulation in Python which is visualized using X-Plane. Dynamics and control are developed in the Matlab environment, then applied in a Python script which communicates with X-Plane in order to apply the dynamics of *Elysium*, as seen in Fig. 15.9. The pilot interacts with the Python simulator using joystick controls, which are passed through the controller and into the vehicle. Two simulations are presented, the first with open loop control of the helicopter and the second with closed loop attitude rate command. Both profiles are flown by an untrained pilot. Figures 15.11 and 15.10(b) show the vehicle position and corresponding pilot inputs when the vehicle dynamics are implemented without control, and Figs. 15.11(a) and 15.11(b) show position and pilot input with closed loop feedback control. In both cases, the test profile flown begins with heave motion, followed by small lateral inputs to test roll response, and finally pitching for forward flight. Control inputs in the open loop case begin modestly, but as the pilot begins to fly the vehicle forward, rapid and occasionally large inputs are required in order to maintain the vehicle on the desired flight profile. The closed loop case shows a very similar position output for the vehicle, but with much smoother and smaller control inputs. Comparing the figures between open and closed loop control is a reflection on the poles of the system, where the open loop shows instability in both pitch and roll, while the closed loop system stabilizes all of the poles, making the vehicle much easier to fly.

16 Acoustics

16.1 FAA Noise Requirement

The acoustic signature of *Elysium* was analyzed by using an in-house acoustic code based on formulation of the Ffowcs Williams-Hawkings equation. The thickness and loading noise of the rotor in hover were calculated and sound pressure levels (SPL) in decibels (dB) were presented on a sphere surrounding the aircraft, as well as on the ground. The calculations were made at two altitudes: (1) 492 ft (150 m) which is standard altitude of FAA noise regulation, and (2) 1500 ft (457.2 m), the operating altitude of *Elysium*. In all flight conditions, the maximum noise level was 62.3 dB, which is much lower than the FAA noise limit. For a small helicopter, which has maximum takeoff weight under 7,000 pounds, FAA noise regulation (FAR 36 Appendix J) requires the flyover test at an altitude of 492 ft (150 m). Figure 16.1 shows the noise limit (FAR 36.805) based on gross takeoff weight of aircraft and indicates that the maximum allowable noise is 82 dB for *Elysium*. The flyover speed is $0.9V_H$=54.381 ft/s, where V_H is defined as the

(a) Position

(b) Control inputs
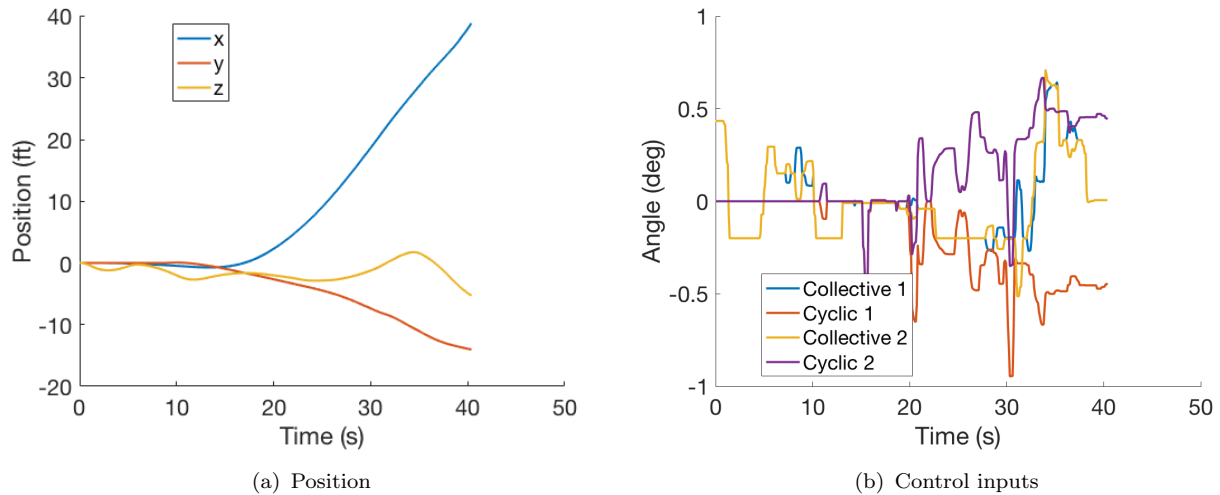
FIGURE 15.10: X-Plane Open Loop Position

(a) Position

(b) Control inputs
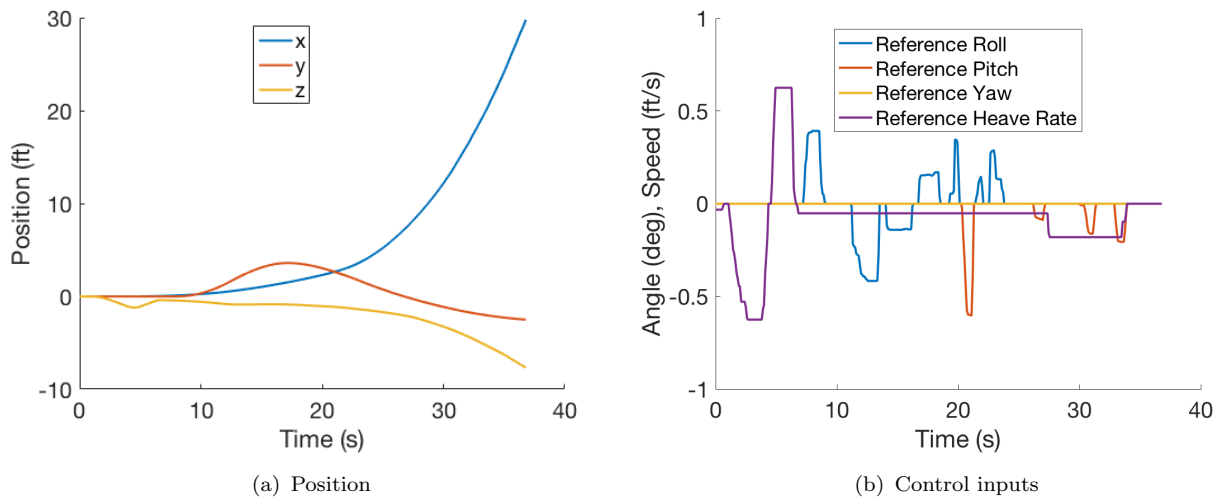
FIGURE 15.11: X-Plane Open Loop Position

airspeed in level flight obtained using the minimum engine power.

16.1.1 Rotor Noise

In general, the noise of the rotor is mainly comprised of: (1) Thickness noise, caused by the air displaced by a blade, (2) Loading noise, caused by the accelerating force on the air induced by the blade surface, (3) High speed impulsive (HSI) noise, and (4) Blade vortex interaction (BVI) noise. HSI noise is caused by transonic flow over the advancing side of the rotor disk resulting in a shock formation, which travels in the plane of the rotor. *Elysium* features a low tip-speed rotor, which results in a tip Mach number of 0.39 at the start of the mission and 0.33 towards the end of the mission. Because of the low hover tip-Mach number and the low advance ratio of the aircraft in forward flight, HSI noise is not a factor for acoustic design.

BVI noise can be a possible source of noise considering the low disk loading of *Elysium*. A high disk-loading rotor would convect the tip-vortex further away from the plane of the rotor
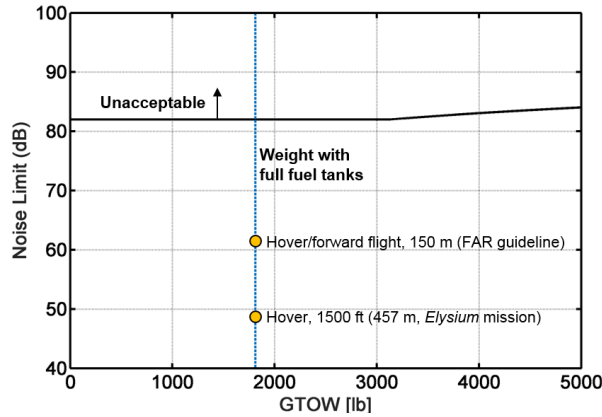
FIGURE 16.1: FAA noise regulations based on FAR 36.805, Appendix J.

preventing a rotor blade from interacting the tip-vortex released from the previous blade. With the baseline rectangular blade tip of *Elysium*, there is a possibility that the tip-vortex interacts with the subsequent passing blade resulting in potential BVI noise. However, as shown in Section 19.1.3, a modified anhedral blade has been designed with the use of in-house three-dimensional CFD solver, which diffuses the vortex by 85% and convects it axially to a greater distance than the baseline blade. Therefore, if the magnitude of BVI noise is greater than the FAA limit, the modified anhedral blades will be used that largely mitigates BVI.

TABLE 16.1: Comparison of maximum noise levels at altitude of 492 ft and 1,500 ft.

Altitude [ft]	Flight condition	Thickness noise [dB]	Loading noise [dB]	Total noise [dB]
492	Hover	51.15	61.65	62.22
492	Forward Flight	53.68	62.08	**62.34**
1,500	Hover	41.45	46.81	48.49

Thickness and loading noise were computed using an in-house developed code. Table 16.1 shows the maximum noise and their breakdown into the thickness and loading noise at altitudes of 492 ft (FAR requirement) and 1,500 ft (mission altitude). At an altitude of 492 ft (150 m), the maximum noise is close to 62 dB in both hover and forward flight; as a result of combination of low tip Mach number and low forward flight speed. At 1,500 ft (457 m), the noise level drops down to 48.49 dB. For comparison, 62 dB is the noise level in a work environment and 48 dB is regular conversation [43].

For the altitude outlined in Table 16.1, the pressure levels on the ground and a hemisphere around the aicraft in hover is shown in Fig. 16.2. The forward flight condition was omitted because of its similarity to the hover results. Loading noise, which is directed below the rotor, is the primary contributor to the total noise signature, seen mostly towards the advancing (outer) side of the rotor disk. The thickness noise is low because of the low tip-speed of the rotor. The noise levels are further reduced when the hover is performed at 1,500 ft (457 m) owing to attenuation. In summary, the low initial tip-speed (which decreases through the mission) and the low disk-loading (1.9 lb/ft^2), keep the decibels levels of *Elysium* well far below the FAA requirements for a vehicle in the same weight class.

(a) Noise at altitude of 492 ft (150 m))

(b) Noise at altitude of 1,500 ft (457.2 m)
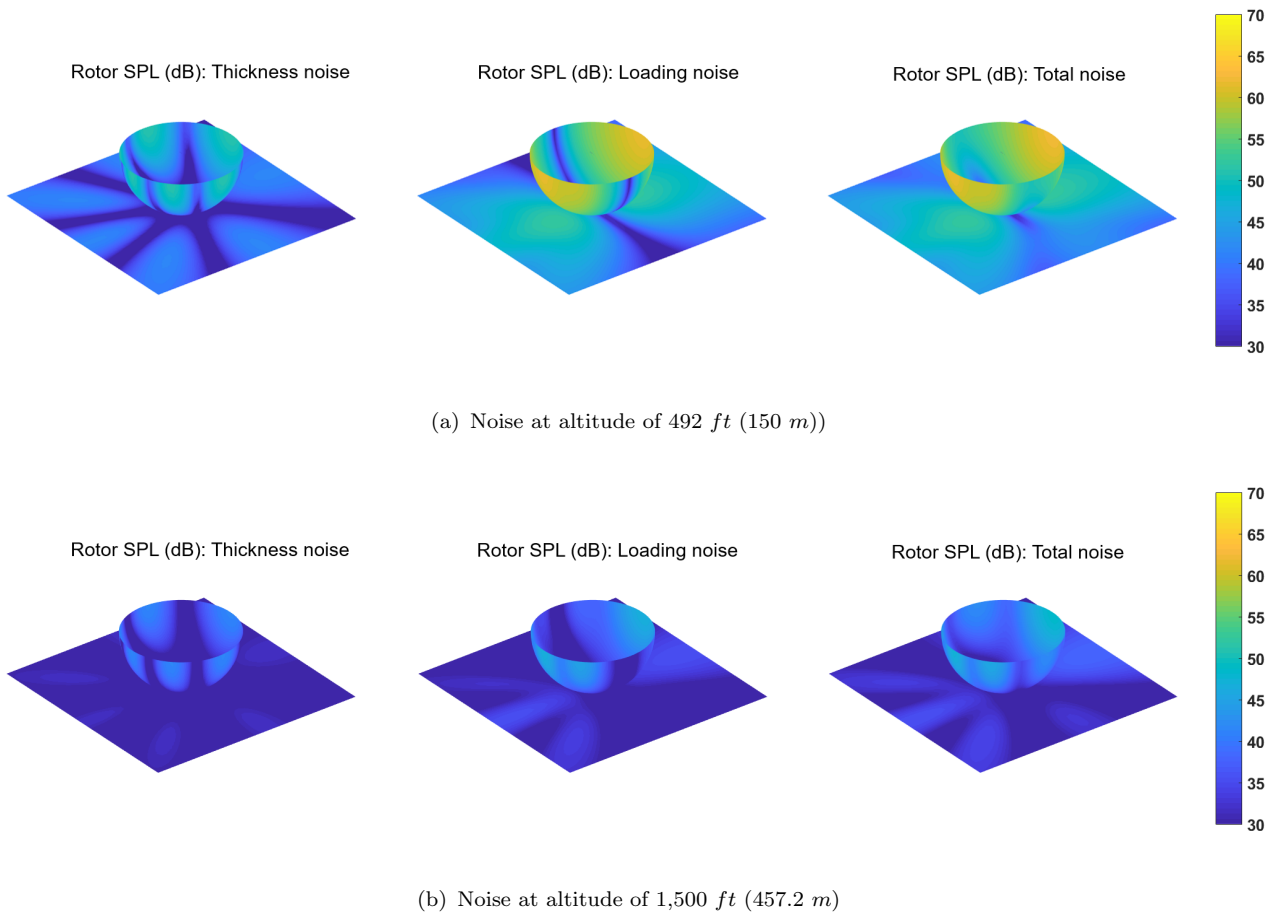
FIGURE 16.2: Comparison of thickness and loading noise in hover at altitude of 492 ft and 1,500 ft.

17 Crashworthiness

17.1 Landing gear

Fixed, skid-type landing gear is used on *Elysium* to decrease the empty weight and complexity of the aircraft. The cruising speed during the forward flight segments of the mission was not high enough to justify the weight penalty of a retracting mechanism. Rather than wheeled landing gear with oleo struts, typically used on aircraft with a GTOW greater than 10,000 lb [44], skid gear is sufficient for *Elysium* and is a simpler system that requires less maintenance.

As shown in Fig. 17.1, the front cross-tube fits into an aluminum sleeve bonded to two fiberglass, honeycomb-sandwich bulkheads that run between the payload compartment floor and underbelly skin. The rear cross tube attaches to the aft bulkhead from within the engine compartment by way of two aluminum brackets, designed to take the shear and bending loads of a hard landing. In the event of a crash, the location of the rear cross tube ensures loads will be transferred to the aft bulkhead rather than into the fuel tank.

73% of the length between the cross-tubes is positioned ahead of the x-position of the center of gravity. This ratio was driven by turnover requirements, higher landing loads at the rear tube, and a desire to keep the weight down. Geometry of the fuselage underbelly also restricted cross-tube placement. Using 2.2g vertical landing loads and an in-house 3-D beam element analysis

(a) Front cross tube

(b) Rear cross tube

FIGURE 17.1: Mounting position of: (a) Front cross tube between fiberglass bulkheads, and (b) Rear cross tube to aft bulkheads.

(a) Lateral turnover angle

(b) Longitudinal turnove angle
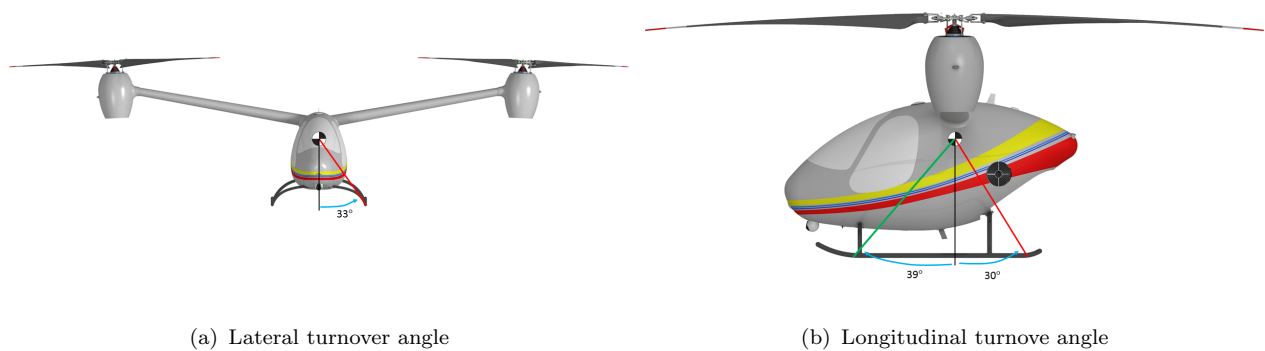
FIGURE 17.2: Landing gear turnover angles.

with a safety factor of 3, the thickness of the cross-tubes and skids was sized to 20% of the tube radius.

According to US military standards, the lateral and longitudinal turnover angles must be greater than 30° if the fuselage is not the first surface to contact the ground during turnover, as is the case with *Elysium*. However, these standards were formulated for conventional rotorcraft rather than twin-rotor vehicles. The small fuselage and large rotors on *Elysium* make it more liable for lateral turnover in the case of gusty conditions. Therefore, rather than 30°, the turnover angle was chosen to be 33°. These angles can be seen in Fig. 17.2.

18 Failure Mode Analysis

As with any vehicle manned or unmanned safety and survivability are essential aspects of a successful mission. Not only does the helicopter represent a significant investment in technology and manpower, but the safety of the ground crew is of the upmost concern. Therefore the possible failure modes at each stage of operation were reviewed, and the cause, impact, and likelihood for each failure mode was identified and mitigated to ensure no excessive riskers were taken in the design for operation.

TABLE 18.1: Failure mode severity definition

Level of Impact	Description	Level of Likelihood	Description
I	Catastrotpic - loss of life possible	A	Very high likelihood ($> 75\%$)
II	Major concern - vehicle unrecoverable	B	High likelihood (50–75%)
III	Moderate concern - failure to complete mission	C	Moderate likelihood (25–50%)
IV	Low concern - modified mission segment	D	Low likelihood (5–25%)
V	No concern - Mission completed as planned	E	Negligible likelihood ($< 5\%$)

18.1 Failure Modes, Effects, and Criticality Analysis

While preventative action, such as regular inspections, maintenance, and repairs, are the best way to identify an issue before failure and protect the personnel and aircraft from damage the unexpected still occurs. To identify the potential risks involved in this design, Failure Modes, Effects, and Criticality Analysis (FMECA) was performed. Table 18.1 shows the likelihood of occurrence and the degree of impact for used each failure mode. Each failure mode is assigned a letter, A–E, to indicated the likelihood of occurrence and a Roman numeral, I–V, to indicate the potential degree of impact to the mission. Failures that pose the greatest risk to the aircraft, I-A, must be identified and mitigated. Table 18.2 shows the likelihood of occurrence, degree of impact, consequences, and mitigation strategies of each failure mode identified. There are no A-I events, and the 1 level-I events that have a low likelihood of occurring. Therefore, the system has adequate safety.

18.2 Generator and Engine Failure

Elysium's rotor system is capable of utilizing power from multiple sources. In the event that the LF-39 MD engine and/or generator fails, the power junction box switches to the Ni-Cd battery to continue supplying power to the rotor drive system. The Li-ion battery is capable of three minutes of maximum power to enable the aircraft to transition to forward flight, locate a safe landing area, and execute a safe landing. The NiCad battery continues to power critical avionics systems during the loss of main generator power.

18.3 Rotor Drive Motor and Gearbox Failure

Elysium's rotor system was designed with the clutch on the high-torque output of the gearbox to mitigate catastrophic loss of the rotor in the event of gearbox and/or failure. A failure in the rotor drive motor or gearbox will result in the rotor being disengaged from the drive system. This allows the rotor to continue to rotate unpowered. The control algorithms will initiate the autorotation protocols and the vehicle will land.

TABLE 18.2: *Elysium's* Failure Modes, Effects, and Criticality Analysis

Failure Mode	Impact	Likelihood	Consequence	Mitigation
Engine/Generator failure	III	D	Forced landing of vehicle	Backup battery installed to allow 3 minutes of max hover power to transition to forward flight and land
Gearbox/rotor drive motor failure	II	D	Forced autorotation of vehicle	Rotor clutch allows the rotor to disengage and continue rotation
Autopilot failure - one computer	III	E	Loss of redundant flight computer	Engage second autopilot computer and land vehicle
Autopilot failure - both computers	I	E	Loss of autonomous flight capability	Total vehicle loss
PPP GNSS failure	III	D	Loss of high precision positioning	Rely on low accuracy GPS
Loss of contact to GCS	III	D	Data loss, no manual control	Autonomous return to base
Gimbal failure	IV	E	Cannot redirect optical sensors	Continue mission and perform manual landing
Optical or IR Camera failure	IV	E	Obstacle detection compromised	Rely on Lidar for obstacle detection
Lidar Failure	IV	E	Landing and obstacle detection compromised	Continue mission, rely on cameras for obstacle detection and perform manual landing
Radar Altimeter failure	III	E	Altitude tracking compromised	GPS and Lidar for altitude measurements, manual landing
ECBU failure	II	E	Avionics power overload	See individual avionics failure modes; land vehicle
ADS-B transponder failure	IV	D	Cannot communicate position to other vehicles	Use telemetry and cameras to monitor traffic

18.4 Limit Load Factors

Figure 18.1 shows the limit loads for the vehicle as a function of forward flight speed. Per MIL-S-8698, *Elysium* is a Class 1 rotorcraft with structural design limit load factors of 3.5g and -0.5g [45]. The structural elements were therefore designed to an ultimate load factor of 1.5 times the design load, or 5.25g and -0.75g. The aerodynamic envelope was developed by trimming *Elysium* in various steady flight conditions, from which it was determined that the steady aerodynamic load factor was 1.66 at 10 kts. While this steady aerodynamic load provided
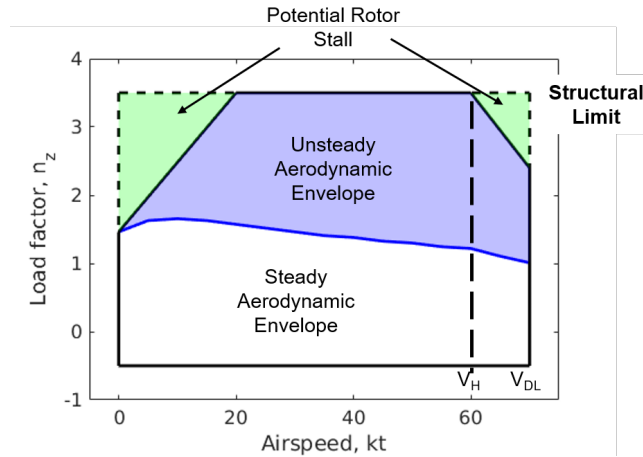
FIGURE 18.1: Load factor vs. velocity diagram for *Elysium*.

a lower limit on load factor, the potential stall boundaries could be used to achieve higher load factors up until the structural design limits.

19 Vehicle Performance

Complementing the aerodynamic performance of the *Elysium* in the 24-hour hover mission presented in Ch. 7, this chapter reviews the performance envelope for *Elysium* in hover, forward-flight, and over each mission segment.

19.1 Hover Performance

TABLE 19.1: *Elysium* Maximum Hover Time at Sea Level

Temperature		
ISA$-18°F$ $(+10°C)$	ISA	ISA$+18°F$ $(-10°C)$
25.9hrs	27.3hrs	28.3hrs

The tip speed of both rotors reduces over time in order to maintain a constant thrust coefficient C_T, allowing the rotors to operate at its most aerodynamically efficient condition for the duration of the mission. Section 7 presents detailed aerodynamics of *Elysium* blades using blade-element theory. The only factor adversely affecting the rotor performance over time is the decreasing Reynolds number, which slightly increases drag and lowers the figure of merit. Figure 19.1(b) shows the roughly constant figure of merit over time as the gross weight of *Elysium* changes.

Elysium was designed to hover with a blade loading of $C_T/\sigma = 0.12$. For hover in conditions other than 1500 ft (457 m) at ISA$+18°F$ $(+10°C)$, the blade loading could be higher or lower than 0.12. Fig. 19.1(b) shows the variation of figure of merit with blade loading obtained from BEMT calculations. In the designed region, the figure of merit stays more or less constant during the flight mission.

19.1.1 Download Penalty

Hover was by far the most important flight regime for consideration in the design of *Elysium*. Any inefficiency in hover would accumulate over 24-hours resulting in higher required power,

(a) Figure of Merit variation with gross weight.

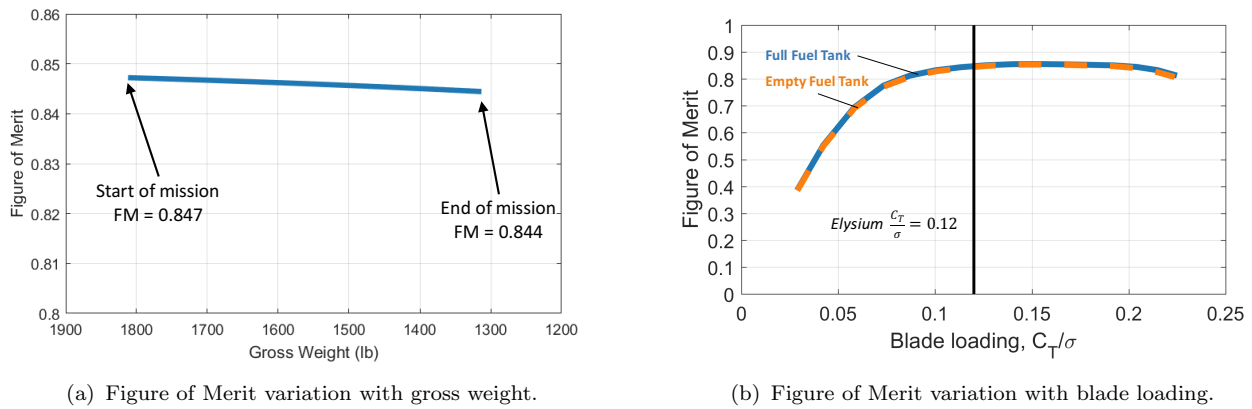(b) Figure of Merit variation with blade loading.

FIGURE 19.1: *Elysium* Figure of Merit variation with gross weight and blade loading coefficient
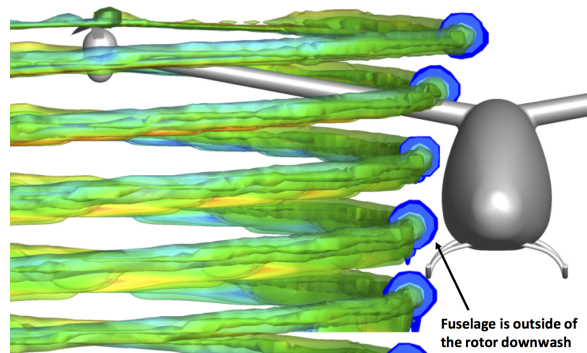

FIGURE 19.2: Free-vortex wake analysis shows the fuselage is not in the direct wake of each rotor.

more fuel, and ultimately a higher GTOW. In Sec. 5.4.1, the tail rotor of a SMR consuming 10% of the main rotor power caused a 20% increase in total vehicle weight for the 24-hour mission. Download penalty on the fuselage is another source of inefficiency in hover. For an aircraft where the fuselage is in the wake of the rotor, the download penalty can account for as high as 5% of GTOW [1]. *Elysium* has the advantage of a low disk loading, which reduces the induced velocity of the rotors in hover. The airframe of the *Elysium* was also designed specifically to have small wetted area in the rotor wakes. Aerodynamic substantiation using an in-house free-vortex solver, presented in Fig. 19.2, shows the vorticity iso-surfaces trailed from the blade tips in hover. The results show wake contraction causing the fuselage to remain entirely out of the wake of each rotor.

From the free-vortex wake profile, only the fuselage arms contribute to the download penalty on *Elysium*. The fuselage arms are elliptical in shape and the drag can be easily computed empirically using two-dimensional drag relations. From Section 10.3.1, the arm cross sections have a height-to-width ratio of 1.5, for which the drag coefficient in the downward direction is approximated as 1.3. The drag coefficient, arm area, and inflow velocity from momentum theory were used to estimate the total download as 0.89% of the vehicle weight. Because *Elysium* maintains a constant thrust coefficient over the entire mission, the non-dimensional inflow also does not change over time. Thrust is therefore directly proportional to drag based on momentum theory:

$$D \propto v_i^2, \quad \rightarrow \quad D \propto 0.0089 \cdot T \tag{19.1}$$

where D is drag, v_i is rotor induced velocity, and T is rotor thrust. The download penalty of 0.89% therefore applies to the full range of gross weights for the entire mission.
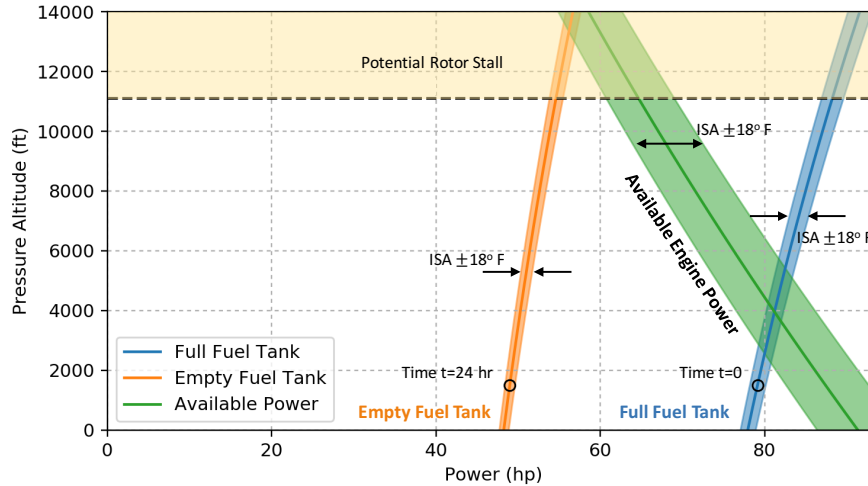
19.1.2 Hover Ceiling

FIGURE 19.3: Hover Ceiling at ISA±18°F (ISA±10°C)

Although the RFP only requires that the *Elysium* hover out of ground effect, the ability to hover at many different altitudes is a valuable and expected attribute of VTOL aircraft. Fig. 19.3 shows the Weight-Altitude-Temperature plot for the *Elysium*. Shown in green, the width of the available power band represents the variation with sea-level temperature ISA±18°F (ISA±10°C). The available power decreases with altitude based on the performance of reciprocating engines at varying temperature and density.

At the start of the 24-hour hover mission, the aircraft at 1500 ft (457 m) is operating near the point of maximum available power. By the end of the 24-hour mission, *Elysium* is overpowered and the hover ceiling is instead limited by blade stall, defined where $C_T/\sigma = 0.16$ at approximately 11,000 ft (3352 m).

19.1.3 Effect of Tip Shape

The use of anhedral rotor blade tips is a popular trend in modern rotor blade design. The goal of using an anhedral at the rotor tip is to force the tip vortex to start further down below the blade, reducing induced velocity and correspondingly induced power. For a blade with little taper and twist where the outboard section of the blade produces the highest lift, pushing the tip vortex down affects most strongly the outboard region where reducing induced power can result lower overall power despite any increase in profile power caused by the anhedral geometry. For higly twisted and tapered blades where the lift is more evenly distributed along the blade as a result of near-uniform inflow, an anhedral tip geometry has shown less favorable results. As shown in the aerodynamic substantiation in Fig. 19.4 , using an anhedral for *Elysium* did show lower tip vortex strength however with approximately a 1% increase in figure of merit. Use of anhedral tip shapes for *Elysium* is not beneficial from a power-reduction standpoint and has therefore not
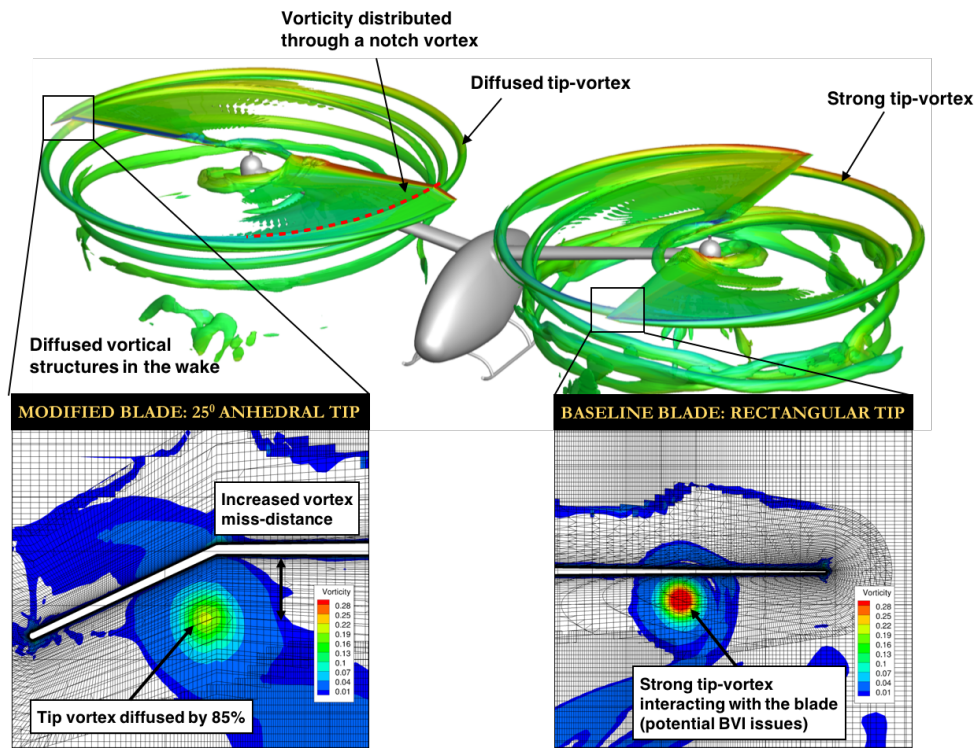
FIGURE 19.4: Effect of blade tip-shape on tip-vortex diffusion in hover.

been included in the final design. From an aeroacoustics and vibrations standpoint, however, if initial testing of *Elysium* shows high blade-vortex or arm-vortex interaction, use of an anhedral tip may mitigate these issues and be considered for future designs. The direction of rotation for each rotor of a twin-rotor aircraft will not affect the hover performance of the vehicle as long as the fuselage is roughly symmetric. In forward flight, however, the direction of rotation dictates whether the advancing side of each rotor is on the outside or inside of the rotor hubs. Both the V-22 and AW-609 tilt-rotors fly in side-by-side configuration in forward edge-wise flight with the rotors advacing on the outside of each hub. Although tilt-rotors are far from hover-efficient, they set a precedent for what is currently feasible in side-by-side edge-wise forward flight. *Elysium* has been designed to fly forward keeping this precedent in mind by also having the advancing blades outside of the rotor hubs.

19.2 Forward Flight

Forward flight cruise makes up less than five minutes of the 24-hour mission time, and consequently through the sizing procedure did not strongly influence the selected vehicle design. Forward flight nevertheless is a requirement for all modern helicopters and Fig. 19.5 shows the predicted performance of *Elysium* at the mission-start and mission-end weight. The plotted orange and blue lines are from blade-element momentum theory for a trimmed aircraft. Using a trimmed result ensures control authority at all flight speeds, which is especially important with the use of highly twisted blades designed for hover. At full-weight, *Elysium* can achieve a maximum flight speed of 60 knots (111 km/h) with an advance ratio of $\mu = 0.23$. At the end of the mission with a near-empty tank, *Elysium* can achieve a maximum flight speed of 65 knots
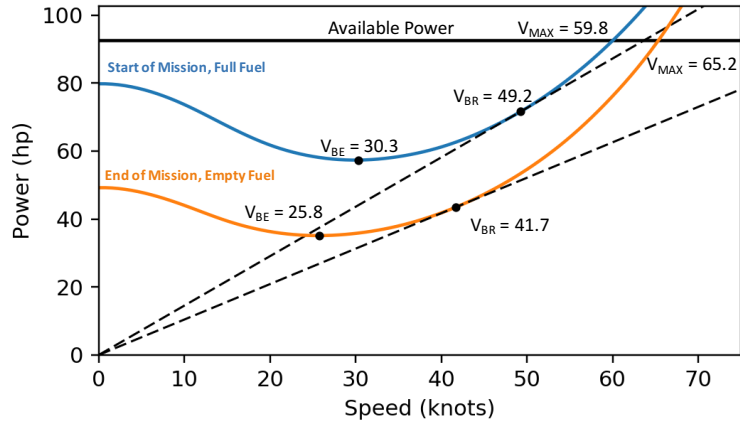
FIGURE 19.5: Cruise performance at 1500 ft (457 m)

(120 km/h) with an advance ratio of $\mu = 0.3$.

Both rotors were trimmed for zero moment at each hub; lift-offset is possible for a twin configuration however would not show a large benefit since the maximum advance ratio is only 0.3. Furthermore, the limiting factor in forward flight speed is available power and not control authority. Twisted, tapered blades intended for hover result in significant profile power drag in forward flight.

The speeds for best endurance are 30.3 and 25.8 knots (56.1 and 47.7 km/h) for the vehicle with full and empty fuel respectively. The speeds for best range are 49.2 and 41.7 knots (92.1 and 77.2 km/h) for the vehicle with full and empty fuel respectively. Although flying at the velocity for best range provides the best fuel economy for a given distance, the small distance between hover stations in the design challenge results in cruise times of less than 2 minutes. For very short flights, factors such as acceleration and deceleration should be considered. Especially with forward flight accounting for such a small fraction of the mission, the cruise speed of 20 knots (37 km/h) for the selected sizing mission is a conservative speed to justify neglecting of unsteady acceleration.

TABLE 19.2: Endurance, range, and approximate flat-plate area of *Elysium* compared to the Robinson R22

	Endurance (hr)	Range		Flat-plate Area	
Elysium	41.7	1460 nm	2703 km	16.8 ft^2	1.6 m^2
Robinson R22	3.5	320 nm	593 km	2.8 ft^2	0.3 m^2

Table 19.2 compares the momentum theory calculation of endurance and range for *Elysium* with performance of the Robinson R22. *Elysium's* endurance is over 11 times that of the R22, which is expected since the R22 is designed primarily for forward flight and *Elysium* for hover. The range of *Elysium* is approximately 4.5 times that of the R22 because the best-range cruise speed for *Elysium* is only 40-50 knots. The R22 and *Elysium* are similar power and weight requirements however the R22 can fly significantly faster because its streamline design results in a small flat-plate area and low corresponding drag. *Elysium* has a streamlined fuselage, however the support arms account for 75% of the entire aircraft flat plate area.

19.3 Aerodynamic Data of Airframe

To predict hover and forward performance of *Elysium*, data for not only the rotor but also for the airframe are required such as parasite drag, and vertical drag. This section describes prediction of aerodynamic data of airframe. Table 19.3 shows equivalent area and volume of parasite lift, drag, pitching moment, and side force at zero degree of vehicle pitch and yaw angle. Because the RFP requires the exclusion of all items related to the rotor system and aerodynamic surface, airframe components were only considered in the table. To calculate aerodynamic data, the following methods were mainly used: (1) USAF Stability and Control Digital DATCOM [46], and (2) methods presented by Keys [47] and Prouty [48]. DATCOM is aircraft design methodology developed by USAF and calculates static stability, dynamic derivatives of aircraft. DATCOM was used to calculate lift, drag, pitching moment of fuselage. The other methods were based on empirical relations and used to calculate aerodynamic data of other components such as landing gear, rotor arm, and gimbal. The resultant output data were built up by adding each component of the airframe.

TABLE 19.3: Equivalent area and volume of airframe

L/q (ft^2)	D/q (ft^2)	M/q (ft^3)	Y/q (ft^2)
0.07	18.66	40.45	0.00

The table shows that the airframe of *Elysium* has low parasite lift area and positive pitching moment volume at zero degrees of vehicle pitch and yaw. Also, because of symmetry of the airframe, side force area is zero. The total parasite drag area was assessed to be about 18.66 ft^2. Table 19.4 shows the breakdown of drag coefficients and equivalent flat plate areas for horizontal drag. To avoid confusion, the drag coefficient was non-dimensionalized by the rotor disk area. The table shows that *Elysium* has a quite high equivalent parasite drag area compared to a helicopter of similar weight [48] because of its rotor arms. However, because *Elysium* has a very low cruise speed (20 *knots*), the ratio of parasite power to total required power during the cruise was only 2.4% and 4.1% at GTOW and empty weight, respectively.

TABLE 19.4: Breakdown of equivalent flat plate area for horizontal drag.

Component	C_d	Drag Area (ft^2)	Contribution (%)
Fuselage	0.0031	1.483	7.95
Rotor Arm×2	0.0348	16.55	88.68
Landing gear	0.0011	0.50	2.68
Gimbal	0.0003	0.13	0.70
Total	0.0393	18.663	100

Similarly, table 19.5 shows a breakdown of equivalent flat plate area for vertical drag. The fuselage of *Elysium* has higher vertical flat plate area than horizontal flat plate area. However, because the fuselage is outside of the rotor wake as shown in Section 19.1 and *Elysium* has very low climb speed (150 ft/min), the download on fuselage and rotor arms were only 20.09 lb during the climb, which is 1.1% of GTOW.

TABLE 19.5: Breakdown of equivalent flat plate area for vertical drag

Component	C_d	Drag Area (ft^2)	Contribution (%)
Fuselage	0.0203	9.64	26.35
Rotor Arm×2	0.0522	24.82	67.86
Landing gear	0.0042	1.99	5.43
Gimbal	0.0003	0.13	0.36
Total	0.0770	36.58	100

19.4 Autorotation Performance

Autorotative performance is a safety consideration for any rotorcraft with a human occupant. Although *Elysium* is designed for the 24-hour challenge with a simulated human occupant, the ultimate goal is for the aircraft to have an actual passenger or pilot. Figures 19.6 and 19.7 show the autorotation capability of *Elysium* compared to conventional rotorcraft.
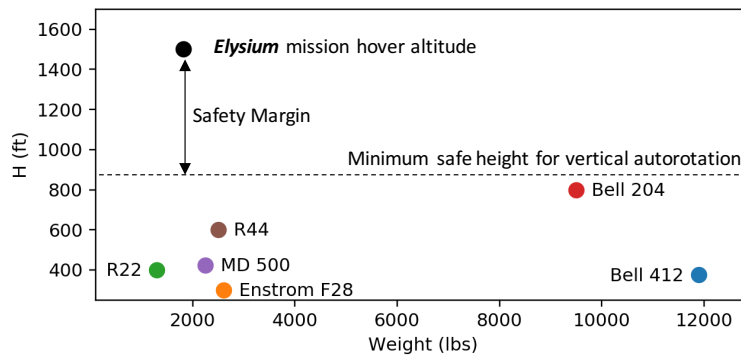
FIGURE 19.6: Minimum save hovering altitude for common helicopters

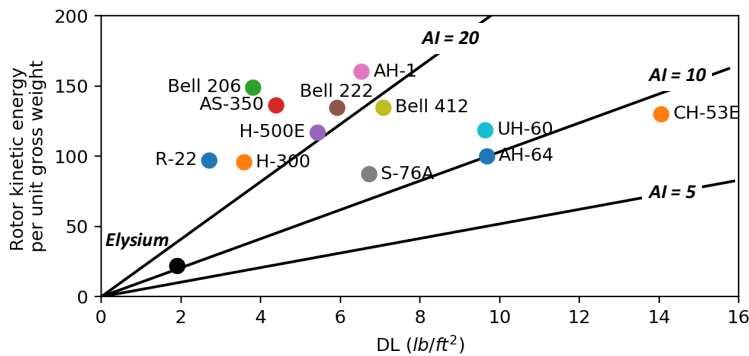FIGURE 19.7: Autorotative index of common helicopters

19.5 Mission Performance

The mission used for sizing *Elysium* (see Section 3.2 for additional details) comprises 10 total segments: idle and climb, followed by three cycles of 8-hour hover and 20 knot cruise, and finishing with descent and idle. The initial climb segment was chosen as axial climb to ensure
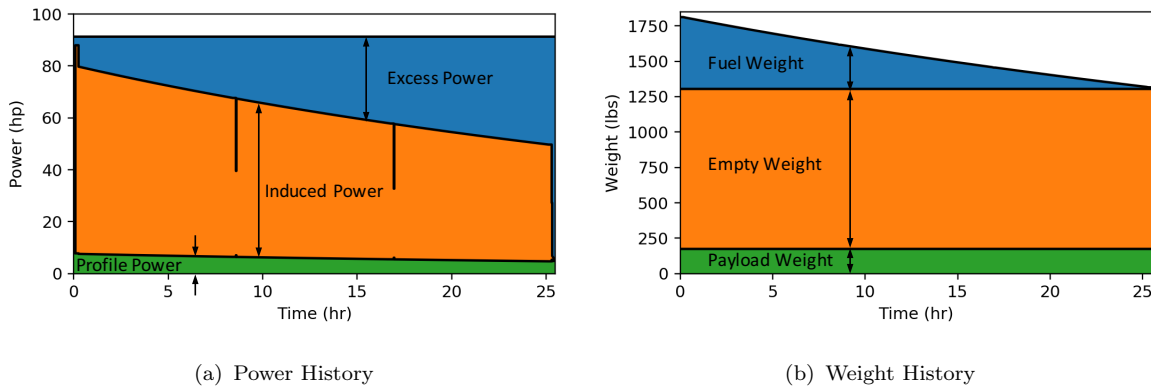
(a) Power History

(b) Weight History

FIGURE 19.8: Power and weight variation over the full mission

Elysium was not required to perform a climb with forward flight speed to ascend to the first hover station. Consequently, this axial climb segment determines the maximum power required as power in vertical climb is greater than for hover. Figure 19.8 shows the variation in the required power across the sizing mission. The initial spike in power reflectes the power required for axial climb.

In an actual 24-hour mission, the temperature will decrease into the night resulting in improved aerodynamic performance. However, to ensure a stringent sizing mission, a constant high temperature of ISA $+18°F$ ($+10°C$) was imposed. Therefore, for a constant temperature and altitude, the available power from the reciprocating engine is unaffected over 24 hours. The maximum available power from this engine, shown in blue in Fig. 19.8, is a flat line over 24 hours.

For a constant tip-speed rotor, the profile power remains constant as the vehicle weight changes. Because *Elysium* incorporates a variable RPM design, the profile power (shown in green in Fig. 19.8(a)) decreases over time. Reducing the RPM allows for a constant blade loading, which is crucial for obtaining a constant figure of merit over time. The three hover segments account for 98% of the mission time. The forward-flight cruise segments in comparison appear as spikes in the power history shown in Fig. 19.8(a) as these segments requires less power than hover. Decrease in vehicle weight over time is directly related to the rate of consumption of fuel, which is shown in Fig. 19.8(b). The weight history shows no noticeable influence of the forward flight in the fuel consumption over 24-hours.

A detailed breakdown of the mission by segment is shown in Table 19.6. Each cruise segment is for a distance of 0.54 nm (1 km), which satisfies the requirements of the RFP. Each hover segment accounts for extra time for periods of gusts that would now count towards hover time for the challenge. The descent rate at the end of the mission of 300 ft/min (1.52 m/s) is insignificant in sizing *Elysium* because this segment requires the least power and occurs at a point when the vehicle is lightest.

20 Concept of Operations

Designing an experimental VTOL aircraft is a challenging task, and designing an aircraft to reliably fly a 24 hour mission includes additional constraints. For any new platform, it is important to develop a thorough understanding and appreciation for vehicle operation, both during flight

TABLE 19.6: Segment breakdown of full mission

	Activity	Duration (hr)	Distance (nm)	Altitude (ft)	Temp (F)	Speed	Avg Weight (lbs)
1	Idle	00:05	0.00	0		0	1811.2
2	Climb	00:10	0.00	0 to 1500		150 ft/min	1811.0
3	Hover	08:20	0.00			0	1715.1
4	Cruise	00:02	0.54			20 kt	1617.6
5	Hover	08:20	0.00	1500	ISA+18°	0	1536.9
6	Cruise	00:02	0.54			20 kt	1456.5
7	Hover	08:20	0.00			0	1386.7
8	Cruise	00:02	0.54			20 kt	1317.0
9	Descent	00:05	0.00	1500 to 0		-300 ft/min	1315.6
10	Idle	00:05	0.00	0		0	1315.4

and on the ground, in terms of inspection, maintenance, and handling. It is also necessary to ensure the aircraft meets all regulations set forth by the Federal Aviation Administration (FAA): while the requirements for autonomous, unmanned helicopters have not yet been published, *Elysium* is designed to meet the current requirements of FAR 27.

20.1 Experimental Aircraft Testing

As an experimental technology demonstrator, *Elysium* will need to successfully complete a proper flight testing regimen before safely attempting the record-breaking 24 hour hover flight for which it has been designed. The unique capabilities of the technologies aboard *Elysium* require new test methods to ensure the necessary reliability and safety required of an experimental aircraft. The test program for *Elysium* was designed to incrementally assess and validate all on-board subsystems as well as the vehicle's capabilities. The testing of the *Elysium* Technology Demonstrator will be broken into three phases. The first phase will consist of ground testing and the following two will all be flight testing, incrementally increasing the flight envelope of *Elysium*. Initially *Elysium's* payload capacity will be used for instrumentation and electronics to support the flight test program, such as the remote multiplexing unit for analog to digital conversion, data combiner unit, a solid state recorder, and transmitter for real-time monitoring. A time-line of the *Elysium* test program is shown in Fig. 20.1. Any issues that arise during a test will be addressed and fully resolved before advancing to the next phase of testing.

20.1.1 Phase 1: Ground Testing

Ground testing will begin with component level bench top testing, including, but not limited to, rotor blades, gearbox, Fly-By-Wire (FBW), and rotor primary electrohydrostatic (EHS) servo subsystems. *Elysium's* rotor blades will undergo fatigue and structural testing for assessment of final manufactured mechanical properties to compare with design values. Because of the unique means of retention of the composite spar to the blade root insert, this joint will receive special attention. Structural and rap tests will determine the mass, structural bending, torsional stiffness, and natural frequencies. The primary rotor control EHS servos will be fully qualified
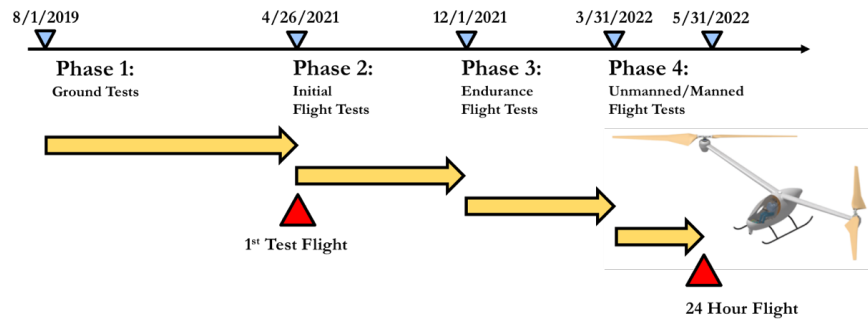
FIGURE 20.1: *Elysium* Technology Demonstrator Test Plan.

with ground testing to include functional characteristic definition, endurance tests, vibration tests, and a temperature test from $-20°C$ to $+50°C$. The gearboxes between the motors and rotors are the most mechanically complex subsystem aboard *Elysium*, and therefore must go through rigorous testing to ensure reliability and sustained performance. Each gearbox will go through a series of no-load lubrication tests to ensure function and performance of lubrication system over a period of 24 hours, and the motors will be tested to ensure the adequacy of the cooling systems for 24 hour operation. Gear rap tests will verify separation of diametral mode and mechanical natural frequencies. Measuring gearbox housing accelerations will monitor resonant responses of any gears throughout the planned operating speed range.

Once component testing is complete, full aircraft tie down ground testing will be conducted including on aircraft acceptance test procedures (ATPs) and endurance tests, before beginning any flight testing. Simultaneously performing component and subsystem tests before integration will speed up flight testing and aid in making installation uneventful and fast. The ground tests will be run with the aircraft tied down to concrete pad with chains or straps, made to react full rotor thrust and moments. First engine integration will be tested, followed by the gearbox and propulsion system accessories. Once all the lubrication, cooling, electrical system and component instrumentation tests are completed with bare head (no blades), the main rotor blades will be installed for initial blade-on ground runs. During these tests, the Fly-By-Wire system operation will be validated and checked for blade balance and tracking. The final set of ground tests will be to demonstrate full capabilities through full control inputs, RPM variation, and avionics communication. Endurance tests will progress as 0.5, 6.0, 12.0, 25.0 hours and culminate in a no tie-down light on the wheel ground run.

20.1.2 Phase 2: Initial Flight Testing

Following completion of the light on wheels ground run, first flight of the *Elysium* Technology Demonstrator will consist of a 30 minute hover and basic systems check. The goal of the subsequent flight is to explore the basic controllability of the aircraft, with basic maneuvers, three takeoffs and landings, and forward flight. This initial flight should show any discrepancy between the actual and desired control system, so any necessary changes in the FBW software can be made for the next flight. Once aircraft control handling quality is satisfactory, *Elysium* must demonstrate: (1) very stable hover, (2) 20 knot forward speed, (3) 10 knot lateral speed, (4) 10°/sec hover turn, (5) 30°/sec roll rate, and (6) 10° angle of bank. Once *Elysium* has met these requirements, Phase 2 is complete and *Elysium* is ready to progress to endurance tests in Phase 3.

20.1.3   Phase 3: Long Endurance Flight Testing

Once *Elysium* has demonstrated sufficient flight worthiness and controllability across the necessary flight envelope, *Elysium* will move to Phase 3 of testing for endurance qualifications. The first test will consist of take-off, vertical climb to 1500 ft, and an 8 hour hover. After successful completion of this first endurance flight, the auxiliary fuel tanks will be installed to reach the 24 hour hover capability. Next, 16 and 24 hour hover flights directly above the landing site will prove *Elysium's* capability to hover for 24 hours without landing or refueling. The last flight will be to attempt the sizing mission to fullfill all RFP and Sikorksy 24 Hour Hover Challenge rules. The position of the three hover stations will be operator-defined prior to starting the mission and wirelessly uploaded to the vehicle as part of the pre-flight procedure. Each hover location will have a ground station with technicians and safety personnel to monitor the vehicle from the onboard instrumentation. *Elysium* will be closely monitored for the duration of the test flight, but will complete the mission fully autonomously, with the option of manual override at any time. A chase aircraft will escort *Elysium* along its mission to ensure line of sight contact for the duration. This vehicle will need to be refueled or replaced, because it will not have the same endurance capabilities. Lessons learned from and modifications due to prior tests will simplify this final sizing mission test and will prepare *Elysium* for success in both the unmanned and manned record breaking flights.

20.2   Ground Procedures and Handling

As a technology demonstrator, *Elysium* was designed with the goal of completing an experimental aircraft test regimen; therefore, the operational requirements are different than a vehicle designed for a customer to use in the field. As an experimental technology demonstrator, it is important to achieve a vehicle design suitable for quick modification and development to reduce the workload and complexity for all technicians and testing personnel. Placement of access panels to all of *Elysium's* internal compartments allows technicians to quickly access any instrumentation or hardware during testing. Minimizing maintenance time between testing is crucial for meeting the five-year timeline for all phases of design, build, and test. Additionally, these panels are crucial for ground testing as component integration and testing will require non-standard production assembly.

21 Life-Cycle Cost Analysis

As a new platform, and model of technological step changes, *Elysium's* costing will vary significantly from conventional production helicopters. *Elysium* will incur high development costs for the advanced technologies incorporated into the design. *Elysium* is designed for ease and cost of manufacturing at low production rates. Only three individual vehicles will be built for flight testing before the lessons learned from the *Elysium* platform are incorporated into a production aircraft, which is not discussed in this report.

The total cost of the *Elysium* Technology Demonstrator Program is broken down into four major categories: (i) the development cost, (ii) the production cost, (iii) the operational cost, and (iv) the end of life cost. The life cycle cost is the sum of each of these four cost elements. The Harris and Scully Method for cost estimation was used to calculate the expected costs of *Elysium* in 2017 USD. This model is based on the total quantity of the aircraft to be manufactured as well as the rate of production each year. The total life cycle cost estimates three aircraft over

the next five years. *Elysium* is an experimental aircraft and therefore difficult to predict from empiracle models built for production aircraft. The additional development cost of advanced engineering work, and production cost because of the low production number requiring special manufacturing will influence these calculations. Historically experimental aircraft experience delays and cost over runs because of these difficulties.

- **Development Cost Prediction**: The *Elysium* design makes use of the most advanced existing and available technologies. Development costs are reduced by using commercial off-the-shelf (COTS) avionics, accessory propulsion components, and flight controls. *Elysium* also consists of many custom built components such as composite blades and structures, and an optimized powerplant system. Developing these unique components will require significant development time, and therefore incur greater costs, for example composite tooling and strength testing. The overhead engineering cost for *Elysium*, a completely new platform, is far greater than for a production aircraft variant upgrade. Assuming the development cost is approximately four times the aircraft cost of production, this results in a total development cost estimate of approximately $6.90 million.

- **Production Cost Prediction**: The production costs for *Elysium* are calculated accounting for the rotor system, structure and powerplant. The cost of avionics suite, and flight controls are based on the cost of COTS components. For a 24 hour mission ready aircraft, the unit cost of *Elysium* is $341,310. For a total production cost of $1.02 million. Compared to the Robinson R22 aircraft, at a $288,000 unit cost, this cost is slightly high, but this is attributed to the advanced avionics and complex carbon fiber structures.

- **Operational Cost Prediction**: Due to the simplicity in design and the short life-span of a technology demonstrator, the operational mission costs for *Elysium's* are low in relation to current production helicopters of the same weight class. During flight testing, the majority of the cost will not come from the aircraft but in the testing personnel and operators who must accompany every flight, and work diligently between tests days. This cost model is based on using $120/hr for engineers and technicians, and $100/hr for mechanics and technitions to make modifications and repairs. An additional 15% of the mission ready aircraft cost accounts for repairs and 40% of the operating costs is added for indirect costs. For *Elysium's* 1000 hr design life, over the next five years the estimated total operating cost is estimated at $9.24 million

- **End of Life Cost Prediction**: At the end of an aircraft's usable life, the aircraft is broken down and reusable materials are sent to recycling centers. The cost is based on the amount of recylcable material in the aircraft. Composites cannot be recylced, while batteries, electronics, and certain mechanical components of the power plant can be recycled. Due to the nearly full composite strucutre, only 40% of *Elysium* can be recycled, which results in a cost of $2.76 million. For such a novel experimental aircraft, the *Elysium* vehicles may retire to be show cased in museums, meaning the aircraft components could not be recycled.

- **Total Life Cycle Cost** : The total life cycle cost of *Elysium* Technology Demonstrator is the sum of the above four components to a total of $13.02 million, and a $4.34 million/unit cost. This number is significantly greater than the Robinson R22, but the low production number and advanced design are large factors in the per unit cost of the aircraft.

22 Summary

The University of Maryland Graduate Team has designed *Elysium* a hybrid electric twin rotor vehicle, to meet all of the vehicle and operational requirements specified in the Request for Proposals for the 2017 AHS International Student Design Competition, to design a 24 Hour Hovering Machine. *Elysium* is designed to maximize hover efficiency while ensuring superior reliability with superb gust tolerance, all within a 5 year design, build, and test timeline.

- Advanced blade aerodynamics allow for a hover optimized rotor that achieves a figure of merit of 0.847

- The hybrid-electric propulsion drive train provides system redundancy, minimum fuel weight, and a platform for all future electric aviation technology to be implemented

- Innovative half-cyclic Fly-By-Wire controls allow for full control authority with minimal weight

- Novel semi-articulated hub design provides unprecedented mechanically compact and maintenance free hub design

Bibliography

[1] Leishman, J. G., *Principles of Helicopter Aerodynamics*, Cambridge University Press, New York, NY, 2006.

[2] Lee, C. H., Min, S. Y., Lee, J. W., and Kim, S. J., "Design, Analysis, and Experimental Investigation of a Cyclocopter with Two Rotors," *Journal of Aircraft*, Vol. 53, No. 5, Aug. 2016, pp. 1527–1537.

[3] Johnso, W., "NDARC NASA Design and Analysis of Rotorcraft," Tech. Rep. 2009-215402, NASA, Dec. 2009.

[4] Pereira, J. L., "Hover and Wind-Tunnel Testing of Shrounded Rotors for Improved Micro Air Vehicle Design," Phd dissertation, University of Maryland College Park, 2008.

[5] Hrishikeshavan, V., "Experimental Investigation of a Shrouded Rotor Micro Air Vehicle in Hover and in Edgewise Gusts," Phd dissertation, University of Maryland College Park, 2011.

[6] Emadi, A. and Gao, Y., *Modern Electric, Hybrid Electric, and Fuel Cell Vehicles: Fundamentals, Theory, and Design*, CRC Press, 2010.

[7] "Compact Fusion," Lockheed Martin, 2014.

[8] "DOE Fuel cell RD roadmap," Motor land, Jan. 2017.

[9] "DOE Fuel Cell market report," Motor land, Jan. 2017.

[10] Manikandan Ramasamy, "Hover Performance Measurements Toward Understanding Aerodynamic Interference in Coaxial, Tandem, and Tilt Rotors," *Journal of the American Helicopter Society*, Vol. 60, No. 3, 2015, pp. 1–17.

[11] Srinivasan, G. R. and Baeder, J. D., "TURNS: A Free-Wake Euler/Navier-Stokes Numerical Method for Helicopter Rotors," *AIAA Journal*, Vol. 31, No. 5, September 1993, pp. 952–962.

[12] Winslow, J., Otsuka, H., Govindarajan, B., and Chopra, I., "Basic Understanding of Airfoil Characteristics at Low Reynolds Numbers," *7th AHS Technical Meeting on VTOL Unmanned Aircraft Systems and Autonomy*, 2017.

[13] Medida, S. and Baeder, J. D., "Application of the Correlation-based -Re t Transition Model to the Spalart-Allmaras Turbulence Model," *20th AIAA Computational Fluid Dynamics Conference*, 2011.

[14] Jude, D. and Baeder, J. D., "Extending a three-dimensional GPU RANS solver for unsteady grid motion and free-wake coupling," *54th AIAA Aerospace Sciences Meeting*, 2016.

[15] Lednicer, D., "The Incomplete Guide to Airfoil Usage," 2010.

[16] Christos Kassapoglou, *Design and Analysis of Composite Structures with Applications to Aerospace Structures*, John Wiley & Sons, Ltd, West Sussex, United Kingdom, 2010.

[17] Core Composites, "Kevlar Honeycomb," 2016, www.corecomposites.com/products/honeycomb/kevlar-honeycomb.html.

[18] Fort Felker, Benton Lau, Stacey McLaughlin, Wayne Johnson, "Nonlinear Behavior of an Elastomeric Lag Damper Undergoing Dual-Frequency Motion and its Effect on Rotor Dynamics," *Journal of the American Helicopter Society*, Vol. 32, No. 4, 1987, pp. 45–53.

[19] Lord Corporation, "Elastomeric Damper Maintenance," 2015, www.aogheliservices.com/lord1.html.

[20] Leonard J. Doolin, Stephen V. Poulin, "Elastomeric Swashplate Configuration for Helicopters," 1990, US Patent 7,598,470.

[21] Tom Bitzer, *Honeycomb Technology: Materials, Design, Manufacturing, Applications and Testing*, Springer Science, Berlin, Germany, 1997.

[22] Hoshi, M., "Reducing Friction Losses in Automobile Engines," *Tribology International*, Vol. 17, No. 4, Aug. 1984, pp. 185–189.

[23] Kovach, J., Tsakiris, E., and Wong, L., "Reducing Friction Losses in Automobile Engines," *SAE Trans.*, Vol. 91, Feb. 1982, pp. 1–13.

[24] Markus, F., "At Least One Automaker Plans to Produce an Opposed-Piston Engine," Motor land, Jan. 2017.

[25] "D-Motor LF-39 Operators Manual," Tech. rep.

[26] Birch, S., "Nanoslide cuts friction on Mercedes-Benz engines," Motor land, Dec. 2011.

[27] "D-Motor LF-26," Tech. rep., Rotax Aircraft Engines.

[28] "OM-912 Operators manual for ROTAX engine Type 912 I Series edition 1 revision 3," Tech. rep., Rotax Aircraft Engines.

[29] "Operators manual for ROTAX engine Type 912 ULS Series edition 3 revision 0," Tech. rep., Rotax Aircraft Engines.

[30] UAV Navigation, "VECTOR Technical Specification," 2015, www.uavnavigation.com.

[31] UAV Navigation, "TELEM05 Technical Specification," 2015, www.uavnavigation.com.

[32] Novatel, "Enclosures FlexPak6," October 2016, www.novatel.com.

[33] UAV Vision, "CM160 Datasheet," 2017, www.uavvision.com.

[34] Freeflight Systems, "Radar Altimeter," 2015, www.freeflightsystems.com.

[35] Sagetech, "MX Family of Transponders," 2017, www.sagetech.com.

[36] UAV Navigation, "GCS-03 Technical Specification," 2015, www.uavnavigation.com.

[37] Whelen, "2017 Helicopter Lighting Catalog," 2017, www.whelen.com.

[38] CorePower Systems, "1162-4," 2017, www.astronics.com.

[39] Sandia Aerospace, "Avionics Cooling Solutions," 2017, sandia.aero.

[40] Willis, S., "OLM: A hands on approach," *Proceedings of the International Committee on Aeronautical Fatigue*, 2009.

[41] Gregory Gremillion, Lina Castano, J. S. H., "Disturbance Rejection with Distributed Acceleration and Strain Sensing," *AIAA SciTech*, 2015.

[42] "Flying Qualities of Piloted Aircraft," Tech. Rep. MIL-STD-1797A, Department of Defense, Dec. 1997.

[43] "Comparative example of Noise Levels," http://www.industrialnoisecontrol.com.

[44] David Crist and L. H. Symes, "Helicopter landing gear design and test criteria investigation," USAAVRADCO TR-81-D-15, U.S. Army Research and Techonology Laboratories, 1981.

[45] "Engineering Design Handbook Helicopter Engineering: Part One Preliminary Design," Tech. Rep. AMCP 706-201, United States Army Material Command, Alexandria, VA, Aug. 1974.

[46] Williams, J. E. and Vukelich, S. R., "The USAF Stability and Control Digital DATCOM," USAF Technical Report AFFDL-TR-79-3032, Air Force Flight Dynamics Laboratory, Dayton, Ohio, April 1979.

[47] Keys, C. N., "Rotary-Wing Aerodynamics: Volume 2 - Perfomance Prediction of Helicopter," NASA Contractor Report 3083, NASA, 1979.

[48] Prouty, R. W., *Helicopter Performance, Stability, and Control*, Krieger Publishing Company, Melbourne, 2002.